FABRICATION OF COPPER/CARBON NANOTUBE NANOCOMPOSITE WIRES FOR SUBSEA APPLICATIONS

A Dissertation

by

FARHAD DANESHVAR FATAH

Submitted to the Office of Graduate and Professional Studies of
Texas A&M University
in partial fulfillment of the requirements for the degree of

DOCTOR OF PHILOSOPHY

Chair of Committee,	Hung-Jue Sue
Co-Chair of Committee,	Mohammad Naraghi
Committee Members,	Lei Fang
	Homero Castaneda
Head of Department,	Ibrahim Karaman

May 2020

Major Subject: Materials Science and Engineering

ABSTRACT

The advent of offshore renewable energy, e.g. wind, wave, and tidal, holds the promise of significant environmental and economic benefits. Once built, the energy produced by offshore renewable energy farms is transmitted to the land by cables installed on the seabed. However, being made of copper, subsea power cables suffer from high density and poor mechanical properties. Recent developments in nanotechnology have provided new alternatives. Among these, carbon nanotubes (CNTs) stand out for their high electrical and thermal conductivity, low density, supreme ampacity and mechanical properties.

In here, incorporation of CNT into Cu matrix to fabricate light-weight and highly conductive wires has been evaluated. CNT surface has very poor wettability towards copper. This challenge was overcome by altering the surface chemistry of the CNTs. Results show that by controlling the CNT surface chemistry, one can tune the composition and morphology of the Cu deposits. Cu-CNT thin films were fabricated by using CNT-Cu hybrid structures via vacuum filtering followed by electroless deposition. Electrical conductivity measurements showed that thin-films that contained Thiol-CNT have remarkably higher electrical conductivity and denser structure.

Accordingly, two routes are undertaken to fabricate Cu-CNT wires. In the first approach, CNT fibers are fabricated via wet-spinning. Surface of the fibers are modified by cysteine and subsequently a layer of Cu is deposited on their surface via electroless deposition, forming a core-shell structure. The electrical conductivity of these fibers is 3.6×10^7 S/m, while their specific strength is twice of copper. In the second approach, CNT-CuNW colloid are mixed

with a polymer-Cu salt solution. Subsequently, after electrospinning the precursor polymer is removed by heating at 400 °C in air followed by purging a reforming gas to reduce the fibers into CNT-Cu fibers. These high aspect ratio fibers have a remarkable performance in transparent conductive electrodes. Its sheet resistance reaches to 39 Ω/□ at 79% transmittance, outperforming commercial counterparts. Moreover, we found out that by proper interface design of CNTs and Cu oxides through introducing Sn_2O intermediate layer, we can produce hybrid structures of CNT and Cu oxides that have specific capacity of 662 F/g and show 94% retention after 5000 cycles. Findings here are versatile and can be used in other metal-CNT structures.

DEDICATION

One of the hardest things for a parent is letting their child leave. They knew they would not see me for a long time, but encouraged me to follow my dreams. For their support, patience, and unconditional love, I dedicate this dissertation to my father, Gholamreza Daneshvar, and my mother, Zahra Jafari.

ACKNOWLEDGEMENTS

I would like to thank my committee chair, Prof. H-J Sue, and my committee members, Dr. Naraghi, Dr. Castaneda, and Dr. Fang, and Dr. Atif Aziz at University of Cambridge for their guidance and support throughout the course of this research.

Microscopy and Imaging Center, Materials Characterization Facility, and Polymer Technology Center are acknowledged. The FE-SEM acquisition was supported in part by the National Science Foundation under Grant No. DBI-0116835.

Thanks also go to my colleagues, specifically Dr. Jamshid Kavosi, Dr. Majid Tabesh, Dr. Michael Mullins, and Dr. Spencer Hawkins and the department staff for making my time at Texas A&M University a great experience.

Finally, thanks to my mother, father, and my brothers for their encouragement and to my fiancé, Katie, for her patience and love.

CONTRIBUTORS AND FUNDING SOURCES

Contributors

This work was supervised by a dissertation committee consisting of Professors Hung-Jue Sue [advisor] and Homero Castaneda of the Department of Materials Science and Engineering and Professor Lei Fang of the Department of Chemistry and Mohamad Naraghi of the Department of Aerospace Engineering.

The electrochemical data analyzed in section 5 was provided by Dr. Atif Aziz of University of Cambridge. The Copper nanowires used in section 4 were synthesized by Dr. Tan Zhang.

All other work conducted for the thesis (or) dissertation was completed by the student independently.

Funding Sources

This work was made possible by Lloyd's Register under Grant Number M1503462 – Nanotechnology in subsea power. Its contents are solely the responsibility of the authors and do not necessarily represent the official views of the Lloyd's Register.

TABLE OF CONTENTS

Page

LIST OF FIGURES

Page

LIST OF TABLES

Page

1. INTRODUCTION

1.1. Background

Subsea power transmission cables and umbilicals are taking greater significance in the smart grids that are set to overhaul the existing power infrastructure. They are responsible for transmitting electricity to offshore installations, finding applications in offshore renewable energy projects, interconnecting national grids, and even down to the seabed with the burgeoning subsea processing technologies sector. According to Navigant Research, the market for subsea power transmission is accelerating; with the global high voltage cable industry alone projected to surpass 5.3 billion USD in annual revenue by 2023, up from 1.4 billion in 2014 [1]. While the first submarine power transmission cable was installed in 1811 [2], the fundamental operating principles behind the electrical cable have not changed significantly in the intervening centuries; however, cable technologies have seen remarkable developments in performance. The cables of today are vastly superior to their predecessors in terms of significantly improved lay length, lay depth, transmission capacity, and system reliability, owing much to the innovations in manufacturing processes, i.e. processing under super-clean conditions [3]. Given the increasing complexity of cable installation projects being proposed today, and that the current approaches in improving cable performance are reaching diminishing yields, advances in cable technologies are sorely needed.

At the core of the submarine cable is the electrical conductor which carries the current. While the conductor fulfils a critical part of the cable's function, it is conceptually simple owing to the limited materials options available. The standard IEC 60228 [4] specifies that electrical conductors are to be fabricated from annealed copper, aluminum or aluminum alloys. There are

several other low resistivity metals and alloys which can be used for more exotic applications, such as silver, but the dominant metals used for cable conductors are aluminum and copper.

The most critical material property of the conductor is its conductivity/resistivity, which is measured relative to the International Annealed Copper Standard (IACS). According to, Table 1-1 the conductivity of aluminum 1350-H19 is about 61% lower than copper, necessitating a larger cross-sectional area for comparable power transmission performance. Even though the aluminum cable might eventually weigh less, the added bulk increases the bending radius, increasing the challenges involved in installation.

Impurities have a severe negative effect on the conductivity of copper. The specified purity of copper for conductors is 100%. Small amounts of phosphorous or arsenic may reduce the conductivity by up to 20%. Thus, traditional techniques to improve the strength of the conductor material through alloying or cold-working come at the expense of conductivity, resulting in the preference of soft annealed copper, according to ASTM standard B3 [5].

The availability and excellent electrical performance of copper are the primary reasons behind its dominant position in the electrical conductor industry. Recent developments in nanotechnology however, have provided new materials which possess the potential to surpass copper in terms of electrical conductivity, weight and ampacity. Among these, carbon nanotubes stand out on the basis of their high electrical and thermal conductivity, low density, abundance of precursor materials, and supreme mechanical properties.

Table 1-1. Direct current resistivity of various metals at 20 °C.

Metal	Volume conductivity (%IACS)	Volume resistivity (Ω-mm^2/m)	Weight resistivity (Ω-lb/mile^2)
Soft copper	100	0.01724	875.5
Hard copper	96.16	0.01793	910.15
Copperweld	39.21	0.04397	2046.3
Al 1350-H19	61.2	0.02817	434.81
Al 5005-H19	53.5	0.03223	497.36
Al 6210 T81	52.5	0.03284	506.85
Alumoweld	20.33	0.08401	3191
Steel	5	0.21551	9574

Individual carbon nanotubes are hollow quantum wires with extremely narrow diameters in the range of several atomic distances. The charge carriers are free to travel only along the axial directions and may show ballistic electron transport, that is, without scattering, as confirmed experimentally [6]. An individual single wall CNT (SWCNT) can have a maximum conductance of $G = 4e^2/h \approx 0.15$ mS (where h is the Planck constant) [7]. Experimental data have shown resistivity values close to theoretical values at 7.7×10^{-7} Ω/cm. The lowest resistivity reported for multi wall CNT (MWCNT) was up to 5×10^{-6} Ω/cm, which was lower than SWCNT, probably due to the fact that MWCNTs have higher diameters than typical SWNTs [8]. Diffusive transport will be observed if the length of CNT is larger than the ballistic regime. Ballistic transport may also be inhibited due to the increase in temperature or high electric fields. Despite this, individual SWCNT at room temperature has exhibited maximum current density up to $10^9 – 10^{10}$ A/cm^2, which is higher than even the critical current density of superconductors.

Apart from the favorable electrical properties, the CNTs have excellent mechanical properties. The experimentally measured values of tensile moduli are approximately 0.3 – 0.95 TPa, tensile strengths at approximately 10 – 100 GPa and tensile strains at approximately 6 –

12% [9]. The density of SWNT is about 1.3 g/cm^3 and that of MWNT is 2.1 g/cm^3. As compared to other typical electric conductors: copper and aluminum at about 8.96 g/cm^3 and 2.7 g/cm^3 respectively.

CNTs are excellent thermal conductors in the axial direction, with thermal conductivity exceeds the best-known bulk heat conductors, including diamond. Thermal conductivities in the axial direction of isolated SWNT and MWNT were experimentally measured to be at 3500 and 3000 $Wm^{-1}K^{-1}$ respectively [10]. Effective heat removal is much more efficient due to the high thermal conductivity and extremely high surface area of CNTs. Due to its low density, nanotubes have very high specific mechanical properties (strength or stiffness divided by density), which exceeds those of steel or other high-performance materials. These properties are highly important for use as electrical conductors and may potentially substitute metal in many applications.

Research into translating these properties from the nanoscale to the macroscale have however, not been advancing as smoothly as many researchers have hoped. Attempts to fabricate macrostructures like sheets and yarns have shown some promising results, such as Behabtu et al. [11] who employed a wet spinning process and produced CNT yarns achieving specific conductivity greater than copper, shown in Figure 1-1, but only through intensive chemical treatment with iodine. While this approach holds promise, the prohibitively expensive and laborious synthesis of CNTs on an industrial scale hampers this approach.

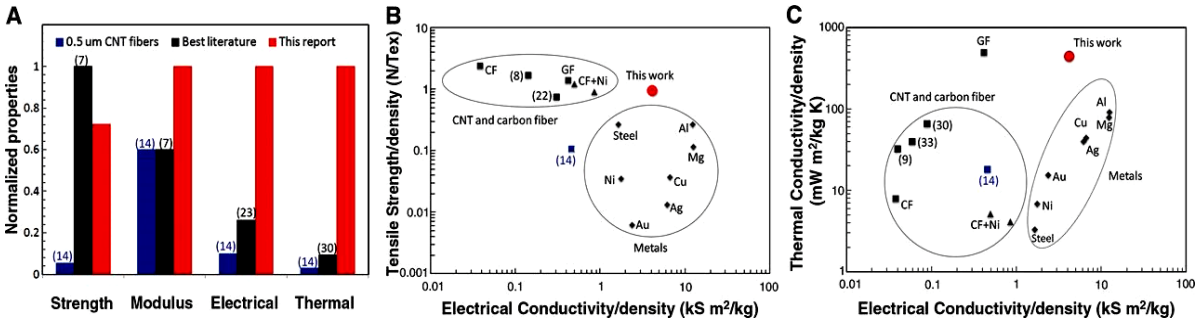

Figure 1-1. Properties of continuous, neat CNT fibers. Black denotes literature values, blue denotes earlier wetspun 0.5-mm CNT fibers (14), and red denotes fibers in [11]. (a) Comparison of properties normalized to the highest value. (b) Specific tensile strength versus specific electrical conductivity of metals (gray diamonds), pitch (GF) and PAN (CF) carbon fibers (gray squares), nickel-coated CF (gray triangles), CNT fibers (black and blue squares), and CNT fibers from this report (red circle). Carbon and CNT fibers fall in a high-strength, low-conductivity region; metals define a high-conductivity, low-strength region. (c) Specific electrical conductivity versus specific thermal conductivity Ashby plot, showing distinct regions for metals and carbon fiber. Reprinted with permission from [11].

A different approach is to employ the CNTs as nanofillers in copper matrixes. Interest in carbon nanotube-metal composites for electrical conductors can trace its roots to a paper by Hjortstam et al. [12], in which a theoretical approach was used to evaluate the possibility of fabricating an ultra-low resistivity carbon nanotube-metal composite. The simple effective-medium model used predicted that at a 30-40 volume % filling factor, metallic, single walled CNT-metal composites could present room temperature electrical conductivities approximately twice that of annealed copper. The confluence of electrical, thermal, and mechanical property enhancements that carbon nanotubes offer when incorporated in metals, leads to the tremendous potential of these materials as electrical cable conductors.

However, several challenges to be overcome before seeing the widespread adoption of CNT-metal composites have been identified, namely the length and quality of the CNTs; the alignment, dispersion, and interfacial contact between CNT and the metal matrix; and lastly the manufacturing cost and scalability of producing the composite. Special attention must also be paid to the behavior of the materials throughout the fabrication route depending on which

processing technique is applied, especially as it relates to the chemical and structural stability of the CNT filler.

Several recent breakthroughs in the field of "ultraconductive copper" (copper composites having electrical conductivity exceeding annealed copper) have been reported in the scientific literature, most prominently in a paper by Subramaniam et al. [13]. The group's groundbreaking results were a result of a novel fabrication protocol which eschews the typical CNT-copper ion dispersion processing route, see Figure 1-2. The process begins with the growth of a vertically aligned CNT forest by a water assisted method, which is then subject to shear forces to align the CNTs horizontally between two glass slides.

The resulting aligned CNT mat is then densified via a liquid densification technique with copper ions. A two-phase electro-deposition process was subsequently employed. The first stage wets the hydrophobic CNT surface with copper ions in an organic solution (copper acetate in acetonitrile) to nucleate copper seeds on the CNT surface. Following that, an aqueous copper ion solution (commercially available electroplating solution) was used to induce the growth of the seed copper particles until the mesopores are filled. A low current density (1-5 mA/cm^2) was used to allow homogenous nucleation as the ion diffusion into the interstices between the CNT matrix was not the rate determining step. After washing in acetonitrile, annealing in a hydrogen atmosphere takes place to reduce the deposited copper oxide phases into copper metal particles, which are then sintered.

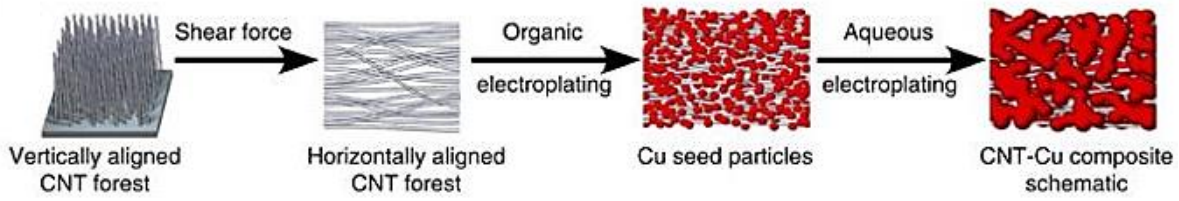

Figure 1-2. Schematic of the two-step electroplating process employed in fabricating CNT-Cu nanocomposite. Reprinted with permission from [13].

The reported performance of the composite material had conductivity comparable to copper, up to 81% IACS (4.7×10^5 S/cm compared with copper's 5.8×10^5 S/cm), but showed two orders of magnitude greater ampacity (6×10^8 A/cm^2). Additionally, the high-volume fraction (45 vol%) of CNTs resulted in a significantly reduced material density, culminating in a specific conductivity 26% greater than neat copper. The thermal properties of the composite material were also markedly improved, with an order of magnitude reduction in the temperature coefficient of resistivity. Consequently, the nanocomposite exceeded the electrical conductivity of copper at elevated temperatures greater than 80 °C, see Figure 1-3. The mechanisms behind the improvements were elucidated to be the suppression of primary failure pathways in copper by the carbon nanotubes, evidenced by increased copper diffusion activation energy.

The exploration of ultraconductive copper has significant commercial and industrial implications, and as such, few scientific papers have been published although there has been much research on the subject. Nevertheless, some information can be gleaned from the patents filed. Nayfeh et al. [14] have developed a technique to die cast CNT-copper composites by loading CNTs into channels within a cartridge. Molten metal is then poured into the chamber and mixed with the CNTs, then injected into the die form where the combination of shear forces and laminar flow results in the alignment of carbon nanotubes parallel to the casting axis.

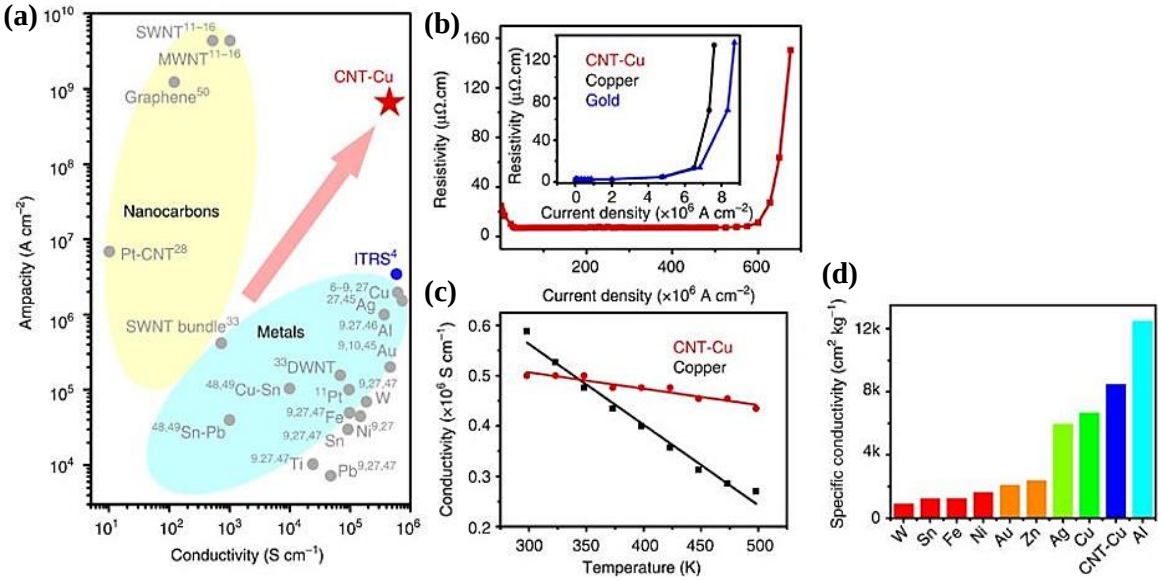

Figure 1-3. (a) Ashby plot of ampacity versus conductivity for various relevant materials, including metals, alloys, nanocarbons and composites. (b) Variation of resistivity with current density for CNT–Cu composite, with similar traces for Cu and Au shown in inset for comparison. (c) Variation of conductivity with temperature for CNT–Cu and Cu. (d) Comparison of specific conductivity of CNT–Cu with different metals. Reprinted with permission from [13].

Composites engineered this way have been reported to have conductivities up to 113% IACS. Furthermore, the patent holder claims that infusing the CNTs with a surface coating of $MgCl_2$ prior to loading allows the formation of intimate electrical contacts between matrix and filler. The rapid cooling of the molten rods also supposedly results in the retention of the alignment of the nanotubes. These two effects would significantly improve the conductivity, by over 10-fold.

A different approach was implemented by Holesinger in designing the CNT-copper composite [15]. Rather than dispersing the CNTs within the copper matrix, his research was directed at sheathing a copper core with an aligned, dense, connected CNT coating. Their methodology begins with the immersion of copper wire segments in a CNT suspension. The wires are then subject to a sweeping acoustic excitation of particular frequencies near the

resonant frequency, agitating and concentrating the suspended CNTs near the central wire, which embeds and fuses the CNTs onto the surface to form a growing sheath. The group reports a specific conductivity 108% that of neat copper.

Perhaps the most promising efforts toward developing ultraconducting copper are the ongoing research activities in Europe, spurred by the inception of the three year, €3 million "Ultrawire" project in 2013. The project links up a 14-member consortium from industry and academia, and aims not only to develop a copper-nanocarbon composite with enhanced overall electrical, mechanical, and thermal performance over bulk copper, but more importantly, to also devise a scalable, continuous method of synthesizing this material with adequate control over the materials' structure and resulting properties.

1.2. Project description

We propose the fabrication of a Cu-CNT metal matrix composite wire which outperform copper wires as electrical conductors. The proposed approach utilizes a spinning technique to afford carbon nanotube fibers from a polymer solution seeded with copper nanoparticles, which will then be plated with copper to form wires.

Two spinning techniques are utilized to fabricate CNT-Cu fibers: (i) electrospinning, and (ii) wet spinning. Electrospinning is a facile, saleable technique based on an electrohydrodynamic process for forming continuous thin fibers ranging from several nanometers to tens of micrometers. The one-dimensional (1D) nanomaterial, CNT, can be oriented by external fields such as flow fields, magnetic fields, electric fields, and electrophoretic processes. Therefore, the CNTs are expected to be highly oriented in an electrified thin jet during electrospinning. As a proof of concept for the electrospinning of CNT

nanofiber assemblies, a number of research groups have recently reported the synthesis of highly aligned CNTs in the electrospun CNT/polymer composites with electrical conductivities inferior to the conventional CNT fibers or yarns [16-18]. Moreover, electrospinning has been used to fabricate copper wires with promising results [19-21]. In this method, electrospinning is carried out using a mixture of a Cu salt (often Cu acetate) and an aqueous polymeric solution. Resulted electrospun fibers have a core–shell structure, with core and shell being made of polymer and a Cu-based compound, respectively. Subsequently, these fibers go through a thermal treatment in air to remove the polymer, followed by a thermal treatment in reforming gas to reduce the fibers to Cu. Macroscopic assemblies of CNT-Cu can be produced by adapting these approaches, by firstly depositing Cu on the surface of CNTs and then electrospinning the Cu seeded CNT/polymer/Cu salt solution, and subsequently subjecting them to thermal treatment in air and reforming gas. Electrodeposition/electroless deposition of the doped fibers can then proceed, with the copper plated fibers subsequently sintered to form the prototype metal matrix composite wires. Seeding the CNTs with copper is a crucial step since CNT has low affinity towards metals. To enhance the interfacial interaction, the surface chemistry of the CNTs are firstly modified and then by utilizing electroless deposition technique, Cu is grown on the CNT's surface. The schematic of the electrospinning and electroless deposition processes are presented in Figure 1-4.

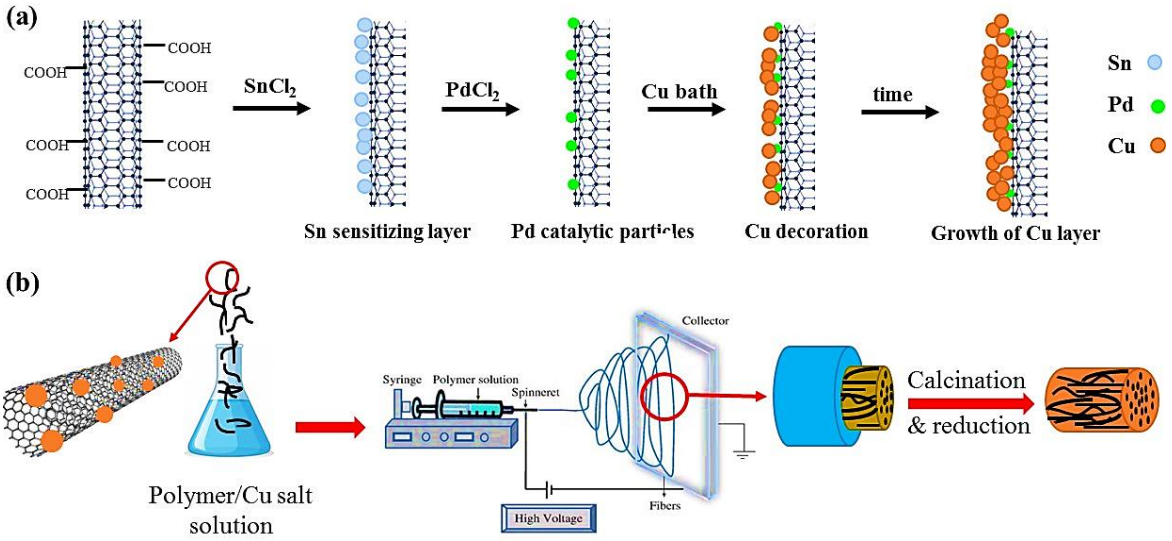

Figure 1-4. Schematic of the proposed processes for depositing Cu on the surface of CNTs using electroless deposition (a), and fabrication Cu/CNT fibers via electrospinning (b). In this example, prior to Cu deposition CNT surface is modified by hydroxyl groups.

Alternatively, wet spinning have been used for fabrication of strong and conductive CNT fibers [11, 22]. In this technique, high purity double wall CNTs (DWCNTs) are dissolved in sulfonic acid or mixed with a polymeric solution such as PVA [23] or polyethylene glycol [24], and spun to a coagulation bath. Subsequently, they are washed with water or heat treated in air to remove the acid or the polymer, respectively. Wet-spinning via sulfonic acid can produce very dense CNT fibers with remarkable tensile strength (1.1 GPa) and very high electrical conductivity (8×10^6 S/m) [25]. However, these fibers still cannot compete with copper in terms of electrical conductivity (Cu: 5.96×10^7 S/m). Accordingly, by adapting wet-spinning process, two routes are undertaken to fabricate Cu/CNT fibers. In the first approach, CNT fibers are produced by dispersing DWCNT in a sulfonic acid-based solution. After washing and removing the acid, the outer surface of the fibers goes through a surface treatment method to prepare them for Cu deposition. In the next step by using electroless deposition, a layer of Cu is deposited on CNT fiber, forming a core-shell structure with CNT fiber as the core and Cu as the shell. The

surface treatment provides better bonding between the CNT and the Cu coating, which is beneficial especially for mechanical properties [26, 27]. In the second wet-spinning route, Cu/CNT hybrid structure are introduced to an aqueous solution of polyvinyl alcohol (PVA) and wet-spun into an acetone bath for coagulation and forming PVA-Cu/CNT fibers. Fibers go through a heat treatment step in air to remove the PVA followed up by a heat treatment in reforming gas to reduce the Cu. These approaches are schematically presented in Figure 1-5.

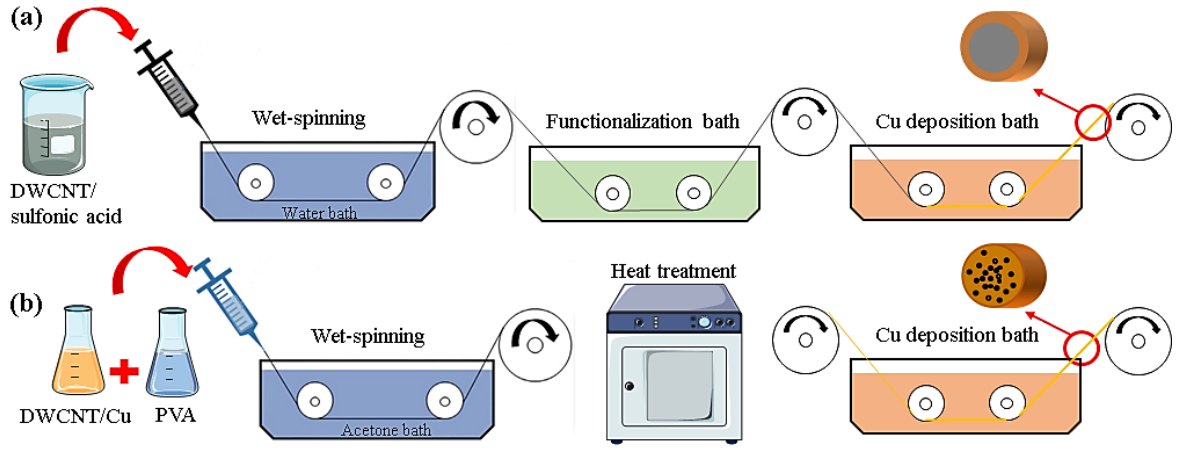

Figure 1-5. Wet-spinning procedures for fabrication of (a) CNT/Cu core-shell, and (b) nanocomposite fibers.

In all the undertaken approaches, creating a strong interaction between CNT and Cu is a critical parameter. Generally, metals have poor wettability towards CNT. This case is even more pronounced for Cu [28]. In the present work, various surface treatment techniques have been implemented to tackle this issue. In addition to pristine CNTs as control sample, three of the most common and promising functionalization groups have been chosen for the study, namely, carboxyl (two different conditions), N-doping and thiol. Then, functionalized CNTs are coated with Cu in nanoscale via electroless deposition method. Based on the CNT surface chemistry, Cu nanostructures with different morphology, size and composition are formed on the CNT

surface. The morphology, interfacial interactions, and composition of these hybrid structures are studied through Transmission Electron Microscopy (TEM), Energy-dispersive X-ray spectroscopy (EDS), X-ray photoelectron spectroscopy (XPS), and X-ray Powder Diffraction (XRD). The metalized CNTs are used in different spinning procedures to produce Cu/CNT fibers. Electrical conductivity of these fibers are obtained through four-probe resistivity measurements according to ASTM B193-16 standard [29]. Tensile strength and modules of the fibers are obtained according to ASTM C1557-14 [30]. In addition, the electrochemical performance of Cu_xO/CNT as electrode materials for supercapacitors has also been investigated.

1.3. References

1. Hamilton, B.D., *Offshore wind market and economic analysis*. 2014, Navigant Consulting, Inc., Chicago, IL (United States).

2. Brinser, H. *Submarine Power Cables*. in *OCEANS'76*. 1976. IEEE.

3. Worzyk, T., *Submarine power cables: design, installation, repair, environmental aspects*. 2009: Springer Science & Business Media.

4. IEC, *Conductors of insulated cables* in *60228*. 2004, IEC.

5. *Standard Specification for Soft or Annealed Copper Wire*, in *B3*. 2018, ASTM.

6. Langer, L., et al., *Quantum transport in a multiwalled carbon nanotube.* Physical review letters, 1996. **76**(3): p. 479.

7. Zhou, X., et al., *Band structure, phonon scattering, and the performance limit of single-walled carbon nanotube transistors.* Physical Review Letters, 2005. **95**(14): p. 146805.

8. Ebbesen, T., et al., *Electrical conductivity of individual carbon nanotubes.* Nature, 1996. **382**(6586): p. 54.

9. Thostenson, E.T., Z. Ren, and T.-W. Chou, *Advances in the science and technology of carbon nanotubes and their composites: a review.* Composites science and technology, 2001. **61**(13): p. 1899-1912.

10. Han, Z. and A. Fina, *Thermal conductivity of carbon nanotubes and their polymer nanocomposites: A review*. Progress in polymer science, 2011. **36**(7): p. 914-944.

11. Behabtu, N., et al., *Strong, light, multifunctional fibers of carbon nanotubes with ultrahigh conductivity.* science, 2013. **339**(6116): p. 182-186.

12. Hjortstam, O., et al., *Can we achieve ultra-low resistivity in carbon nanotube-based metal composites?* Applied Physics A, 2004. **78**(8): p. 1175-1179.

13. Subramaniam, C., et al., *One hundred fold increase in current carrying capacity in a carbon nanotube–copper composite.* Nature communications, 2013. **4**: p. 2202.

14. Nayfeh, T.H. and A.M. Wiederholt, *Nano-engineered ultra-conductive nanocomposite copper wire*. 2013, Google Patents.

15. Holesinger, T.G., et al. *Carbon nanotube composite cables for ultra-deepwater oil and gas fields*. in *Offshore Technology Conference*. 2014. Offshore Technology Conference.

16. Guan, X., et al., *Carbon nanotubes-adsorbed electrospun PA66 nanofiber bundles with improved conductivity and robust flexibility.* ACS applied materials & interfaces, 2016. **8**(22): p. 14150-14159.

17. Arshad, S.N., M. Naraghi, and I. Chasiotis, *Strong carbon nanofibers from electrospun polyacrylonitrile.* Carbon, 2011. **49**(5): p. 1710-1719.

18. Maitra, T., et al., *Improved graphitization and electrical conductivity of suspended carbon nanofibers derived from carbon nanotube/polyacrylonitrile composites by directed electrospinning.* Carbon, 2012. **50**(5): p. 1753-1761.

19. Bognitzki, M., et al., *Preparation of sub‐micrometer copper fibers via electrospinning.* Advanced Materials, 2006. **18**(18): p. 2384-2386.

20. Sun, B., et al., *Recent advances in flexible and stretchable electronic devices via electrospinning.* Journal of Materials Chemistry C, 2014. **2**(7): p. 1209-1219.

21. An, S., et al., *Self‐junctioned copper nanofiber transparent flexible conducting film via electrospinning and electroplating.* Advanced Materials, 2016. **28**(33): p. 7149-7154.

22. Zhang, S., et al., *Macroscopic fibers of well‐aligned carbon nanotubes by wet spinning.* Small, 2008. **4**(8): p. 1217-1222.

23. Xue, P., et al., *Electrically conductive yarns based on PVA/carbon nanotubes.* Composite Structures, 2007. **78**(2): p. 271-277.

24. Lu, W., et al., *State of the art of carbon nanotube fibers: opportunities and challenges.* Advanced materials, 2012. **24**(14): p. 1805-1833.

25. Tsentalovich, D.E., et al., *Influence of carbon nanotube characteristics on macroscopic fiber properties.* ACS applied materials & interfaces, 2017. **9**(41): p. 36189-36198.

26. Bakshi, S.R., D. Lahiri, and A. Agarwal, *Carbon nanotube reinforced metal matrix composites-a review.* International materials reviews, 2010. **55**(1): p. 41-64.

27. Nai, M.H., J. Wei, and M. Gupta, *Interface tailoring to enhance mechanical properties of carbon nanotube reinforced magnesium composites.* Materials & Design, 2014. **60**: p. 490-495.

28. Ilari, G.M., et al., *Carbon–metal interfaces analyzed by aberration-corrected TEM: How copper and nickel nanoparticles interact with MWCNTs.* Micron, 2015. **72**: p. 52-58.

29. *ASTM Standard B193* in *Standard Test Method for Resistivity of Electrical Conductor Materials*. 2016, ASTM International: West Conshohocken, PA.

30. *ASTM C1557*, in *Standard Test Method for Tensile Strength and Young's Modulus of Fibers*. 2014, ASTM International: West Conshohocken, PA.

2. TUNING THE COMPOSITION AND MORPHOLOGY OF CARBON NANOTUBE-COPPER INTERFACE [*]

2.1. Introduction

Copper has been the conductive material of choice in electronic devices for years due to its superior electrical conductivity, abundance, and thermal resistance among others. Future technological advances, from portable electronics to space explorations, demand electronics with smaller size and lower weight, parameters that metals such as copper fail to satisfy. However, recent developments in nanotechnology have provided new materials which possess the potential to surpass copper in terms of electrical conductivity, weight, and ampacity. Among these, carbon nanotubes (CNTs) stand out on the basis of their high electrical and thermal conductivity, remarkable ampacity, low density, abundance of precursor materials, and supreme mechanical properties [1].

Individual CNTs are hollow quantum wires with extremely narrow diameters in the range of several atomic distances. The charge carriers are free to travel only along the axial directions and show ballistic electron transport at room temperature [2]. Nevertheless, research into translating these properties from nanoscale to macro scale have not been straightforward. Attempts to fabricate highly conductive macrostructures like sheets and yarns have shown some promising results, but only through complex processing and intensive and expensive chemical treatments [3-6]. A different approach, inspired by the theoretical work of Hjorstam et al. [7],

---

[*] Reprinted with permission from "Tuning the composition and morphology of carbon nanotube-copper interface" by Daneshvar, Farhad, et al. *Carbon* 157 (2020): 583-593. Copyright 2019 by Elsevier Ltd.

is to employ the CNTs as nanofillers in copper matrix. By simple effective-medium model, it was predicted that at a 30-40 vol% loading, metallic single-walled CNTs (SWCNTs)-copper composites could present room temperature electrical conductivities about twice that of annealed copper. This conclusion is of course under ideal conditions, such as uniform dispersion of CNTs and a perfect interface with the matrix. Unfortunately, experimental efforts have not been able to achieve these predicted conductivities even though a tremendous potential has already been demonstrated. For example, Subramaniam et al. [8] fabricated a Cu-CNT (45 vol%) sheet that had room temperature conductivity comparable to copper (81%), and ampacity and specific conductivity 100 times and 26% higher than copper, respectively.

One of the remedies to close the gap between theoretical and experimental results is to enhance the interfacial interactions between the CNT and the matrix. For polymer-based composites, this subject has been widely studied leading to development of numerous CNT surface treatment approaches with successful results [9-12]. These surface modification techniques have also been implemented in CNT-metal nanocomposites with some promising results, especially in terms of mechanical properties [13-18]. Nonetheless, research that have experimentally and systematically compared the effect of different surface groups on CNT-metal interface are scarce. These studies are necessary when significant number of research efforts are focusing on the CNT-metal and metal oxide systems in various applications such as energy storage, sensors, catalysts, and portable electronics [1, 19, 20].

In the present work, the effect of CNT surface treatment on the morphology, structure, and electrical conductivity of the Cu-CNT system has been investigated. Compared to other metals, Cu has weak interactions with CNTs [21], but this issue has been tackled in this work by

utilizing a proper surface treatment and synthesis method. Three of the most common and promising functionalization groups have been chosen for the study, namely, carboxyl (two different conditions), N-doping and thiol. Functionalized CNTs are coated in nanoscale via a facile and versatile electrochemical method. Our findings show that not only the morphology but also the composition of the metallic deposits is affected by the CNT surface treatment. Thiol group, which is known to have strong interactions with precious metals [22], shows the best affinity towards Cu. The thiol activated CNTs are uniformly coated with Cu and show electrochemical stability. Subsequently, Cu-seeded CNTs with different functionalities were used to fabricate CNT/Cu thin films. These composite thin films are produced via vacuum filtration and a subsequent electroless deposition methods. It is observed that CNT surface groups have significant effect on the electrical conductivity of these fibers; the thiol-activated CNT/Cu system shows the highest conductance, four and seven times higher than systems containing carboxyl and N-doped CNTs, respectively. Our results show that by proper tailoring of the CNT surface functionality, one can develop light-weight Cu-CNT nanocomposite wires with remarkable conductivity. The present findings can be used in a wide variety of applications, such as CNT (or graphene)-inorganic hybrid materials for energy storage, sensors, and catalysts; applications in which high surface area and electrical conductivity are desired.

2.2. Experimental procedure

2.2.1. Materials

Multi-walled CNTs (MWCNT) with a purity of 95 wt.%, diameter of 10 nm and length of 1-10 μm were supplied by Arkema Inc. To be concise, they will be referred to as CNTs. All other chemicals were obtained from Sigma-Aldrich and were used as received.

2.2.2. Pretreatment of CNTs

To study the effect of surface chemistry, CNTs were subjected to four different functionalization treatments, as described below.

I) Mild oxidation: 200 mg of as received-CNTs were dispersed in a mixture of sulfuric (75 mL) and nitric acids (25 mL) and ultrasonicatated in a sonication bath for two hours at room temperature. Subsequently, 150 mL deionized water (DI-H_2O) was added and the solution was sonicated for another hour at room temperature. After oxidation, oxidized MWCNTs were washed four times with DI-H_2O and collected on a polyvinylidine fluoride (PVDF) filter membrane (Millipore, Durapore, 0.45 μm pore size) under vacuum. Finally, they were dispersed in DI-H_2O. From here on these mildly oxidized MWCNTs are going to be referred as MO-CNTs.

II) Harsh oxidation: Similar to the first surface treatment process except that before diluting the CNTs with DI-H_2O, they were stirred for six hours at 70 °C under reflux. They are referred to as HO-CNTs from here on.

III) Nitrogen-doping: N-doping has a low interference with unique structure of CNTs. Also, by first principle calculations, it was recently shown to effectively enhance both mechanical and electrical properties of Cu-CNTs [23]. Respectively, N-doped CNTs (N-CNTs) were provided by from Arkema Inc., and used as substrate for deposition of Copper. According to the supplier, the MWCNTs have an average diameter of 10 nm and average length of 5 μm with 7 at% N.

IV) Thiol functionalization: 100 mg MO-CNTs obtained from the mild oxidation process described above are dispersed in 200 mL ethanol. N, N'-Dicyclohexylcarbodiimide (DCC) was

added to the solution in weight ratio of 1:1 w/w compared with CNTs. This mixture was then sonicated for 30 min and then stirred at room temperature for one hour. Next, 150 mg cysteamine was added in a weight ratio of 3:2 compared with MWCNTs and the mixture was stirred at room temperature for 24 hours. Thiol activated MWCNTs (SH-CNTs) were washed at least four times using PVDF filter membrane (Millipore, Durapore, 0.45 μm pore size) under vacuum.

2.2.3. Preparation of Cu/CNT composites

CNTs with different surface groups (f-CNTs) were similarly coated with Cu using electroless deposition technique as described in [19]. Concisely, 50 mg of f-CNTs were dispersed in 100 mL aqueous solution of $SnCl_2$ (1 g) and HCl (0.25 mL). The mixture was sonicated for 30 min at room temperature. Next, Sn-sensitized CNTs were activated using $PdCl_2$ (0.01 g) and HCl (0.25 mL) 50 mL aqueous solution by ultrasonication for 30 min at room temperature followed by rinsing in DI-H_2O using centrifuge. This washing step should be done carefully to remove all the excessive or unattached Pd and Sn ions from the solution. Finally, the activated CNTs were introduced to a 100 mL Cu electroless deposition bath. The composition and conditions of the plating bath are given in Table 2-1.

Table 2-1. The composition and conditions of the copper electroless bath deposition.

Chemical composition	Quantity
$CuSO_4.5H_2O$	6.2 g/l
2Na-EDTA	40 g/l
CHOH (37 vol% in H_2O)	20 ml/l
Temperature	60 °C
pH (NaOH)	13

2.2.4. Fabrication of Cu/CNT film for electrical conductivity measurements

Vacuum filtration was utilized for fabrication of CNT-Cu films similar to [24]. Firstly, 50 mg f-CNTs were seeded by copper using similar electroless deposition process explained in section 2.3. The only difference is that the concentration of all the metallic salts and 2Na-EDTA were cut in half to minimize the free particle formation and to promote copper nucleation. Free metallic particles and impurities were removed by filtering and centrifuge at 2000 rpm for 5 min. To fabricate the thin films, the aqueous solutions containing f-CNT/Cu hybrid systems were vacuum-filtered using polytetrafluoroethylene (PTFE) membrane filters with pore size of 450 nm (Millipore). The f-CNT/Cu were dried using a vacuum oven at 50 °C for 12 h. To ensure all the hybrid systems have similar amount of copper, dried copper seeded f-CNT films were electroless plated in 150 mL of copper bath with composition presented in Table 1 for 10 to 12 min. The copper coated films were dried using a vacuum oven at 50 °C overnight. The thin films with different CNT functional groups have the same weight after this process. Finally, the f-CNT/Cu films were heated at 250 °C for two hours in controlled flow of nitrogen and immediately followed by one hour in nitrogen-hydrogen (5 vol%) gas under 1 kPa pressure using dynamic mechanical analyzer (DMA) (ARES 300-G2, TA instruments). For comparison, the same process was used to fabricate thin film of pristine MWCNTs (P-CNTs).

2.2.5. Characterization

The structural properties and the morphologies of the synthesized Cu/MWCNT hybrid systems were examined using transmission electron microscopy (TEM) (FEI Teccai G2 S-Twin, Philips), X-Ray diffraction (XRD) (Bruker D8 Advance ECO) with CuKα incident radiation (λ = 0.1506 nm), and X-ray photoelectron spectroscopy (XPS) (Omicron DAR 40 dual

Mg/Al x-ray source). XPS plots were deconvoluted based on Gaussian–Lorentzian peaks and Shirley background subtraction. Prior to XRD and XPS experiments the samples were filtered and centrifuged to remove all the free Cu particles formed in the solution. FEI Tecnai Osiris S/TEM working at 200 keV was used to obtain STEM and EDX. The EDX detectors were FEI Super-X systems employing 4 Bruker silicon drift detectors for high collection efficiency (>0.9 sr solid angle) and high-count rates (>250 kcps).

To investigate the effect of surface treatment on electrical conductivity of the hybrid systems, thin films of Cu/MWCNT were made using vacuum filtering approach. Four-point-probe conductivity measurements were carried out on free-standing Cu/MWCNT films with a four-point-probe (Signatone, SP4-40045TBY) on a resistive stand (Signatone, Model 302). The conductivity was calculated by using the following formula:

$$\sigma = \frac{I.ln2}{\pi.V.t.k} \qquad 2\text{-}1$$

where σ is the electrical conductivity (S/m), I (A) is the current going through the outer two probes, V (V) is the voltage drop measured across the two inner probes, t is the thickness of the film (m) (which was obtained by SEM), and k is a correction factor. Three to four samples were analyzed for each functionalization method and 10 to 15 measurements were carried out on each sample. The average and standard deviation are reported.

2.3. Results and discussion

2.3.1. Surface treatment of CNTs

XPS was used to investigate the surface and interfacial chemistry of functionalized CNTs. The results show that all the samples contain C and O. In addition, N 1s peak at 399.3 eV and S 2p peak at 169.3 eV are detected for N-CNT and SH-CNT, respectively. The C 1s peak for

all the samples is situated almost at the same binding energy of 284.35 eV, which will be further analyzed in detail. It should be added that the O 1s peak binding energy depends on the surface modification technique and varies from 531.5 eV for SH-CNT to 532.5 eV for MO-CNT (Figure 2-1).

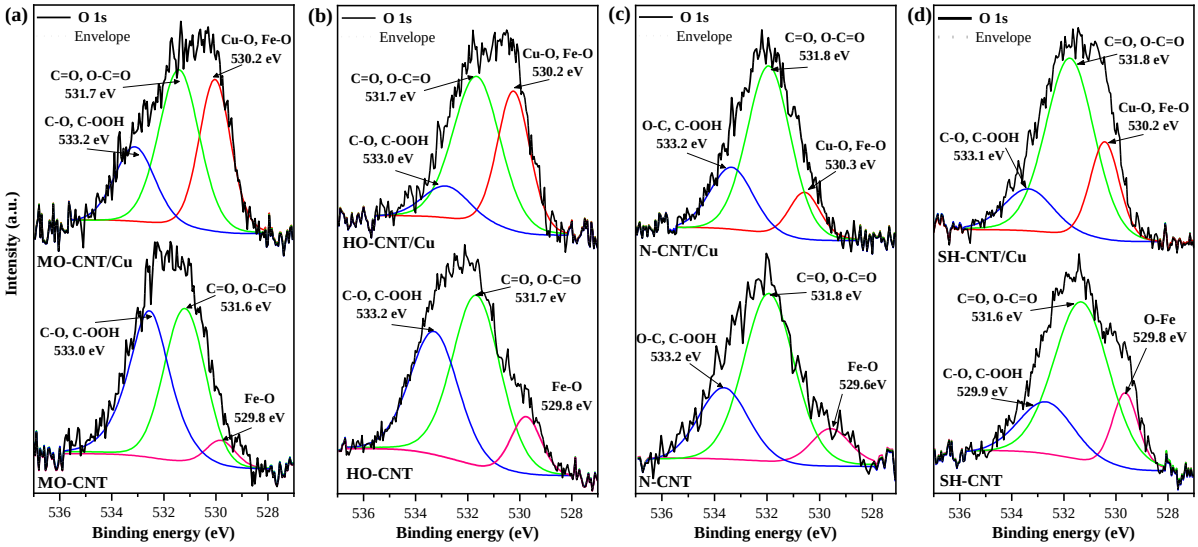

Figure 2-1. Resolved O 1s peaks of functionalized CNT and CNT/Cu hybrid systems (a-d) and their relative composition (e). As it can be observed, lattice oxide bonds were detected for functionalized CNT systems at 529.8 eV which are attributed to the Fe-O of CNT catalyst. Moreover, peaks at around 531.8 ev and 533.2 eV are assigned to C=O/O-C=O and C-O/C-OOH bonds, respectively.

The high resolution XPS data of C 1s peaks for f-CNTs and their deconvoluted peaks are represented in Figure 2-2a and 1b. As can be observed, MO-CNT sample is mainly consisted of C=C (284.3 eV) and C-C (285.5 eV) structures. The strong C 1s peak corresponding to sp^2 carbon, which is more or less common for other samples as well, shows that the conjugated bonds in CNT lattice are preserved after the surface treatments. Also, C-O-C (or C-O) peak at 286.6 eV, O-C=O peak (or C=O) at 288.3 eV, C-OOH peak at 289.5 eV, and broad π-π peak at 291.5 eV are resolved [25]. With increasing the intensity of the acid treatment, the C 1 peak becomes more asymmetric due to emergence of the shoulder at higher binding energies. The

resolved peaks show that the relative intensity of C=C peak (sp^2) slightly decreases while the C-C and oxygen containing species become stronger suggesting that the CNT structure is more distorted and more defects are introduced to the HO-CNT surface. The carboxyl group content in each sample is estimated based on the area beneath the resolved peaks. The result shows that carboxyl group content in MO-CNT and HO-CNT samples are around 7.5 at% and 12 at%, respectively. Moreover, based on the deconvolution of O 1s, the HO-CNT sample contained contains relatively higher C=O bonds concentration.

Compared to carboxyl functionalized samples, the full width at half maximum (FWHM) is higher for N-CNT and SH-CNT samples even though the oxygen containing groups have almost the same intensity. This is attributed to formation of a new peak at 286.0 eV which is ascribed to C-N for N-CNT and C-S or C-N for SH-CNT samples. Finally, compared with MO-CNT and HO-CNT samples, the intensity of oxygen containing groups decrease in the N-CNT and SH-CNT samples, which indicates that the oxygen functionalities reduction occurs by N-doping and thiol grafting. The nature of these changes can be revealed by analyzing the high resolution XPS of N 1s and S 2p respectively.

High resolution XPS shows that the N 1s core level spectra for N-doped CNTs (Figure 2-2c) can be deconvoluted in two peaks related to pyrodinic N at 298.7 eV and graphitic N at 400.7 eV [26]. As illustrated in Figure 2-2e, the former represents the substitution of an N atom with a C atom adjacent to a defect while the latter represents substitution of N atom with a C atom in a perfect benzene ring [26]. Moreover, the atomic ratio of these two structures are calculated by integrating the fitting curve area of N 1s peak, showing that doped N is almost 70 at% in pyrodinic form and the rest is in graphitic form.

Figure 2-2d displays the S 2p spectra corresponding to the SH-CNT showing that the thiol groups are successfully formed on the CNT's surface. S 2p has two main peaks with one situated at 168 eV which is attributed to sulfates and one around 164 eV which is a result of cysteine and thiol formation. The latter is the peak of interest here. Cysteine peak fitting results revealed that it can be deconvoluted to three components corresponding to C-S $2p_{1/2}$ at 163.3 eV, C-S $2p_{3/2}$ at 164.5 eV and a sharp peak at 163.9 eV which is assigned to SH tail of the thiol group [27]. These results suggest that thiol groups are formed by the amidation reaction between the amine groups of cysteine and the carboxylic groups of CNTs [27]. The surface composition of the CNTs was also determined using XPS, which indicated a 3.2 at% of S.

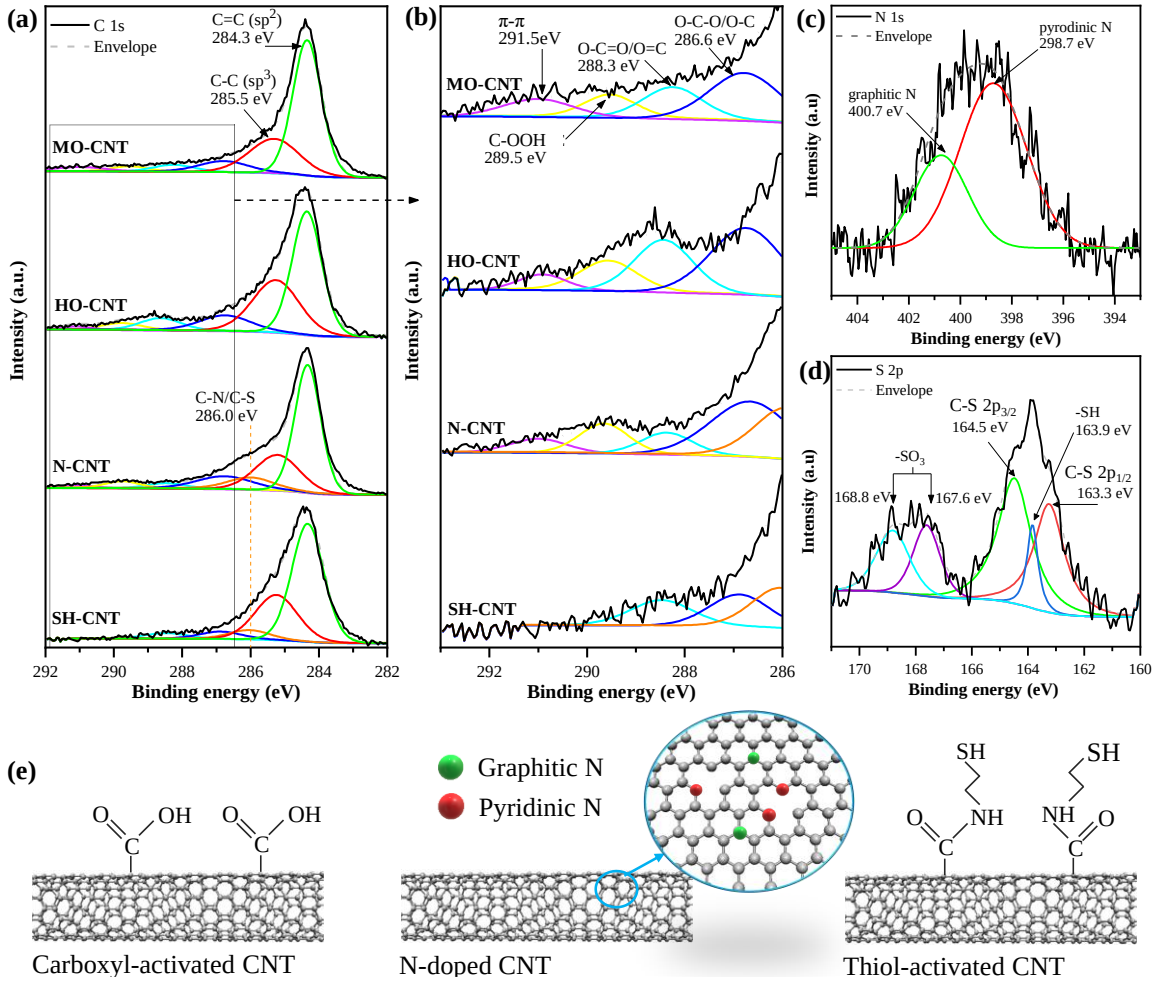

Figure 2-2. High resolution XPS spectra of (a) C1s, (b) C1s between 286-293 eV of the CNTs with different surface groups, (c) N 1s peak of N-CNT system, and (d) S 2p of SH-CNT. The dominant surface functional group for each type of surface treatment is schematically presented in (e). It should be noted that both MO and HO treatments create similar surface functional groups but in the latter these surface groups will be more abundant.

2.3.2. Morphology and composition of Cu/CNT systems

TEM analyses of the hybrid systems show that the functional group on the CNT surface can significantly affect the morphology and density of the copper deposits. Figure 2-3 shows a representative set of TEM images for Cu/CNT hybrid systems for four different functional groups. In Cu/MO-CNT system, Cu deposits randomly and scarcely cover the MO-CNTs surface. While some of the CNTs have no or only a small amount of Cu, some large deposits

can be observed specifically at the tube ends showing that seeding of Pd and subsequently deposition of Cu do not occur uniformly on all the CNTs.

This defect-dependence deposition has been previously reported in electroless deposition of Cu on graphene [28]. CNT ends and defects are proper sites for deposition of Cu. Due to the anisotropy of CNT system, carbon atoms at the tips are more reactive, can form strong covalent bonds and show stronger interactions with metals [29]. Moreover, CNT sidewalls are resistant to acid treatment so oxidation usually initiates at and mostly affects nanotube tips and defects [30]. As a result, oxidation in the mild acid treatment does not occur uniformly and the distance between proper nucleation centers may be too far from each other to form a continuous Cu layer.

The scattered deposits on the sidewalls have smaller size and are readily oxidized which impedes the autocatalytic growth of Cu. On the other hand, the already defective tube ends are mostly affected by acids and carboxyl groups are densely generated at these locations. This leads to formation of scattered Cu deposits on the MO-CNT sidewalls and big Cu aggregates at the tips. It should be noted that free Cu particles were observed in this sample (not shown here) possibly due to detachment of Pd particles from the surface during rinsing or detachment of Cu particles during sonication prior to TEM sample preparation. Due to high curvature, the surface energy of CNTs is high. Therefore, if a strong interaction between the CNT and the metallic particles does not exist, they will detach from the CNT side-wall. Therefore, MO-CNT fails to provide a proper substrate for nucleation and growth of Cu layer.

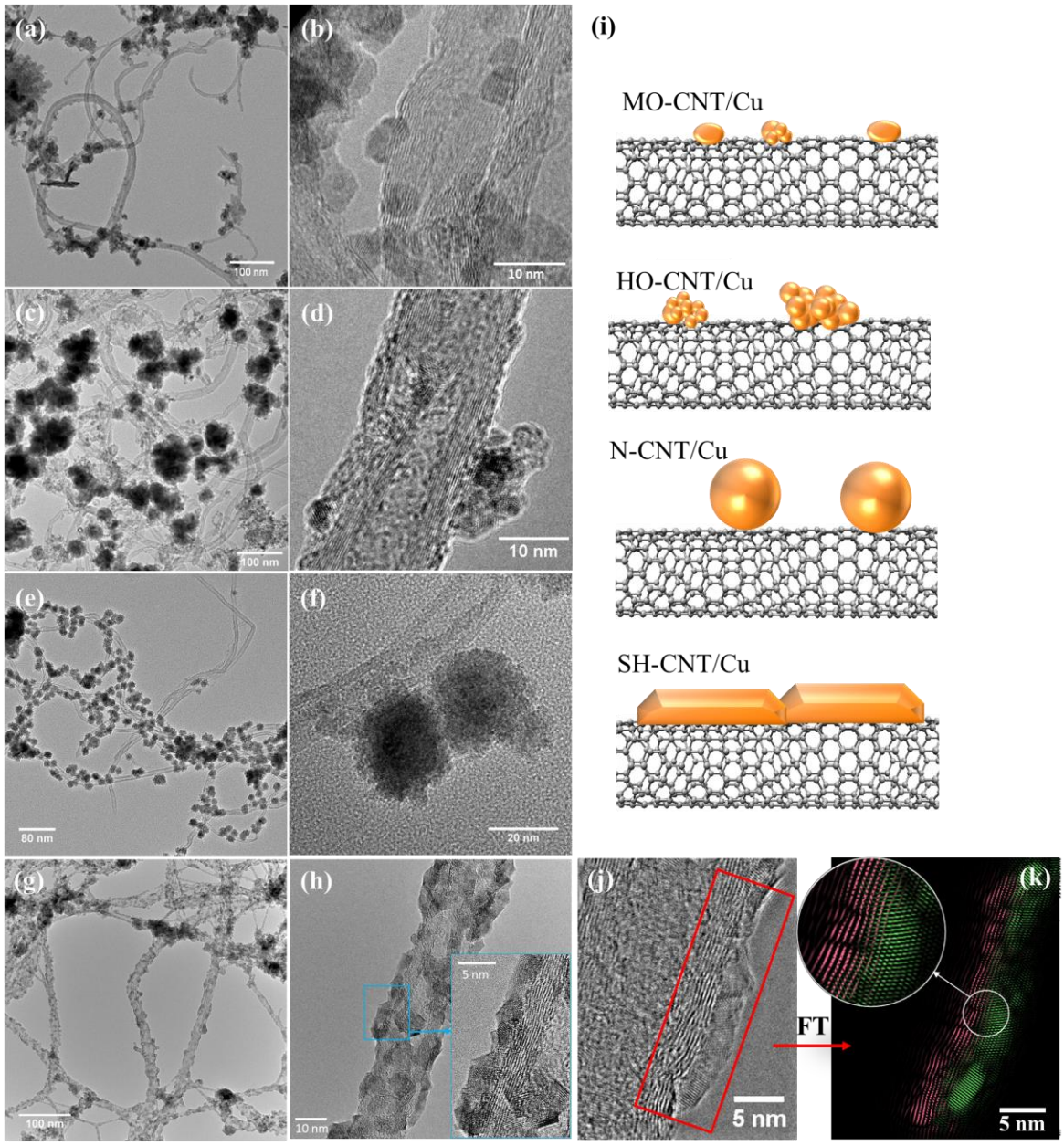

Figure 2-3. Morphology of the Cu deposits on the sidewalls of CNTs with different functional groups. Scattered Cu deposits with diameter ~4 nm formed on the surface of MO-CNTs (a-b). Big aggregates of Cu (~100 nm) are observed at the HO-CNT tube ends along with scattered deposits on the sidewalls (c-d). When the CNTs are doped with nitrogen Cu aggregation at the tube ends decreases and sphere shape deposits (~20 nm) are formed on the sidewalls while some of the N-CNTs are not coated at all (e-f). SH-CNT surface is wetted by Cu and all the SH-CNTs are uniformly coated with a thin layer of Cu (~4 nm) and negligible Cu aggregation is observed at tube ends (g-h). The effect of CNT's surface group on the morphology of the Cu deposits is schematically represented in (i). High resolution TEM of SH-CNT/Cu at the interface (j) and the corresponding processed image based on Fourier transformation (FT) shows how Cu deposits (green) are integrated in CNT (purple) (k).

By increasing the intensity of the acid treatment, more carboxyl groups are expected to from on the surface of CNTs which provides abundant proper locations for nucleation of Pd and Cu, and leads to a denser Cu coverage. However, this phenomenon is not observed in our work. By increasing the surface oxidation intensity, the density of the Cu deposits on the CNT sidewalls shows a slight enhancement while the size of the deposits shows a more vivid increase; specifically, large aggregates are formed at the tube ends. In addition to the deposit size, acid treatment intensity also affects the morphology of the deposits. As observed in high resolution TEM image of MO-CNT/Cu system (Figure 2-3b), the Cu deposits have a regular oval shape with diameter around 4 nm. However, in HO-CNT/Cu sample, the Cu deposits have irregular shapes and are generally larger. Based on shape irregularity and different fringe directions, it is speculated that they are formed by growth and aggregation of a few Cu nuclei. It should be noted that based on the zeta potential measurements, more aggressive acid treatment results in a more negative surface charge in HO-CNTs. By considering the XPS results, it can be deduced that larger and more abundant defect sites are formed on the HO-CNT surface. However, these sites are not uniformly distributed on the CNT surface and large Cu aggregates (that can reach to 100 nm in size) are formed at the tips of some of the CNTs. While these aggregates were also observed on MO-CNT, their size rarely exceeded 40 nm. Strong electrostatic forces at these locations attracts more Pd^{+2} and Cu^{2+} ions. Therefore, large spheres at the HO-CNT tube ends are the result of formation of functional groups, and subsequently larger catalytic particles that effectively initiates Cu deposition.

The deposits on the surface of the N-CNTs have a more uniform shape and morphology. TEM results show that most of the N-CNTs sphere metallic deposit with diameter around 20

nm (Figure 2-3 e and f). Similar to carboxyl group, N-doped CNTs contains atoms with lone electron pair which theoretically can bind with metal ions through sharing an electron pair [31]. Recently, by theoretical and experimental studies, Milowska et al. [23] showed that N-doping of CNTs would enhance the adhesion of sputtered Cu to CNTs and results in a composite with improved mechanical and electrical properties. However, N-doped CNTs are hydrophobic and show poor dispersion in water compared to MO-CNTs and HO-CNTs. This can impede interactions between Pd^{+2} and Cu^{2+} ions with N-doped CNTs in aqueous solutions. In addition, N-doped CNTs are protonated in water which shifts the pH at point of zero charge (pH_{zpc}) to higher values compared with MO-CNTs and HO-CNTs. This will cause a repulsive electrostatic force between divalent metal ions, such as Cu^{2+} and N-CNTs, and reduces the Cu adsorption on N-CNTs' surface. On the other hand, the N atoms are able to share their electrons with the Pd^{+2} and/or Cu^{2+} ions. The combination of repulsive forces between the hydrophobic inert CNT surface and the ions, and the attraction of metallic ions to the pyrodinic N can lead to the formation of spherical Cu structure with minimal contact to the CNT surface, as observed in Figure 2-3e and f.

The morphology of the SH-CNT/Cu hybrid system is represented in Figure 2-3g, h and j. The crystalline structure of SH-CNTs indicates that the CNT structure is preserved after surface treatment. In addition, the SH-CNTs are more uniformly coated and almost all of the CNTs are covered by Cu deposits. It is well-know that thiol has strong affinity for some metals and can bond with them through its sulfur group [32-34]. Moreover, as previous studies have shown when CNTs are thiol activated, the noble metal particles are not agglomerated but uniformly attached to CNT sidewall surface [32, 33]. As a result, it can be deduced that Pd has been seeded

uniformly on SH-CNT surface. Cu nucleation is initiated from these seeds and then grow and form Cu clusters, forming a uniform coating on SH-CNT surface. By investigating at the Cu deposits morphology at higher magnifications, another interesting difference against other treatment conditions becomes apparent. Unlike the MO-CNT/Cu and HO-CNT/Cu samples, the Cu particles on SH-CNT are not spherical but have elongated trapezium shape, showing a better wetting toward the SH-CNT surface, suggesting that there is a stronger interaction between Cu and SH-CNT (Figure 2-3j). As a result, CNT surface functionality strongly influences not only the Cu coverage but also their shape.

STEM images and nanoscale elemental maps of the electroless deposited CNTs are presented in Figure 2-4. For each sample several locations were investigated. In all cases, Cu was the main constituent of the deposits along with oxygen and in tin. Also, in almost all the cases, Pd was not detected showing its content is below the detection limits of the equipment. The only exception was the HO-CNT/Cu sample in which Pd was detected in specific areas. As it was discussed before, this sample contains relatively large Cu particles which can be formed due to accumulation of catalytic seeds. Pd was only detected around the large aggregates showing that indeed they are formed due to densely packed catalyst particles at HO-CNT defect sites.

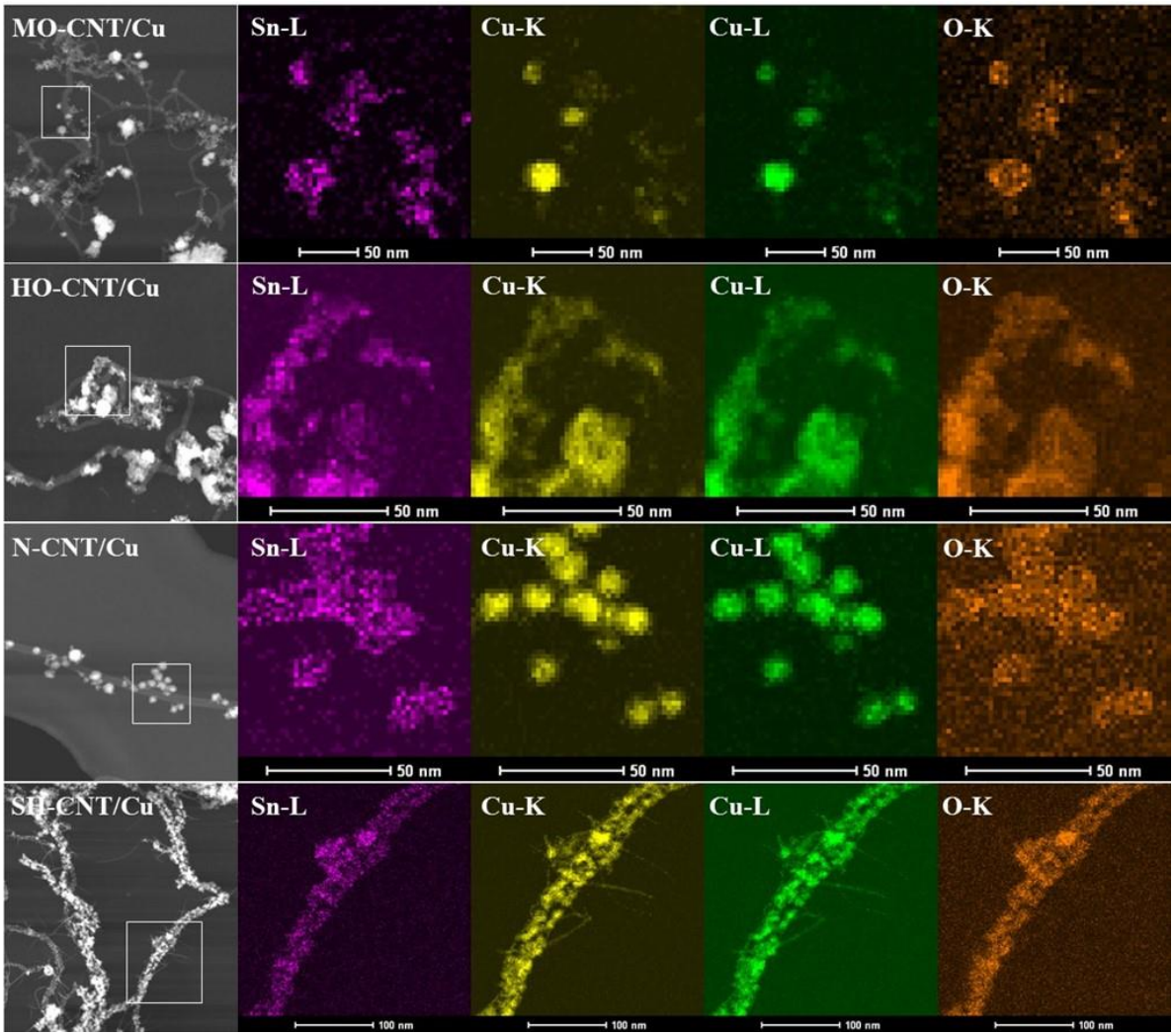

Figure 2-4. STEM and EDS maps of hybrid systems. Cu, O and Sn are the main constituents of the coatings. No Pd was detected. Large clusters of Cu can be observed in MO-CNT/Cu and HO-CNT/Cu systems specifically at the CNT ends. In N-CNT/Cu system uniform Cu spheres are formed on the CNT surface. Thiol-activation will result in a uniform coating of Cu on the surface SH-CNTs. It seems a thin layer of tin is still present on the surface of the f-CNTs.

XPS was used to analyze the surface chemistry of functionalized CNTs and hybrid systems. After Cu deposition, all the hybrid systems contain Cu, O, C, and to a lesser extent Sn and Pd (Figure 2-5). Peaks at binding energies of 335, 486.6 and 932.5 eV are associated with Pd 3d, Sn 3d and Cu 2p respectively. C 1s and O 1s peaks are located at 284.5 and 530 eV, respectively. Except for Cu 2p, the rest of the metallic peaks have similarly symmetric shape

independent of the CNT surface functional groups. Hence, they will not be discussed further. More details about Pd 3d and Sn 3d peaks were presented in our previous work [19].

Figure 2-5a shows the the normalized high resolution XPS spectra of Cu 2p of CNT/Cu systems. Two characteristic peaks of Cu 2p can be observed for all the systems. One is the Cu $2p_{3/2}$ at around 932.5 eV and the other is located at binding energy of 951.6 eV, which represents the Cu $2p_{1/2}$ component. Cu^{2+}, and specifically Cu^{+} and metallic Cu main peaks are located very closely to each other. However, CuO presence can be identified by the strong satellite peaks at 961.8 and 941.6 eV, which can be attributed to metallic Cu or Cu_2O [35-38]. Compared with other systems, MO-CNT/Cu system contains significantly stronger satellite peaks which indicates that a significant amount of CuO is present in this sample. Accordingly, less pronounced satellite peaks are detected for HO-CNT/Cu and SH-CNT/Cu systems while they are not observed for N-CNT/Cu sample. Although during electroless deposition process, reducing and complexing agents were used, due to the small size of the particles, detection of metallic oxide is not surprising. It has previously been shown that CNTs inclusion into metallic systems can result in structure refinement [1, 13, 14]. Consequently, high surface area of these nanoparticles makes them more susceptible to oxidation [39-41]. In addition to the composition, oxidation also affects the coating morphology. CuO nanoparticles are inert and can hinder autocatalytic reduction of Cu. Therefore, it is rational to assume that Cu on MO-CNT system is readily oxidized after reduction by formaldehyde which hampers the autocatalytic reduction and leads to discrete and small deposits of CuO on CNTs. On the other hand, at CNT ends where functionalization is more intense, larger Cu deposits are formed. In other words, in these areas, stronger interaction between the CNT and metallic particles exist. Hence, bigger and

more stable catalytic sites are formed which are more resistant to oxidation. As a result, nucleation and growth becomes quicker at the CNT tube ends or other defect sites on the surface [1, 42].

The role of CNT surface chemistry on the morphology of the deposits can also be explained based on thin film growth mechanisms. During electroless deposition, Cu ions have some degree of mobility on the surface of CNTs. These ions travel on the surface until they are trapped at either the surface defects to form a new nucleus, or meet and join an existing Cu island. The coverage or uniformity of the coating is directly proportional to the diffusion rate of Cu ions on CNT surface. In other words, a more uniform coating can be achieved if the mobility of Cu ions on CNT surface is enhanced. Respectively, it is postulated that in N-CNT system, the Cu mobility on the surface of CNT is hampered. As a result, lateral growth does not occur. Also, due to poor wettability of N-CNT surface, the Cu nucleus formed at the nitrogen defect grows spherically to minimize its contact and interface energy with the CNT. On the other hand, for the SH-CNT sample, the surface diffusion of ions is facilitated which leads to lateral growth of Cu deposits in a Volmer-Weber mode. This lateral growth continues until Cu islands meet each other and coalesce [43].

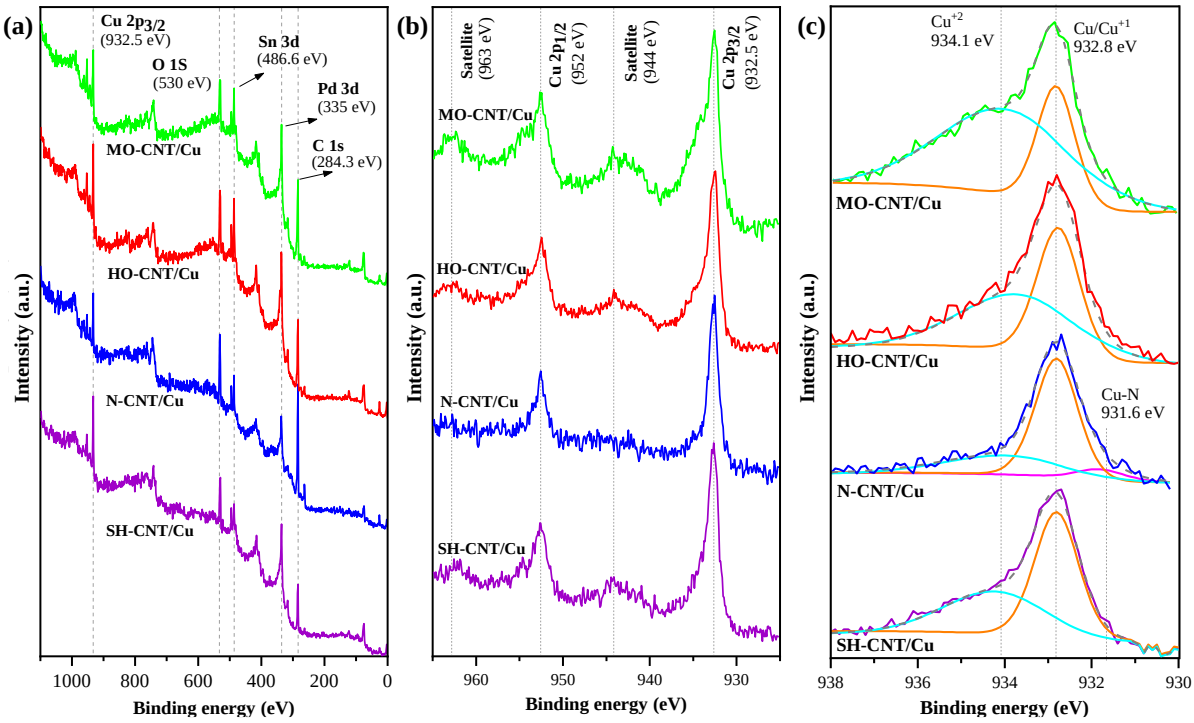

Figure 2-5. Wide scan spectra of hybrid systems showing that Cu, O, Pd and Sn are present in the coating (a). High resolution Cu 2p can be used to determine the state of the copper (b). Deconvoluted Cu $2p_{3/2}$ peaks shows that the MO-CNT/Cu system has the highest amount of CuO while N-CNT/Cu system has the lowest amount of CuO (c).

Compared to MO-CNT sample, weaker Cu satellite peaks are detected for HO-CNT/Cu and SH-CNT/Cu samples showing that the CuO formation is limited. For more details, the Cu $2p_{3/2}$ peak at 932.5 eV was resolved and the result is presented in Figure 2-5b. By resolving this peak, two deconvoluted peaks appear, one at binding energy of around 932.4 eV, which is attributed to Cu^{+} (i.e., Cu_2O), and the other at slightly higher binding energies which is attributed to Cu^{2+} (i.e., CuO). It should be noted that it has been reported that formation of a Cu_2O thin layer on the surface is inevitable [44, 45]. It should be noted that since metallic Cu peak is located almost at the same binding energy as that of Cu^{+}, it is assumed that the peak at lower binding energies is the result of both Cu and Cu^{+} components.

The molar ratio of Cu/Cu_2O and CuO are calculated based on the integrated peak area of their deconvoluted Cu $2p_{3/2}$ peaks [35]. Accordingly, there is 51 at%, 23.8 at% and 15.8 at% CuO in MO-CNT/Cu, HO-CNT/Cu, SH-CNT/Cu systems, respectively. Consequently, compared with other samples, the Cu in MO-CNT/Cu tends to be in higher oxidation states and more CuO is formed. This is attributed to the discrete deposits of finer particle size, which facilitates reaction with electrophilic neighboring protons (H^+) and oxidation [46]. On the other hand, in thiol treated and harshly oxidized samples, not only particle size is larger but also proper nucleation sites are more abundant and closer to each other, which leads to formation of a continuous Cu layer. This will reduce the surface area and preserves the deposits from oxidation. Note that based on the previous studies, we speculate that thiol may also be able to stabilize the Cu deposits. Thiol has strong interactions with metallic particles due to free electron pair which forms donor centers. These donor centers are readily polarized and can form strong interaction with Cu ions [47]. Rigo et al. [48] studied the interactions between Cu and thiol using electron spin resonance (ESR), nuclear magnetic resonance (NMR). They found that thiol groups such as cysteine are able to reduce Cu^{+2} to Cu^+ probably via free radical mechanism. In addition, it has been reported that thiol has anti-oxidation effect on Cu nanoparticles [49] and can protect Au nanoparticle against chemical attacks [50]. All of these previous reports point out that thiol have strong interaction with metallic nanoparticles and is able to stabilize and protect them against oxidation.

In the N-CNT/Cu system, no satellite peak is observed, suggesting there is negligible amount of CuO in this hybrid system. As observed in Figure 2-3e and f, large spherical Cu particles are formed on N-CNTs with comparatively high volume to surface ratio. A thin oxide

layer is formed on the surface of the particle, protecting Cu at the core of the sphere from oxidation. As a result, they are mostly composed of Cu or Cu^{+}.

The peak shift concept in XPS can be considered to obtain a better understanding of the interactions between the Cu and functionalized CNTs. If there is a Cu peak shift towards higher binding energies, it means electron clouds are migrated to the atoms with higher electronegativities, i.e., O, C, N, or S. Also, the magnitude of the shift indicates stronger interaction [46, 51]. For example, in CuO, the Cu peak will shift to a higher binding energy because it shares some electrons with oxygen or when Cu bonds with sulfur. Consequently, in N-CNT/Cu sample, the Cu $2p_{3/2}$ peak resides at 933.1 eV, which is very close to the Cu binding energy reported in the literature (933 eV) [35-38], suggesting that the Cu particles in this sample do not have much interaction with the N-CNT or oxygen. Moreover, the O 1s resolved peaks show that Cu deposition does not have any effect on the relative intensity of the C-O/COOH and C=O bonds. This also applies for SH-CNT system. On the other hand, in MO-CNT and HO-CNT systems, after Cu deposition, the concentration of C-O/COOH bonds decreases significantly. This can be due to the fact that in MO-CNT and HO-CNT samples, Cu deposits are mostly interacting with C-O/C-OOH, whereas in SH-CNT and N-CNT systems the N and thiol groups bond with Cu. It is worth noting that the N 1s peak analysis can give a better understanding of the interactions between Cu and N-CNT. However, this peak was not detected after Cu deposition because of the N low weight ratio and being covered by large Cu spheres. On the other hand, the Cu $2p_{3/2}$ peak for other samples similarly show a shift towards a higher binding energy of around 933.5 eV. Since each sample has a different fraction of copper oxides, it is deduced that this shift has a different source in each sample. The shift for MO-CNT/Cu is

attributed to comparatively higher CuO content while in SH-CNT/Cu sample, the shift is mostly caused by strong interactions between copper and sulfur of thiol functional group. For further evidence, the $S2p_{3/2}$ peak at binding energy of around 164 eV needs to be studied. However, this peak disappeared in the SH-CNT hybrid system due to its low content and being covered by the metallic particles.

To confirm the crystalline properties of the nanocrystals, the as-synthesized hybrid systems were examined using XRD. As presented in Figure 2-6, the nanoparticles display high crystallinity. Due to low content, Sn and Pd peaks are not detected. The detected peaks belong mostly to a lower oxidized state of Cu, i.e., Cu_2O and metallic Cu. In carboxyl-treated systems, i.e., MO-CNT/Cu and HO-CNT/Cu, diffraction peaks at 2θ of 36.5°, 42.5°, 61.6°, and 73.4° are present which can be indexed as the (111), (200), (220), and (311) planes of Cu_2O, respectively (JCPDS card no. 01-080-3714). In addition, the XRD patterns of N-CNT/Cu and SH-CNT/Cu systems show peaks at (200) peaks at 43.2°, 50.4° and 74.1° which can be identified as (111), (200), and (220) planes of metallic copper (JCPDS card no. 01-071-3761). Due to relatively low content of CNT, only a weak peak of (200) graphite is detected at 2θ of 26° (JCPDS card no. 01-071-3739). Differentiation of (111) and (220) peaks of Cu from (200) and (311) peaks of Cu_2O is challenging since they are situated very close to each other (compare 43.2° and 74.1° for Cu to 42.5° and 73.4° for Cu_2O). Here, these peaks are located at slightly lower degrees for carboxyl-activated samples. Therefore, they are attributed to Cu_2O. Also, the metallic copper (200) peak at 50.4° only appears for SH-CNT/Cu and N-CNT/Cu samples. As shown, the strong Cu_2O peak at 2θ of 36.5° is common in all samples along with a weak (220) peak of Cu_2O at 61.6°. However, the intensity of these common peaks is relatively lower in amine and thiol

treated samples. These results confirm the XPS analyses, indicating that Cu is present mainly in oxide state in MO-CNT/Cu and HO-CNT/Cu samples while there is metallic copper along with Cu_2O in SH-CNT/Cu and N-CNT/Cu. The presence of metallic copper in amine-treated sample is expected since most of the reduced copper are large particles formed in the solution which are not as easily oxidized. In other words, in amine-treated sample, unlike the thiol-activated one, formation of metallic copper is not related to the CNT interface but is a result of larger Cu particle size and lower surface area. Finally, in all samples, the [111] faces are the dominant crystal orientation regardless of the oxidation state of deposits. This is due to the fact that growth direction strongly depends on parameters such as complexing agent and pH which is similar in all samples [39, 52]. It is worth mentioning that the direction of growth for Cu-based nanoparticles becomes important in catalysis applications since some of the planes have higher reactivity [41].

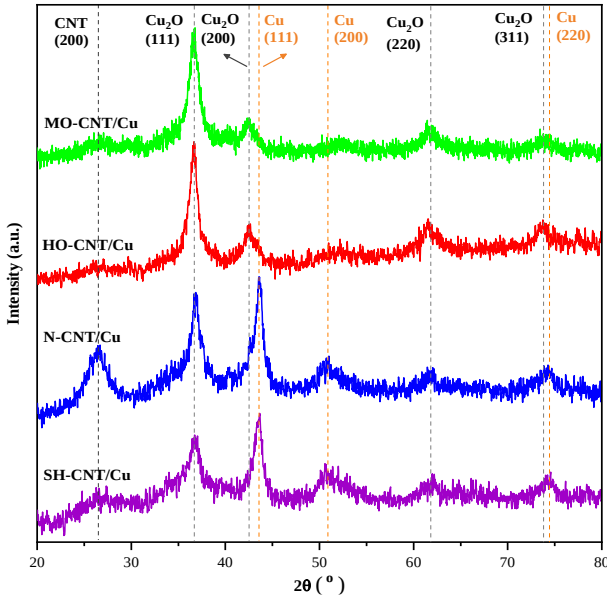

Figure 2-6. XRD patterns of hybrid systems. These results show that N-CNT/Cu and SH-CNT/Cu systems mostly contain metallic copper while the MO-CNT/Cu system contain significant amounts of CuO. Sn or Pd are not detected.

2.3.3. Electrical conductivity

The thin films with different CNT surface functional groups have a similar weight of around 300 mg after Cu electroless deposition, suggesting they have equal amount of copper. This means each thin film contains around 16 wt% (45 vol%) of f-CNTs and the composite thin film has a theoretical density of 5.8 g/cm^3. Consequently, it can be deduced that any difference in the electrical conductivity is the results of the interaction between Cu and CNTs containing different surface functional group types. The electrical conductivity measurement results are presented in Table 2-2. The SH-CNT/Cu film has the highest conductivity of 0.82 MS/m, which is more than seven times higher than that of the N-CNT/Cu sample. The conductivity of samples containing carboxyl-activated CNTs, i.e., MO-CNT/Cu and HO-CNT/Cu, are similar at around 0.20 MS/m.

Indeed, the thiol groups show the highest affinity towards copper. TEM results show that all the SH-CNTs are coated and copper is able to effectively wet SH-CNT surfaces. Also, based on XPS results, copper deposits have the strongest interaction with SH-CNT and are better preserved against oxidation. As a result, these thiol functionalized sites act as preferred sites for deposition of copper and promote uniform deposition of Cu (Figure 2-7). This leads to higher conductivity of SH-CNT/Cu system compared with other systems. Compared with MO-CNTs, HO-CNTs show better affinity towards Cu. However, their composite film shows a slightly lower conductivity. XPS results show that, as a result of the harsh acid treatment, the defects population increases significantly. These defects, specifically oxygen in carboxyl groups, can scatter the electrons and impair ballistic conductance of CNTs [53]. More importantly, harsh

acid treatment can shorten the length of CNTs which can reduce the conductivity as a result of increase junctions of CNTs and the matrix [54].

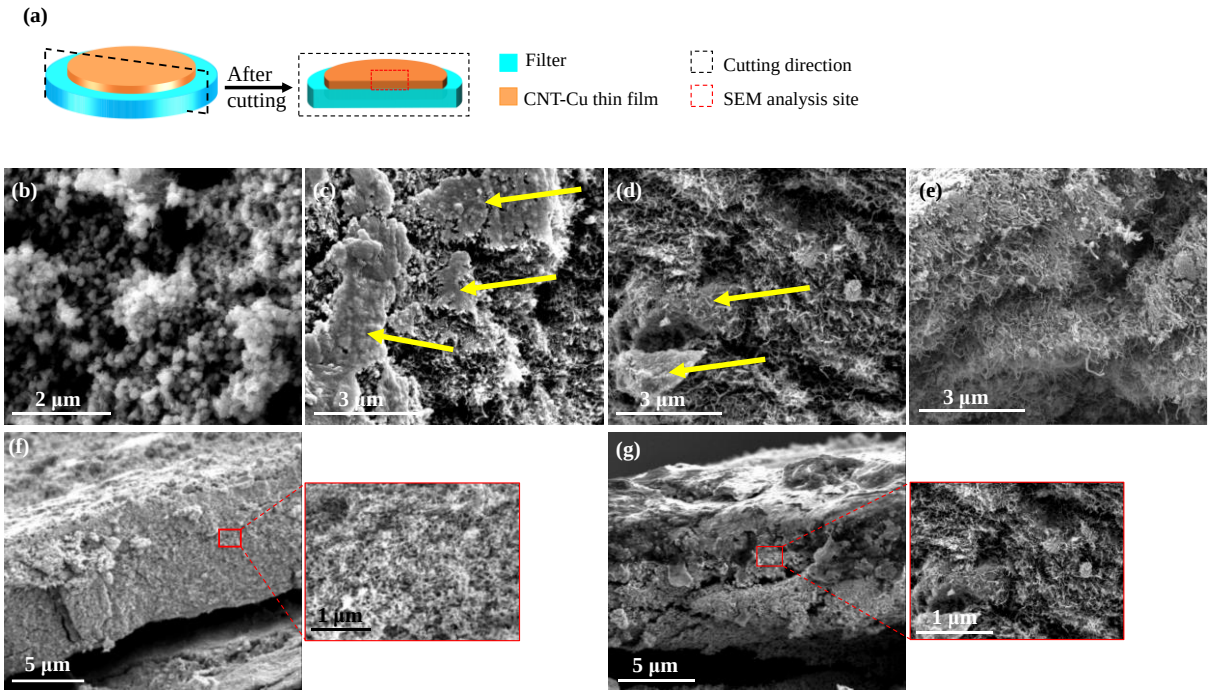

Figure 2-7. The schematic shows the location of SEM analysis on thin films (a). The thin films were cut at the center using a fresh razor. The razors and the thin films were immersed in liquid nitrogen for one minute before cutting. The SEM images of the thin films cross section before and after the reduction heat treatment are presented in figures b to g. Before heat treatment, Cu has spherical shape on N-CNT thin film (b). After the heat treatment, the Cu deposits for N-CNT/Cu and oxidized-CNT/Cu thin film form non-uniform patches indicated by yellow arrows (c and d, respectively). For SH-CNT thin film (e), Cu was more uniformly dispersed and did not form large islands. After the compaction step, the density of the thin films for SH-CNT/Cu (f) and to a lesser extent for N-CNT/Cu (g) increased. The oxidized-CNT/Cu thin films had a similar structure to Figure g.

The N-CNT/Cu system shows the lowest conductivity. Although it has been reported that N-doping will cause the least disturbance in the pure sp^2 structure of CNT and can even enhance the conductivity of Cu/CNT systems [23], N-CNTs are not seeded effectively and show the lowest affinity towards copper, hence resulting in the lowest electrical conductivity due to hydrophobicity and stereo-hindrance effect. Examining the cross section of the thin films

reveals that the N-CNT/Cu thin films were not as compact as other systems and Cu deposits formed discrete patches (Figure 2-7 c and g); while for SH-CNT/Cu system, Cu was more uniformly distributed within the thin film (Figure 2-7 e and f).

The above findings show that functional groups on the surface of CNTs have a great effect on the morphology, composition and final properties of CNT-Cu composites. It should be noted that length and quality of CNTs can significantly affect the final properties of the composite. In this work we used commercially available CNTs but it is speculated that by using longer CNTs, higher conductivities can be achieved. By understanding the effect of CNT surface functionalization on the deposited Cu morphology and composition, we can design new hybrid systems for specific application needs. For example, thiol activation can remarkably enhance the wettability of CNT surface towards Cu and improve the electrical conductivity of CNT/Cu system. As a result, portable and flexible electronics, and nanocomposites for structural applications can benefit from the uniform coating of Cu on SH-CNTs. On the other hand, in application where surface area and reactivity are important, such as catalysis and energy storage, carboxylated and N-doped CNTs can perform better. Also, the above findings are not limited to CNT/Cu systems and can be applied to other carbon nanostructures metals.

Table 2-2. Electrical properties of thin films made of pristine CNTs and different CNT/Cu systems.

Sample	**Electrical conductivity (S/m)**	**Specific conductivity (Sm^2/Kg)***
P-CNTs	3×10^3 (± 760)	0.33
MO-CNT/Cu	1.9×10^5 (± 2000)	32.76
HO-CNT/Cu	2.0×10^5 (± 2100)	34.48
N-CNT/Cu	9.8×10^4 (± 1860)	16.90
SH-CNT/Cu	8.2×10^5 (± 1530)	141.38

* Specific conductivity numbers are based on theoretical densities.

2.4. Conclusion

CNTs were functionalized by N-doping, carboxyl (7 at% and 12 at%, respectively) and thiol groups. They were subsequently coated with copper via electroless deposition approach. The interaction between CNT functionalized with the above four different surface functional groups and copper were examined. By utilizing HRTEM, STEM, EDX, XPS, and XRD, the effect of CNT surface functional groups on the interaction, morphology and composition of copper deposits were studied in detail. The nanoscale analyses have revealed how the CNTs surface functional groups interact with Cu to form different morphologies and chemical states. Moreover, the effect of CNT surface functionality on the electrical conductivity of CNT/Cu films produced by vacuum filtration was analyzed by using four-point electrical conductivity measurements, indicating that the thiol group can enhance the wettability of the CNTs towards copper deposition. Thiol has lone pairs of electrons and can be deprotonated, resulting in formation of a strong bond with palladium and subsequently copper. Uniformly adsorbed palladium particles on CNT acts as nucleation sites for copper. These nuclei that are located in a proximity of each other, resulting in a dense and uniform coating on SH-CNT surface. This dense coating helps protect against oxidation. On the other hand, the carboxyl treated CNTs do not have the same affinity towards metal ions. The wettability is low and copper will form as discrete and small spheres on the MO-CNT and HO-CNT surfaces which are prone to oxidation due to their higher surface energy state. Moreover, on N-CNTs, spherical Cu particles with diameter around 20 nm are formed that have minimal contact with the CNT surface. Thus, copper coating on N-CNTs cannot be effectively achieved mainly due to their hydrophobicity and low wettability. Accordingly, thin films made of SH-CNT/Cu system in which copper is

seeded uniformly shows the highest electrical conductivity, which is four times higher than composites containing carboxylated CNTs and seven times higher than N-doped CNTs.

2.5. References

1. Eder, D., *Carbon nanotube− inorganic hybrids.* Chemical reviews, 2010. **110**(3): p. 1348-1385.

2. Poncharal, P., et al., *Room temperature ballistic conduction in carbon nanotubes*. 2002, ACS Publications.

3. Behabtu, N., et al., *Strong, light, multifunctional fibers of carbon nanotubes with ultrahigh conductivity.* science, 2013. **339**(6116): p. 182-186.

4. Lekawa-Raus, A., et al., *Electrical properties of carbon nanotube based fibers and their future use in electrical wiring.* Advanced Functional Materials, 2014. **24**(24): p. 3661-3682.

5. Zhang, S., et al., *Carbon-Nanotube-Based Electrical Conductors: Fabrication, Optimization, and Applications.* Advanced Electronic Materials, 2019: p. 1800811.

6. Zhang, S., et al., *Ultra-high conductivity and metallic conduction mechanism of scale-up continuous carbon nanotube sheets by mechanical stretching and stable chemical doping.* Carbon, 2017. **125**: p. 649-658.

7. Hjortstam, O., et al., *Can we achieve ultra-low resistivity in carbon nanotube-based metal composites?* Applied Physics A, 2004. **78**(8): p. 1175-1179.

8. Subramaniam, C., et al., *One hundred fold increase in current carrying capacity in a carbon nanotube–copper composite.* Nature communications, 2013. **4**: p. 2202.

9. Kim, J.A., et al., *Effects of surface modification on rheological and mechanical properties of CNT/epoxy composites.* Carbon, 2006. **44**(10): p. 1898-1905.

10. Ma, P.-C., et al., *Dispersion and functionalization of carbon nanotubes for polymer-based nanocomposites: a review.* Composites Part A: Applied Science and Manufacturing, 2010. **41**(10): p. 1345-1367.

11. Yang, S.-Y., et al., *Effect of functionalized carbon nanotubes on the thermal conductivity of epoxy composites.* Carbon, 2010. **48**(3): p. 592-603.

12. Sahoo, N.G., et al., *Polymer nanocomposites based on functionalized carbon nanotubes.* Progress in polymer science, 2010. **35**(7): p. 837-867.

13. Daneshvar-Fatah, F. and F. Nasirpouri, *A study on electrodeposition of Ni-noncovalnetly treated carbon nanotubes nanocomposite coatings with desirable mechanical and anti-corrosion properties.* Surface and Coatings Technology, 2014. **248**: p. 63-73.

14. Nasirpouri, F., et al., *Magnetic Properties of Electrodeposited Nickel-Multiwall Carbon Nanotube Composite Films.* IEEE Transactions on Magnetics, 2015. **51**(11): p. 1-4.

15. Cha, S.I., et al., *Extraordinary strengthening effect of carbon nanotubes in metal-matrix nanocomposites processed by molecular-level mixing.* Advanced Materials, 2005. **17**(11): p. 1377-1381.

16. Wildgoose, G.G., C.E. Banks, and R.G. Compton, *Metal nanoparticles and related materials supported on carbon nanotubes: methods and applications.* Small, 2006. **2**(2): p. 182-193.

17. Bakshi, S.R., D. Lahiri, and A. Agarwal, *Carbon nanotube reinforced metal matrix composites-a review.* International Materials Reviews, 2010. **55**(1): p. 41-64.

18. Nai, M.H., J. Wei, and M. Gupta, *Interface tailoring to enhance mechanical properties of carbon nanotube reinforced magnesium composites.* Materials & Design, 2014. **60**: p. 490-495.

19. Daneshvar, F., et al., *Porous SnO_2–Cu_xO nanocomposite thin film on carbon nanotubes as electrodes for high performance supercapacitors.* Nanotechnology, 2018. **30**(1): p. 015401.

20. Wu, B., et al., *Noble metal nanoparticles/carbon nanotubes nanohybrids: synthesis and applications.* Nano Today, 2011. **6**(1): p. 75-90.

21. Ilari, G.M., et al., *Carbon–metal interfaces analyzed by aberration-corrected TEM: How copper and nickel nanoparticles interact with MWCNTs.* Micron, 2015. **72**: p. 52-58.

22. Xue, Y., et al., *Quantifying thiol–gold interactions towards the efficient strength control.* Nature communications, 2014. **5**: p. 4348.

23. Milowska, K.Z., et al., *Carbon nanotube functionalization as a route to enhancing the electrical and mechanical properties of Cu–CNT composites.* Nanoscale, 2019. **11**(1): p. 145-157.

24. Oluwalowo, A., et al., *Electrical and thermal conductivity improvement of carbon nanotube and silver composites.* Carbon, 2019. **146**: p. 224-231.

25. Singh, B., et al., *Pt based nanocomposites (mono/bi/tri-metallic) decorated using different carbon supports for methanol electro-oxidation in acidic and basic media.* Nanoscale, 2011. **3**(8): p. 3334-3349.

26. Sharifi, T., et al., *Nitrogen doped multi walled carbon nanotubes produced by CVD-correlating XPS and Raman spectroscopy for the study of nitrogen inclusion.* Carbon, 2012. **50**(10): p. 3535-3541.

27. Van Tam, T., S.H. Hong, and W.M. Choi, *Facile synthesis of cysteine–functionalized graphene quantum dots for a fluorescence probe for mercury ions.* RSC Advances, 2015. **5**(118): p. 97598-97603.

28. Bosch-Navarro, C., J.P. Rourke, and N.R. Wilson, *Controlled electrochemical and electroless deposition of noble metal nanoparticles on graphene.* RSC Advances, 2016. **6**(77): p. 73790-73796.

29. Banhart, F., *Interactions between metals and carbon nanotubes: at the interface between old and new materials.* Nanoscale, 2009. **1**(2): p. 201-213.

30. Datsyuk, V., et al., *Chemical oxidation of multiwalled carbon nanotubes.* Carbon, 2008. **46**(6): p. 833-840.

31. Czerw, R., et al., *Identification of electron donor states in N-doped carbon nanotubes.* Nano Letters, 2001. **1**(9): p. 457-460.

32. Showkat, A.M., et al., *Dispersion of gold nanoparticles into thiol-functionalized carbon nanotubes by γ-radiation.* Diamond and related materials, 2007. **16**(8): p. 1688-1692.

33. Kim, Y.-T. and T. Mitani, *Surface thiolation of carbon nanotubes as supports: A promising route for the high dispersion of Pt nanoparticles for electrocatalysts.* Journal of catalysis, 2006. **238**(2): p. 394-401.

34. Pakiari, A. and Z. Jamshidi, *Nature and strength of M− S Bonds (M= Au, Ag, and Cu) in binary alloy gold clusters.* The Journal of Physical Chemistry A, 2010. **114**(34): p. 9212-9221.

35. Wan, Y., et al., *Electrochemical formation and reduction of copper oxide nanostructures in alkaline media.* Electrochemistry Communications, 2013. **36**: p. 99-102.

36. Biesinger, M.C., et al., *Resolving surface chemical states in XPS analysis of first row transition metals, oxides and hydroxides: Sc, Ti, V, Cu and Zn.* Applied Surface Science, 2010. **257**(3): p. 887-898.

37. Poulston, S., et al., *Surface oxidation and reduction of CuO and Cu2O studied using XPS and XAES.* Surface and Interface Analysis: An International Journal devoted to the development and application of techniques for the analysis of surfaces, interfaces and thin films, 1996. **24**(12): p. 811-820.

38. Svintsitskiy, D.A., et al., *In situ XRD, XPS, TEM, and TPR study of highly active in CO oxidation CuO nanopowders.* The Journal of Physical Chemistry C, 2013. **117**(28): p. 14588-14599.

39. Mott, D., et al., *Synthesis of size-controlled and shaped copper nanoparticles.* Langmuir, 2007. **23**(10): p. 5740-5745.

40. Kawasaki, H., et al., *Microwave-assisted polyol synthesis of copper nanocrystals without using additional protective agents.* Chemical Communications, 2011. **47**(27): p. 7740-7742.

41. Gawande, M.B., et al., *Cu and Cu-based nanoparticles: synthesis and applications in catalysis.* Chemical reviews, 2016. **116**(6): p. 3722-3811.

42. Fan, Y., B.R. Goldsmith, and P.G. Collins, *Identifying and counting point defects in carbon nanotubes.* Nature materials, 2005. **4**(12): p. 906.

43. Nasirpouri, F., *Electrodeposition of nanostructured materials*. 2017: Springer, p. 90-91.

44. Saikova, S., et al., *Conditions for the formation of copper nanoparticles by reduction of copper (II) ions with hydrazine hydrate solutions.* Russian Journal of General Chemistry, 2010. **80**(6): p. 1122-1127.

45. Lin, Y.-M. and S.-C. Yen, *Effects of additives and chelating agents on electroless copper plating.* Applied surface science, 2001. **178**(1-4): p. 116-126.

46. Kim, J.Y., et al., *Preparation, characterization and catalytic properties of Pd-decorated carbon nanotubes possessing different linkers.* Journal of Materials Chemistry, 2011. **21**(16): p. 5999-6005.

47. Zhang, C., et al., *Efficient removal of heavy metal ions by thiol-functionalized superparamagnetic carbon nanotubes.* Chemical Engineering Journal, 2012. **210**: p. 45-52.

48. Rigo, A., et al., *Interaction of copper with cysteine: stability of cuprous complexes and catalytic role of cupric ions in anaerobic thiol oxidation.* Journal of inorganic biochemistry, 2004. **98**(9): p. 1495-1501.

49. Ghelichkhah, Z., et al., *L-cysteine/polydopamine nanoparticle-coatings for copper corrosion protection.* Corrosion Science, 2015. **91**: p. 129-139.

50. Kang, J.S. and T.A. Taton, *Oligothiol graft-copolymer coatings stabilize gold nanoparticles against harsh experimental conditions.* Langmuir, 2012. **28**(49): p. 16751-16760.

51. Zhang, H. and H. Cui, *Synthesis and characterization of functionalized ionic liquid-stabilized metal (gold and platinum) nanoparticles and metal nanoparticle/carbon nanotube hybrids.* Langmuir, 2009. **25**(5): p. 2604-2612.

52. Susman, M.D., et al., *Chemical deposition of Cu_2O nanocrystals with precise morphology control.* ACS nano, 2014. **8**(1): p. 162-174.

53. Bockrath, M., et al., *Resonant electron scattering by defects in single-walled carbon nanotubes.* Science, 2001. **291**(5502): p. 283-285.

54. Yan, K., et al., *The interface effect of the effective electrical conductivity of carbon nanotube composites*. Nanotechnology, 2007. 18(25): p. 255705.

3. CARBON NANOTUBE/COPPER CORE-SHELL FIBERS FOR SUBSEA APPLICATIONS

3.1. Introduction

There is an increasing demand to reduce the size and weight of the conductors, from consumer electronics to power transmission. For example, with the development of renewable energies, subsea power transmission cables are becoming more important in integrating with smart grids. In this rapidly growing industry [1], cables are mainly made of copper, which has high density, or aluminum alloys which are not as conductive. Recent advances in nanotechnology have led to development of new materials better performance than copper and aluminum alloys in terms of electrical conductivity, weight and ampacity [2-8]. Carbon nanotube (CNT) is considered to be an excellent alternative due to their remarkable electrical and thermal conductivity, ampacity, electrochemical stability, low density, and excellent mechanical properties [9-13]. Continuous CNT fibers have been fabricated with remarkable tensile strength of 800 to 1230 MPa, but their one order of magnitude lower electrical conductivity remains to be a major concern [6-8]. Therefore, there has been a great interest to improve the electrical performance of these fibers by metallization [4, 5, 14-18]. Subramaniam et al. [4] combined several fabrication approaches to produce high density CNT (45 vol%)-Cu composite films with specific conductivity 26% greater than copper. Similarly, Leggiero et al. [17] used a chemical vapor deposition method to seed Cu on CNT roving. After plating and densification, a dense and uniform CNT hybrid conductor with 94.2% w/w Cu was obtained that has an electric conductivity of 2.81 × 10 7 S/m, which is five times higher than the samples

that were not seeded. The key issue in these studies was introducing Cu seeds to the CNT surface prior to plating to promote formation of uniform Cu deposits with strong adhesion on CNT. Although their fabrication procedures are not easily scalable, their results show that by promoting uniform Cu deposition on CNT with enhanced interfacial interactions, highly conductive nanocomposites can be made.

A scalable alternative approach is to coat the spun fibers with a metal like Cu and form a core-shell structure. Wet spinning followed by electrodeposition [19-25] or physical vapor deposition (PVD) [26-28] methods have been implemented to fabricate Cu/CNT core-shell fibers. Promising results have been reported including electrical conductivity as high as 2.6 × 107 S/m and tensile strength of 1.01 GPa after densification via rolling [27]. One of the main reasons that hinders achieving superior properties is the poor interaction of CNT with Cu [29, 30]. A successful solution to tackle this issue is to design the interface between the CNT core and the Cu shell. In addition to pre-seeding that was discussed above, creating an intermediate layer between the CNT and Cu [20, 28] or modifying the surface chemistry of CNT fibers [19, 26] have been shown to be effective strategies. For example, Zou et al. [20] electroplated a thin layer of Ni in between Cu and CNT, leading to more than two folds of improvement in electrical conductivity and tensile strength.

In this research, through tuning the CNT surface chemistry we have developed a scalable method to fabricate high performance Cu/CNT core-shell fibers via a modified electroless deposition. Compared with electroplating, this process yields dense and uniform coatings and is suitable for irregular and inaccessible surfaces [31]. Conventionally, this process starts with immersing the substrates in a tin-based solution to improve the CNT wettability and to facilitate

the absorption of seeding particles. Unfortunately, presence of tin can have an adverse effect on the adhesion of the Cu layer with the substrate [32-34]. To eliminate tin usage, the outer surface of the CNT fibers was functionalized with thiol groups. As a result, the Pd catalyst could be directly seeded on the CNT fibers, similar to the works of Subramaniam et al. [4] and Leggiero et al. [17]. Moreover, the thiol functional groups create a strong bonding between the fiber core and Cu shell [29]. Consequently, dense and smooth coating of Cu were deposited on the Pd-seeded fibers and light-weight core-shell fibers with remarkable electrical conductivity of 3.4 × 10 7 S/m and tensile strength of 642 MPa were fabricated. The procedure proposed here is facile and scalable and our findings can be implemented in other deposition techniques and for other metals. In addition to power cables, these low-density conductors can be used in a wide variety of applications where weight reduction is critical, from aerospace industries to portable electronics.

3.2. Experimental procedure

3.2.1. Fiber Fabrication

The CNT fibers were fabricated from double-wall carbon nanotubes provided by Dexmat according to [8]. They had diameter between 40 to 100 μm. To introduce carboxyl groups to the CNT fibers, thin a typical process they are immersed in a solution of sulfuric acid and nitric acid (3:1 volume ratio) for 20 min, and then rinsed with deionized DI-water four times. For creating thiol groups on the CNT fiber, the acid treated CNTs are immersed in an 100 ml aqueous solution containing 100 mg N,N′-Dicyclohexylcarbodiimide (DCC) and (Sigma-Aldrich) and 150 mg cysteamine (Sigma-Aldrich) for 2 hr. Copper electroless deposition for P-CNT and O-CNT fibers started with sensitizing them in a 100 ml aqueous solution of tin

chloride (1 g) (Sigma-Aldrich) and 37% hydrochloric acid (0.6 ml) (Sigma-Aldrich) for 2 min. After rinsing one time with DI-water they were activated by immersion in 100 ml aqueous solution of palladium chloride (20 mg) (Sigma-Aldrich) and 37% hydrochloric acid (0.5 ml) for 2 min. For preparing the SH-CNT/Cu fibers for Cu deposition a different route was undertaken. It started with dipping them in a 100 ml aqueous bath of 10 mg palladium chloride and 100 mg sodium chloride (Sigma-Aldrich). Then, 0.2 ml 50 vol% hydrazine hydrate solution (Sigma-Aldrich) was added to the bath. All wet chemistry procedures explained above were carried out at room temperature and under stirring using a magnetic bar. Before inserting them into the Cu deposition bath, they were thoroughly washed in DI-water. The recipe of the Cu electroless deposition bath is provided in Table 1. The deposition was carried out between 30 min to 90 min. Subsequently, the CNT/Cu fibers were rinsed with DI-water 3 times and with ethanol two times and finally dried in vacuum oven at 30 ºC over night. Annealing was carried out in a reforming gas (5 vol% hydrogen-nitrogen) for three hours at 300 ºC with a ramp rate of 15 ºC/min.

3.2.2. Characterization

The morphology of the fibers was examined via scanning electron microscopy (SEM) (FEI-Quanta 600) equipped with Oxford energy-dispersive X-ray (EDS). Transmission electron microscopy (TEM) (FEI Teccai G2 S-Twin, Philips) was used for studying the morphology of the Cu at the CNT interface. X-Ray diffraction (XRD) (Bruker D8 Advance ECO) with CuKα incident radiation (λ = 0.1506 nm) was used to study the microstructure of the composite fibers. For analyzing the surface chemistry of the CNTs X-ray photoelectron spectroscopy (XPS) (Omicron DAR 40 dual Mg/Al x-ray source) was utilized. XPS plots were deconvoluted

based on Gaussian–Lorentzian peaks and Shirley background subtraction. To obtain the dimensions of the fibers laser confocal microscopy (LCM) (Keyence VK 9700) was used and the results were verified by SEM.

The electrical conductivity of the fibers was measured with a four-point-probe (Signatone, SP4-40045TBY) on a resistive stand (Signatone, Model 302) at room temperature. The ampacity was measured by applying a DC current, steadily increasing the voltage and recording the current in air. High temperature performance of the fibers was investigated in a glove box filled with Ar using two-point probe testing. Mechanical properties of the fibers were studied using a dynamic mechanical analyzer (DMA) (RSA G2, TA instruments). For bending tests, fiber with a gage length of 2 cm was first put under a small tensile force (< 10 mN) to align it vertically. Then the gage length was reduced to 1.4 cm followed by retraction to its initial stage. Cycles of contraction and retraction with a frequency of 1 Hz were applied for 10 s to 10 min. This corresponds to around 45º bending every second.

3.3. Results and discussion

Figure 3-1a illustrates the schematic fabrication process of CNT/Cu core-shell wires. The CNT fibers were produced by wet spinning process using sulfonic acid as described in [8]. Then, these fibers went through oxidation and thiolation surface treatment to create carboxyl (COOH) or thiol (SH) groups, respectively. Carboxyl modified samples were soaked in Sn bath followed by immersion in Pd bath. Sn readily wets the surface of CNT fibers, allowing for direct Pd absorption. On the other hand, thiol-activated fibers have superior wettability towards metals [29] and can interact with Pd directly, hence eliminating a need for Sn sensitization on the CNT fibers. Sodium borohydride was used to reduce the Pd on the SH-CNT fibers. After thoroughly

washing the fibers with deionized water (DI-water), they are immersed in Cu deposition bath where absorbed Pd acts as a catalyst for nucleation and growth of Cu. The composition and conditions of Cu deposition bath is provided in Table 3-1. After drying, the fibers went through an annealing step in 5 vol% hydrogen-nitrogen mixture (reforming gas) and their mechanical and electrical properties were studied after this step.

Table 3-1. Composition and conditions of Cu electroless deposition bath.

Chemical composition	Quantity
$CuSO_4.5H_2O$	6.2 g/l
2Na-EDTA	20 g/l
2,2'-dipyridyl	10 ppm
CHOH (37 vol% in H_2O)	20 ml/l
Temperature	65 °C
pH (NaOH)	13

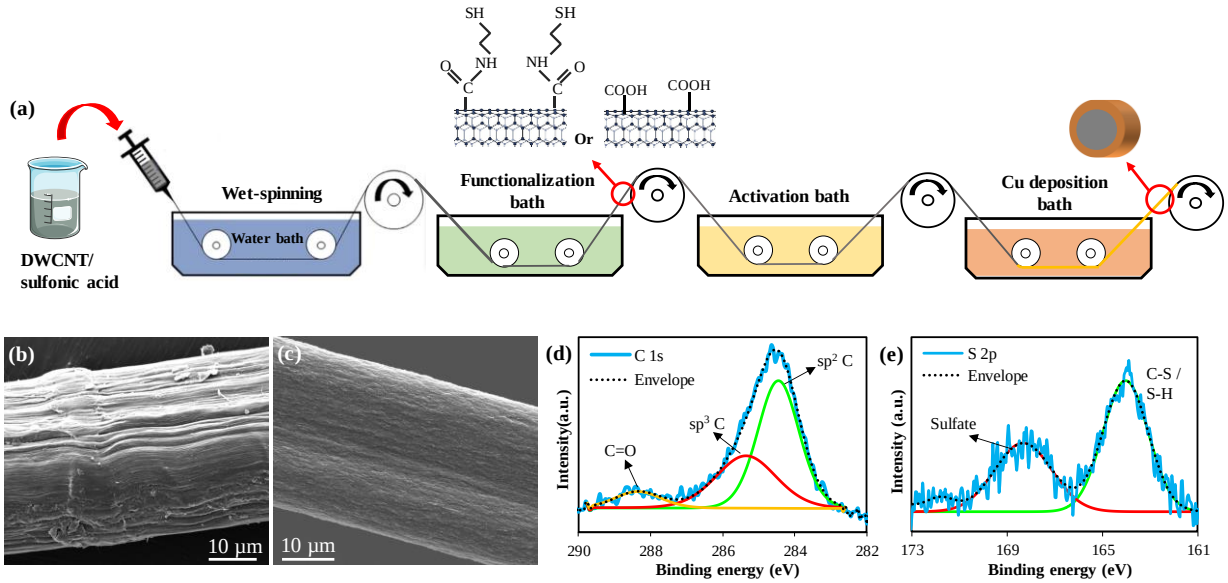

Figure 3-1. (a) Schematic of a typical process for fabrication of CNT/Cu core-shell fibers. Fibers after functionalization and activation baths are rinsed with DI-water. Morphology of the fibers before (b) and after (c) acid treatment shows that the cross section of the fibers reduces between 15 to 20%. XPS analysis on the fibers after 20 min of acid treatment (d) and thiolation indicate that carboxyl and thiol groups are formed on the surface of the fibers, respectively.

3.3.1. Interface Design and Morphology

Prior to Cu deposition two different surface groups were introduced to pristine CNT fibers, namely carboxyl (O-CNT/Cu) and thiol (SH-CNT/Cu). Carboxyl groups were formed by oxidizing the outer surface of the fibers in a mixture of nitric and sulfuric acids. This is a common method for functionalization of CNTs and improving their interaction toward metals and polymers. Similarly, Meng et al. [35] modified the surface of CNT fibers using nitric acid and observed a significant improvement in their electrical conductivity and tensile strength which was attributed to the densification of fibers after acid treatment. Electrochemical anodization is another method that has been implemented to oxidize CNT fibers [19, 20, 36]. This technique can improve the bonding of CNT fiber with metallic coatings, but does not cause fiber densification (compare Figure 3-1b and c). In our experiments we also observed that acid treatment can densify the fibers, depending on the duration of the process and fiber diameter. In XPS analysis (Figure 3-1d), it is demonstrated that only 15 to 20 min of acid treatment is sufficient to create carboxyl groups on the surface and densify the fiber packing. For example, the diameter of fiber core after acid treatment is reduced from 38 to 32 μm, while their electrical conductivity and tensile strength are enhanced by almost 30% and 25%, respectively. Over longer periods of acid exposure, more carboxyl groups are formed, but the crystalline structure of CNTs begins to deteriorate [29] and the fiber starts to disintegrate. It is noted that this acid treatment method is very effective in compacting thinner fibers (diameter < 50 μm), whereas it is detrimental to the integrity and properties of fibers with larger diameter (diameter > 80 μm).

Thiol groups were introduced by soaking the acid treated CNT fibers in a mixture of N, DCC and cysteamine. The high resolution XPS data of S 2p peak for samples after this process

is presented in Figure 3-1e. This plot is mainly consist of two peaks at around 168 eV which corresponds to sulfates and a stronger peak at around 164 which is attributed to C-S and S-H bonds which confirms the formation of thiol groups on the fiber surface [29]. The average diameter of the fibers after this step increases slightly, from 30 to 32 μm, and small drops in electrical conductivity and tensile strength are observed. Despite of these changes, SH-CNT fibers still have a smaller cross section and superior properties compared with the pristine fibers. Thiol has a pair of free electrons and can form strong bonding with metals through its donor centers [29, 37, 38].

As mentioned before, electroless deposition typically starts with dipping the substrates into a tin-based solution. Tin and its complexes readily adhere to any substrate including glass [31] and prepare the surface for adsorption of Pd catalyst. However, after performing Cu electroless deposition on individual CNTs traces of tin in the deposits were found. It has been reported that a tin-free activation can improve the adhesion of Cu coatings with the substrate [32-34]. Therefore, eliminating tin in the process not only is more environmentally friendly but also can produce Cu deposits with superior adhesion to the fiber surface. By functionalization of the fibers with thiol, Pd nanoparticles were able to directly nucleate at the surface of fibers. As it can be observed in Figure 3-2a, Pd nanoparticles, with a narrow particle size distribution of around 20 nm are formed on SH-CNT fibers. On the other hand, the same procedure was carried out on O-CNT fibers; but instead of forming uniformly distributed fine nanoparticles, a few large agglomerations of Pd were observed. Electroless deposition of Cu on these samples failed. It is worth noting that we were able to directly decorate the SH-CNTs with uniform Cu seeds with the same method used for Pd decoration. These seeds were uniform with a narrow size

distribution of around 4 nm; however, uniform Cu coatings through electroless deposition could not be fabricated. It is speculated that due to their small size, these seeds oxidize quickly and become inactive for promoting autocatalytic Cu deposition.

Figure 3-2b to f compares the surface morphology of fibers with different surface groups after Cu deposition. P-CNT/Cu fiber has a rough surface and shows large faceted crystallites. The O-CNT/Cu fiber does not have a significant effect on the morphology of the Cu deposits. while SH-CNT/Cu fiber shows the smoothest surface compared to the other systems. This is in alignment with our earlier work in which it was observed that thiol functional group is able to significantly improve the CNT wettability towards Cu, allowing deposition of ultrathin Cu films (< 3 nm) [29]. Moreover, the evolution of the coating with time for different fibers was studied. It was observed that the Cu thickness increases with the deposition duration. Generally, the deposition rate is in the order of SH.CNT/Cu > O.CNT/Cu > P.CNT/Cu. This is attributed to the fact that thiol functionalized CNTs have more abundant Pd catalytic sites compared to the other systems [29]. Small and dense Pd catalysts sites ensures deposition of thin and continuous electroless Cu layer since nucleation and growth of Cu initiate from these catalytic sites. On the other hand, a non-uniform distribution of or agglomeration of Pd seeds leads to insufficient sites for initiation of Cu deposition which prolongs the process and leads to a discontinuous and rough Cu coating [39].

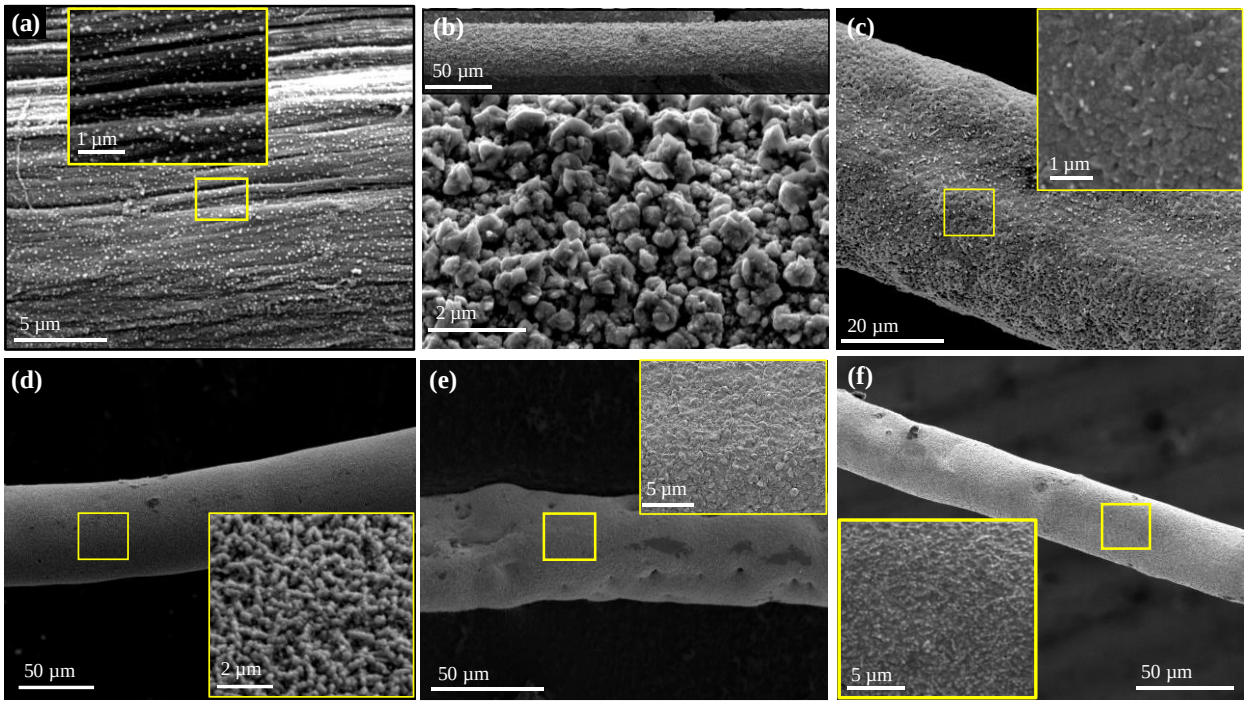

Figure 3-2. SEM images of the metallized fibers: (a) SH-CNT fiber after seeding with Pd, (b) the P-CNT/Cu fiber before annealing and (c) after annealing. O-CNT/Cu and SH-CNT/Cu fibers have similar microstructure before annealing (d). After annealing O-CNT/Cu fiber (e) and SH-CNT/Cu (f) structure is smoothened and looks very dense.

XRD analysis shows that crystalline structure of the core-shell fibers is similar, irrespective of different surface treatments. As represented in Figure 3-2e, the (111) and (200) peaks of cubic copper were found at 43.4° and 50.5°, respectively. At the early stages of electroless deposition, the grain structure of the Cu is mainly determined by the morphology of the CNT substrate. However, as the process continues and the coating thickens, the bath composition becomes the dominant factor and controls the grain structure. As a result, it is not surprising that all the samples have similar lattice structure. Williamson-Hall method was used on the main peaks to estimate the Cu crystallite size [40]. Results reveal that P-CNT/Cu has the largest crystallite size of around 76 nm; while for O-CNT/Cu and SH-CNT/Cu, their sizes are 50 nm and 45 nm, respectively. On the P-CNT fiber, there are very limited numbers of preferential

sites for nucleation and growth of the Cu seeds which results in larger Cu particles (as reflected by the rough surface of P-CNT/Cu fiber shown in Figure 3-2b. On the contrary, for the surface treated samples the active sites for anchoring Cu seeds are abundant and the growing islands of Cu meet and coalesce with each other early in the deposition process. This results in a fine grained film which provides high quality and dense Cu deposits [41]. It should be noted that comparison of the crystallite size of the two functionalized fibers should be carried out with care since their sizes are similar. Also, these numbers do not represent the actual crystallites size but rather are only suitable for relative comparison. After annealing in the reforming gas at 300 °C, the crystallite size increases and becomes more uniform among all samples and the morphology of the Cu layer is smoothened (Figure 3-2c, e, and f).

The density of the Cu film has a major effect on the physical properties of the coating including their electrical conductivity and strength. The density of the annealed fibers was calculated based on mass gained and thickness increase and the results. Regardless of the surface functionalization, the density of the Cu films slightly increases with the thickness. Also, it is apparent that surface modification of the fibers leads to Cu shells with a higher density. After coating a 9 to 10 μm thick Cu film, the shell density is 7.6, 8.2, and 8.4 g/cm^3 for P-CNT/Cu, O-CNT/Cu, and SH-CNT/Cu fibers, respectively. This is consistent with our previous findings [29] and the literature [20]. It has been reported that Cu can readily wet and bond to the surface of CNTs with thiol functionalization leading to packed and void free structures. Meanwhile, P-CNT and Cu have very poor affinity towards each other which leads to segregation and formation of CNT-rich and Cu-rich regions with high porosity [29].

3.3.2. Mechanical Properties

Figure 3-3a presents the tensile properties of the core-shell fibers, with 9 to 10 μm Cu layer on the shell. P-CNT fibers have remarkable tensile strength of 650 ± 14 MPa before acid treatment and 810 ± 24 MPa after acid treatment, while the tensile strength of a typical Cu wire is around 230 MPa. Owing to the high tensile strength of the core CNT fiber, the composite fibers show higher tensile strength compared with Cu. The P-CNT/Cu (42.9 vol% CNT) shows the lowest tensile strength among core-shell fibers, around 430 ± 20 MPa, which can be attributed to the poor bonding between the core and the shell. In fact, it was observed that during handling of P-CNT/Cu fiber, the coating can be detached from the substrate easily. Therefore, it is speculated that the Cu coating does not have any effect on the strength of the composite fiber. On the other hand, functionalization of the fibers creates anchors for the Cu shell to be firmly attached to the CNT core, leading to tensile strength enhancement. Accordingly, by introducing carboxyl groups to the CNT fiber through acid treatment, the tensile strength improves to 540 ± 20 MP (41 vol.% CNT). This is close to the tensile strength of electrochemically anodized CNT/Cu core-shell fibers in the literature [19, 20]. Introducing thiol groups to the interface of CNT/Cu proves to be most effective as the tensile strength of SH-CNT/Cu (42.8 vol.% CNT) sample reaches 640 ± 20 MPa, similar to the P-CNT fibers alone. By considering the density, the specific strength of the SH-CNT/Cu fiber is almost five times higher than commercial Cu wire. This remarkable performance is attributed to the bridging effect of thiol surface groups and the tin-free activation process which leads to creation of a strong bonding between the CNT fiber and the Cu shell. As shown in Figure 3-3b, Cu slightly diffuses into the SH-CNT structure and form a firm binding. This strong interaction leads to a

more efficient stress transfer between the core and shell. The fracture surface of the fibers is given in Figure 3c to e. For P-CNT/Cu fibers, a significant pull out at the break point, up to 100s μm long bare CNT bundles are found. Tailoring the interface by thiol functional group decreases this pull-out length to only a few μm, meaning minimal sliding and pull-out has occurred. Therefore, it is speculated that the load transfer from the shell to the core and vice versa has taken place more effectively and CNT breakage is likely to have occurred.

The SH-CNT/Cu fibers also has an excellent performance against fatigue bending cycles. To evaluate this property, fibers were bent 45º with a frequency of 1 Hz up to 600 cycles (Figure 3-3f). Morphologies of the composite fibers were investigated and cracks were observed in P-CNT/Cu only after 10 cycles and O-CNT/Cu after 200 cycles (Figure 3-3g), but for the SH-CNT, crack or debonding of the Cu shell was not observed even after 600 cycles. Weak adhesion of catalytic sites can lead to voids and defects between deposits and substrate and cause premature film peeling [39]. Therefore, for the SH-CNT/Cu sample, strong bonding and free of tin at the interface results in a strong adhesion between CNT fiber and Cu shell. The tensile strength of fibers after 100 cycles were tested and interestingly the tensile strength of the P-CNT/Cu does not change significantly. Meanwhile, the tensile strength of the SH-CNT/Cu and O-CNT/Cu drop by 10% and 25%, respectively. This is in support of our speculation that in P-CNT/Cu the bonding between the core and the shell is very poor to begin with and the bending cycles basically does not cause deterioration of the already weak interface. On the contrary, the O-CNT/Cu exhibits some interaction between the core and the shell which is weakened during the bending cycles; hence a reduction of tensile strength was observed. Due

to the strong interfacial interaction of the thiol groups with the Cu shell, the tensile strength of the SH-CNT/Cu is mostly preserved even after the bending cycles.

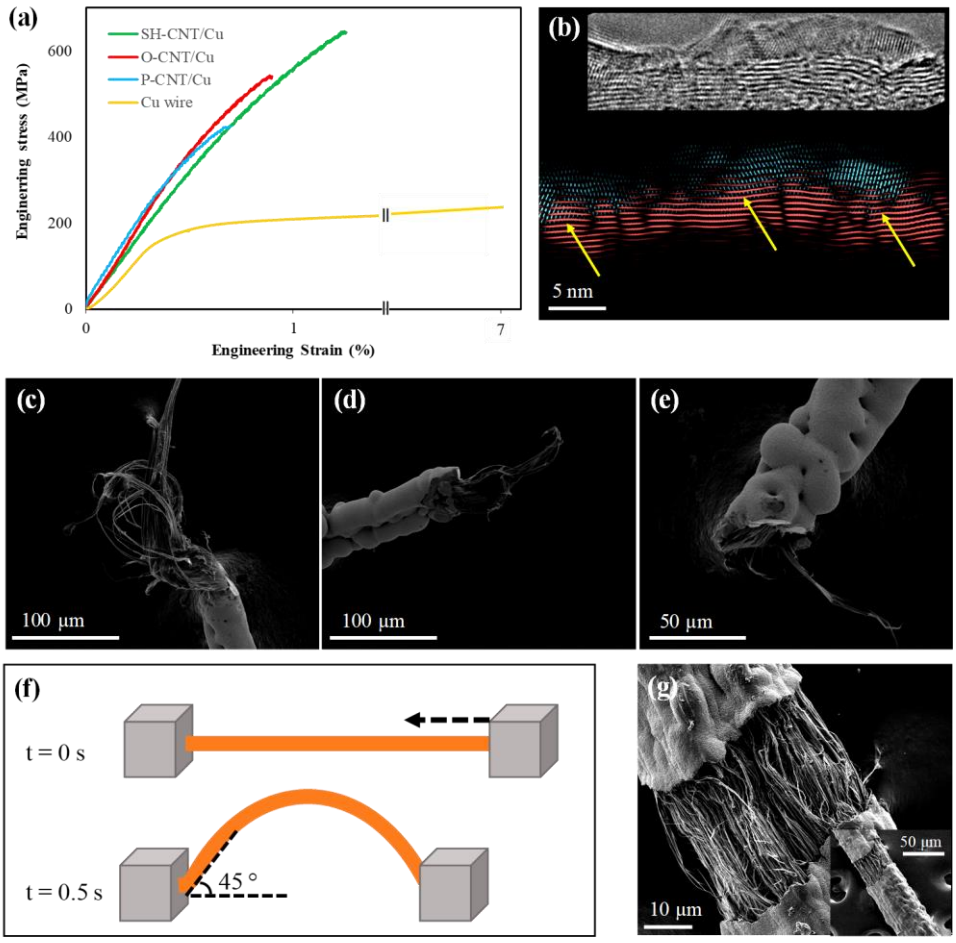

Figure 3-3. The mechanical properties of the fibers and their morphology after failure. (a) Engineering stress-strain curve of the composite fibers and a commercial Cu wire. (b) the diffusion of Cu inside the SH/CNT structure indicating a strong bonding between the two. The fracture surface of the P-CNT/Cu (c), O-CNT/Cu (d), and SH-CNT/Cu (e) composite fibers after the tensile tests. Schematic of the bonding test (f). Shell of the P-CNT/Cu and O-CNT/Cu fibers was cracked similarly after 10 and 200 cycles, respectively (g).

3.3.3. Electrical Properties

The electrical conductivity of the fibers was measured using four-point-probe tests and the results are presented in Figure 3-4a. In this method the sensing terminals of current and voltage

are separated which eliminates the effects of contact resistance and provides a more accurate measurement. Results show that electrical conductivity of the composite fibers depends on microstructural defects and the interface between CNT and Cu. Measurements were carried out at room temperature, on core-shell fibers with a Cu thickness of 9 to 10 μm. Electrical conductivities of $7.2 \pm 0.1 \times 10^6$, $2.1 \pm 0.2 \times 10^7$, and $2.5 \pm 0.2 \times 10^7$ S/m were obtained for P-CNT/Cu (42.9 vol. % CNT), O-CNT/Cu (41 vol. % CNT), and SH-CNT/Cu (42.8 vol. % CNT), respectively. These numbers are about 6 to 20 times higher than that of the P-CNT fibers (1.3×10^6 S/m). It is speculated that the quality of the deposits and the strong interfacial interaction between CNT and Cu play the dominant roles in the electrical properties of the composite fibers. As observed in Figure 3-2b, the P-CNT/Cu surface was not as packed nor as smooth as its interface modified counterparts which explains its inferior performance.

It should be noted that some of the best results in the literature were obtained through pre-seeding of the samples. For example, Subramaniam et al. [4] achieved an electrical conductivity of 4.7×10^7 S/m for Cu/CNT thin films after pre-seeding the CNTs with Cu particles. Moreover, Leggiero et al. [17] used CVD to seed the CNT roving and reported conductivity of 2.8×10^7 S/m for their composite, 22% higher than the samples that were not pre-seeded. Here, application of Pd seeds coupled with electroless deposition produces dense and uniform coating of Cu with strong interaction with the CNT fiber, which leads to superior electrical conductivity. It should also be noted that after acid treatment, the CNT fibers are densified and the electrical conductivity is improved significantly. As a result, the functionalized fibers not only have a smoother surface but also packed better at their core, which leads to a higher electrical conductivity.

Annealing the composite fibers improves the electrical conductivity which is consistent with the previous reports [20]. Accordingly, the conductivity of the O-CNT/Cu and SH-CNT/Cu improve to $2.9 \pm 0.1 \times 10^7$ and $3.4 \pm 0.2 \times 10^7$ S/m, respectively. This improvement is more significant for the P-CNT/Cu sample, where it reaches $1.5 \pm 0.1 \times 10^7$ S/m. The microstructure of P-CNT/Cu before annealing was very coarse with visible gaps between the grains. After heat treatment, it is apparent that the surface smoothness of the fiber improves and the faceted crystallites are replaced by smooth and uniform microstructure. In addition to modifying the microstructural defects, annealing can lead to recrystallization and produce larger grains. As the grain size increases, the electron scattering reduces hence the conductivity enhances. Moreover, formation of Cu_2O is common during electrochemical deposition but annealing in reforming gas can reduce any oxides to their metallic state. Furthermore, the composite fibers become much lighter and their density is almost half of Cu (4.72 g/cm^3). Accordingly, the specific conductivity of the SH-CNT/Cu is around 7.37×10^7 $S.m^2/kg$ which is about 12% higher than that of a commercial Cu wire. It is worth noting that after one week of storage, the P-CNT/Cu fibers that did not go through the heat treatment step became mate brown and lost 35% of their conductivity; while for annealed P-CNT/Cu fiber, this drop was just 10% after three days and stabilized afterwards.

The electrical performance of the SH-CNT/Cu fiber at higher temperature was compared with the commercial Cu wires (Figure 3-4b). Cu wire and core-shell fibers were transferred to an inert environment and their resistance were recorded as a function of temperature by using a two-point-probe setup. The commercial Cu wire has a resistance of 2×10^{-6} Ω.cm at room temperature (25 ºC) and its resistance linearly increases to 4.37×10^{-6} Ω.cm at 300 ºC,

corresponding to a temperature coefficient of resistance (α) of 4.15 × 10^{-6} °C. This is because as the temperature increases, Cu atoms jostle more violently, increasing the chances of scattering as a result of their collision with vibrating atoms, i.e., inelastic scattering. Electron migration in CNTs, on the other hand, has a different mechanism and the electrical conductivity is not affected much by temperature above room temperature [6]. Therefore, by increasing the temperature of a CNT/Cu core-shell structure, the inelastic scattering in Cu is alleviated by elastic scattering in the CNT fiber resulting in a lower α compared with the one of Cu. Accordingly, the α for SH-CNT/Cu fiber is reduced by half (α ≈ 2.1 10^{-6} °C) and, interestingly, at around 300 °C, the conductivity of the SH-CNT/Cu is similar to the conductivity of a commercial Cu wire.

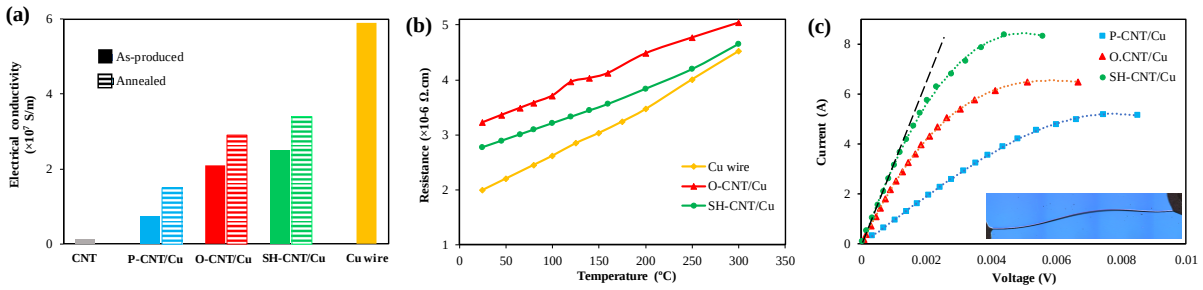

Figure 3-4. The electrical performance of the composite fibers. (a) electrical conductivity, (b) Temperature dependence of the electrical conductivity, and (c) the I-V curves for determining the maximum current carrying capacity (ampacity) of the composite fibers. The inset shows the fiber during the ampacity test. The dash line corresponds to the conductivity of the fiber. For latter the length of SH and O-CNT/Cu fibers were 2 cm and O-CNT/Cu fiber was 1.5 cm.

The current-carrying capacity (i.e. ampacity) of the composite fibers was evaluated and compared with commercial Cu wire. Ampacity is defined as the maximum current that a wire can carry divided by its cross-sectional area. As current passes through a wire, charge carriers are transferred in the direction of the electric field. On their way, they may collide with the wire ions and scatter in a random fashion. This converts the kinetic energy of the electrons to thermal

energy which is known as Joule heating. The produced heat can reduce the wire conductivity, cause oxidation, electromigration, and finally wire failure. Owing to its strong C-C bond, CNT does not follow the classical Joul's law and is not much affected by Joule heating, which results in a remarkably high ampacity, up to three orders of magnitude higher than Cu [42, 43]. This makes them promising candidates for interconnects in next generation electronics.

The results of ampacity tests are shown in Figure 3-4c. For the commercial Cu wire, an ampacity of $0.90 \pm 0.03 \times 10^5$ A/cm^2 is obtained. The ampacity of the P-CNT/Cu fiber with a 9 μm coating is measured to be $0.64 \pm 0.05 \times 10^5$ A/cm^2. The ampacity improves for O-CNT/Cu and SH-CNT/Cu to $0.87 \pm 0.04 \times 10^5$ A/cm^2 and $1.03 \pm 0.05 \times 10^5$ A/cm^2, respectively. The ampacities of core-shell fibers are surprisingly lower than what was expected, and are very close to commercial Cu. This is attributed to the fact that copper has a higher conductivity, denser structure, and less defects which facilitates the regular motion of electrons in the direction of the electric field, alleviating the Joule heating [43]. On the other hand, our results show that the Cu layer in core-shell fibers have lower electrical conductivity and density compared with copper wire which can lead to more pronounced Joule heating and disrupt heat exchange with the surrounding. Among the composite fibers, the SH-CNT/Cu fiber outperforms the other fibers. It is speculated that this stems from two major factors: (i) its higher density and conductivity as discussed previously, and (ii) strong bonding between Cu layer and CNT fiber (as discussed in bending results) which facilitates heat exchange between the core and the shell. As a result of this effective heat exchange, thermal energy is transferred to the core and distributed quickly along the fiber, avoiding localized heat spots.

In transportation and microelectronic applications where energy efficiency is of utmost concern, the weight and size of the electrical components are of interest. By considering the density and comparing the specific ampacity, for an SH-CNT/Cu fiber with 10 μm thick shell, the specific ampacity is 2.1×10^4 A.cm/g which is more than two folds higher than the commercial Cu wire of 1×10^4 A.cm/g. Similarly, the other two core-shell composite fibers that are much lighter compared with Cu wire, have also superior specific ampacities; $\approx 1.5 \times 10^4$ A.cm/g and $\approx 1.8 \times 10^4$ A.cm/g for P-CNT/Cu and O-CNT/Cu, respectively. These results show that by tuning the interface of CNT/Cu fibers, one can produce ultrastrong, light-weight and highly conductive fibers that are suitable for many applications ranging from power transmission in subsea applications to portable electronics, and to electric vehicles. The present findings can also be implemented in other deposition techniques including electrodeposition for rapid fabrication of high-performance metal/CNT core-shell fibers.

Moreover, Figure 3-5 the electrical and mechanical performance of the fabricated core-shell fibers with commercial Cu wire and the recently published works on CNT-Cu hybrid structures and lightweight core-shell fibers. As it can be observed, among the hybrid fibers shown, SH-CNT/Cu fibers stands out in terms of its remarkable specific tensile strength and conductivity. Owing to the Cu shell dense structure and strong bonding with the CNT core, this fiber outperforms many similar fibers in the literature. Common practices in the industry such as extrusion can compact the structure and expect to further increase the mechanical and electrical performance of the core-shell CNT/Cu fibers.

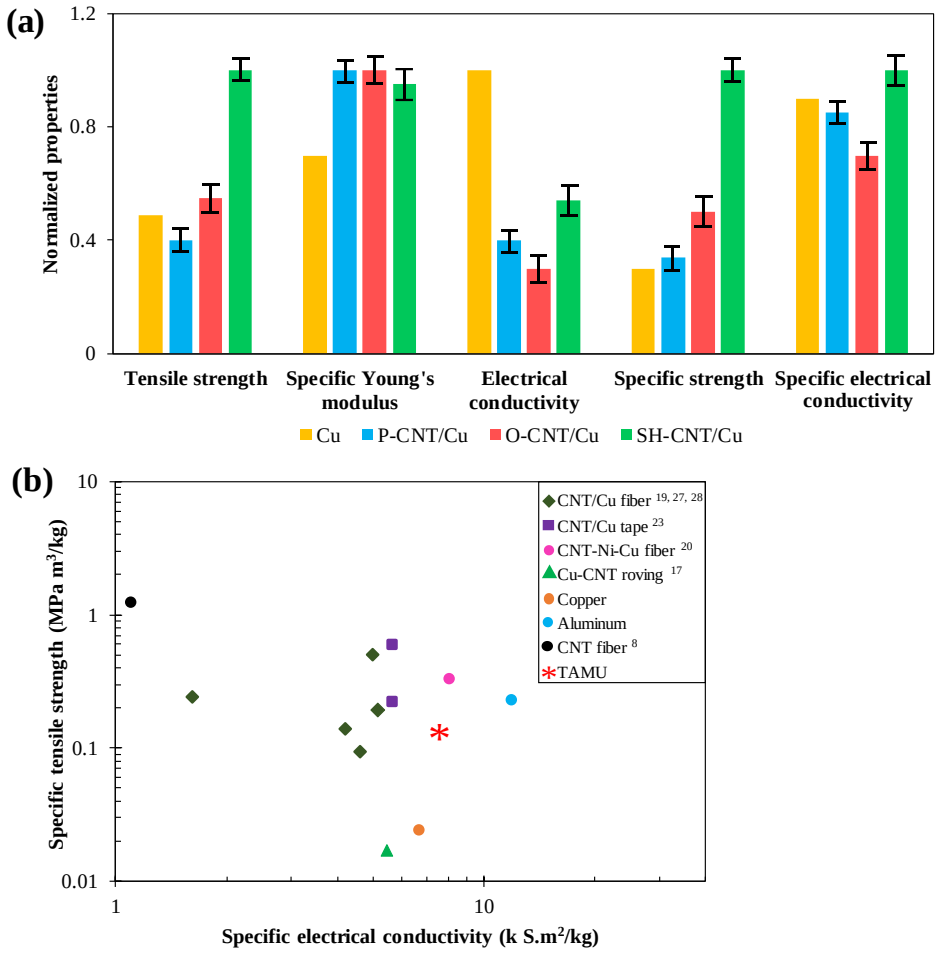

Figure 3-5. The comparison of the composite fibers with the commercial Cu wire (a), and the SH-CNT/Cu performance compared with the literature (b).

3.4. Conclusion

In this study, a tin-free electroless deposition method was used to fabricate light-weight, robust, and highly conductive CNT/Cu wires. This has been achieved through introduction of thiol groups to the surface of CNT fibers. This creates preferential sites for chemisorption of Pd atoms to the fiber. As a result, a continuous and uniform coating of Cu can be plated on the surface of CNT fiber. Electrical conductivity of the core-shell fibers was improved due to successful design of the interface and densely deposited Cu layer. Measurements showed that

the specific conductivity of composite fibers can exceed that of commercial Cu and their specific ampacity and specific conductivity of two folds and 12% higher than commercial Cu wires, respectively. Moreover, a remarkable tensile strength of 642 MPa was achieved for SH-CNT/Cu fiber, which corresponds to five times higher specific tensile strength than common Cu wires. Bending tests revealed that avoiding tin in the process and using thiol groups can enhance the bonding between the core and the shell which not only makes the fiber robust, but also facilitates heat transfer and increases its life.

3.5. References

1. Technavio, *Global Power Cables Market 2017-2021*. 2017: Chicago. p. 70.

2. Aziz, A., et al., *1D copper nanowires for flexible printable electronics and high ampacity wires.* Nanoscale, 2017. **9**(35): p. 13104-13111.

3. Kim, S.J., et al., *Ultrastrong graphene–copper core–shell wires for high-performance electrical cables.* ACS Nano, 2018. **12**(3): p. 2803-2808.

4. Subramaniam, C., et al., *One hundred fold increase in current carrying capacity in a carbon nanotube–copper composite.* Nature Communications, 2013. **4**(1): p. 1-7.

5. Chun, K.-Y., et al., *Highly conductive, printable and stretchable composite films of carbon nanotubes and silver.* Nature Nanotechnology, 2010. **5**(12): p. 853.

6. Behabtu, N., et al., *Strong, light, multifunctional fibers of carbon nanotubes with ultrahigh conductivity.* Science, 2013. **339**(6116): p. 182-186.

7. Zhao, Y., et al., *Iodine doped carbon nanotube cables exceeding specific electrical conductivity of metals.* Scientific Reports, 2011. **1**: p. 83.

8. Tsentalovich, D.E., et al., *Influence of carbon nanotube characteristics on macroscopic fiber properties.* ACS Applied Materials and Interfaces, 2017. **9**(41): p. 36189-36198.

9. Langer, L., et al., *Quantum transport in a multiwalled carbon nanotube.* Physical Reviews Letters, 1996. **76**(3): p. 479.

10. Zhou, X., et al., *Band structure, phonon scattering, and the performance limit of single-walled carbon nanotube transistors.* Physical review letters, 2005. **95**(14): p. 146805.

11. Ebbesen, T., et al., *Electrical conductivity of individual carbon nanotubes.* Nature, 1996. **382**(6586): p. 54-56.

12. Thostenson, E.T., et al., *Advances in the science and technology of carbon nanotubes and their composites: a review.* Composite science and technology, 2001. **61**(13): p. 1899-1912.

13. Daneshvar, F., et al., *Porous SnO_2–Cu_xO nanocomposite thin film on carbon nanotubes as electrodes for high performance supercapacitors.* Nanotechnology, 2018. **30**(1): p. 015401.

14. Chen, T., et al., *Synthesis of aligned carbon nanotube composite fibers with high performances by electrochemical deposition.* Journal of Materials Chemistry A, 2013. **1**(6): p. 2211-2216.

15. Zhang, D., Y. Zhang, and M.J.N. Miao, *Metallic conductivity transition of carbon nanotube yarns coated with silver particles.* Nanotechnology, 2014. **25**(27): p. 275702.

16. Qiu, L., et al., *Enhancing the interfacial interaction of carbon nanotubes fibers by Au nanoparticles with improved performance of the electrical and thermal conductivity.* Carbon, 2019. **141**: p. 497-505.

17. Leggiero, A.P., et al., *High Conductivity Copper–Carbon Nanotube Hybrids via Site-Specific Chemical Vapor Deposition.* ACS Applied Nano Materials, 2018. **2**(1): p. 118-126.

18. Li, Q., et al., *Structure-dependent electrical properties of carbon nanotube fibers.* Advanced Materials, 2007. **19**(20): p. 3358-3363.

19. Xu, G., et al., *Continuous electrodeposition for lightweight, highly conducting and strong carbon nanotube-copper composite fibers.* Nanoscale, 2011. **3**(10): p. 4215-4219.

20. Zou, J., et al., *Ni nanobuffer layer provides light-weight CNT/Cu fibers with superior robustness, conductivity, and ampacity.* ACS Applied Materials and Interfaces, 2018. **10**(9): p. 8197-8204.

21. Randeniya, L.K., et al., *Composite yarns of multiwalled carbon nanotubes with metallic electrical conductivity.* Small, 2010. **6**(16): p. 1806-1811.

22. Sundaram, R., et al., *The importance of carbon nanotube wire density, structural uniformity, and purity for fabricating homogeneous carbon nanotube–copper wire composites by copper electrodeposition.* Japanese Journal of Applied Physics, 2018. **57**(4S): p. 04FP08.

23. Han, B., et al., *Fabricating and strengthening the carbon nanotube/copper composite fibers with high strength and high electrical conductivity.* Applied Surface Science, 2018. **441**: p. 984-992.

24. Hannula, P.-M., et al., *Observations of copper deposition on functionalized carbon nanotube films.* Electrochimica Acta, 2017. **232**: p. 495-504.

25. Hannula, P.-M., et al., *Carbon nanotube-copper composites by electrodeposition on carbon nanotube fibers.* Carbon, 2016. **107**: p. 281-287.

26. Milowska, K.Z., et al., *Breaking the electrical barrier between copper and carbon nanotubes.* Nanoscale, 2017. **9**(24): p. 8458-8469.

27. Han, B., et al., *Fabrication and densification of high performance carbon nanotube/copper composite fibers.* Carbon, 2017. **123**: p. 593-604.

28. Wang, G., et al., *Overcoming the strength-conductivity trade-off dilemma in carbon nanotube/aluminum-copper fiber by diffusion interface and chemical reaction interface.* Carbon, 2019. **146**: p. 293-300.

29. Daneshvar, F., et al., *Tuning the composition and morphology of carbon nanotube-copper interface.* Carbon, 2020. **157**: p. 583-593.

30. Ilari, G.M., et al., *Carbon–metal interfaces analyzed by aberration-corrected TEM: How copper and nickel nanoparticles interact with MWCNTs.* Micron, 2015. **72**: p. 52-58.

31. Wei, X. and D.K.J.J.o.t.E.S. Roper, *Tin sensitization for electroless plating review.* Journal of the Electrochemical Society, 2014. **161**(5): p. D235-D242.

32. Yu, W., et al. *Electroless plating of copper and nickel via a Sn-free process on dielectric SiLK/spl reg/surface*. in *4th Electronics Packaging Technology Conference, 2002.* 2002. IEEE.

33. Wang, Y., C. Bian, and X.J.A.s.s. Jing, *Adhesion improvement of electroless copper plating on phenolic resin matrix composite through a tin-free sensitization process.* Applied Surface Science, 2013. **271**: p. 303-310.

34. You, J.B., et al., *A vapor-phase deposited polymer film to improve the adhesion of electroless-deposited copper layer onto various kinds of substrates.* Langmuir, 2014. **30**(3): p. 916-921.

35. Meng, F., et al., *Carbon nanotube fibers for electrochemical applications: effect of enhanced interfaces by an acid treatment.* Nanoscale, 2012. **4**(23): p. 7464-7468.

36. Wang, H., et al., *Ultra-Lightweight and Highly Adaptive All-Carbon Elastic Conductors with Stable Electrical Resistance.* Advanced Functional Materials, 2017. **27**(13): p. 1606220.

37. Rigo, A., et al., *Interaction of copper with cysteine: stability of cuprous complexes and catalytic role of cupric ions in anaerobic thiol oxidation.* Journal of Inorganic Biochemistry, 2004. **98**(9): p. 1495-1501.

38. Zhang, C., et al., *Efficient removal of heavy metal ions by thiol-functionalized superparamagnetic carbon nanotubes.* Chemical Engineering Journal, 2012. **210**: p. 45-52.

39. Chang, S.-Y., et al., *Integrated electrochemical deposition of copper metallization for ultralarge-scale integrated circuits.* Journal of The Electrochemical Society, 2004. **151**(1): p. C81-C88.

40. Daneshvar-Fatah, F., F.J.S. Nasirpouri, and C. Technology, *A study on electrodeposition of Ni-noncovalnetly treated carbon nanotubes nanocomposite coatings with desirable mechanical and anti-corrosion properties.* Surface and Coatings Technology, 2014. **248**: p. 63-73.

41. Deckert, Cheryl. "Electroless copper plating, a review: Part I." Plating and surface finishing 82.2 (1995): 48-55.

42. Deshpande, V.V., et al., *Spatially resolved temperature measurements of electrically heated carbon nanotubes.* Physical Review Letters, 2009. **102**(10): p. 105501.

43. Wang, X., et al., *High-Ampacity Power Cables of Tightly-Packed and Aligned Carbon Nanotubes.* Advanced Functional Materials, 2014. **24**(21): p. 3241-3249.

4. FABRICATION OF HIGHLY CONDUCTIVE COPPER-CARBON NANOTUBE COMPOSITE FIBERS VIA ELECTROSPINNING

4.1. Introduction

As new electronic devices become smarter, smaller, and faster, they require more efficient power to function. Simultaneously, there are stringent restrictions on weight and size of new devices and their components. Therefore, simply using larger electrical pathways for transmitting higher currents is not an option. Alternatively, novel materials that have superior current-carrying capacity, i.e., ampacity, are needed. Owing to the strong C–C bond, carbon nanotubes can show ampacity 1000 times higher than copper, making them an attractive option [1, 2]. Recently, a significant amount of research has been carried out on fabrication of conductive CNT-based structures to address these needs. Thin films [3, 4], tapes [5], and wires [6-9] with remarkable electrical properties have been fabricated. However, fabrication processes implemented in these studies usually consist of several complex and time-consuming steps which limits their mass production potential and their practicality. Moreover, these techniques are often unable to produce continuous sub-micrometer diameter fibers. In contrast, electrospinning represents a cost-effective and scalable technique that allows simple fabrication of high-quality conductive nanofibers. The morphological and physical properties of the electrospun fibers can easily be tailored to a wide range of applications [10]. Electrospinning of metallic nanofibers is expected to replace more expensive processes, such as lithography, in the production of nanogrids and nanowires for conductive electrodes and low-cost microelectromechanical systems (MEMS) [10, 11]. Furthermore, electrospinning allows

preparation of ultralong nanofibers with extremely high aspect ratios, which ensure better electronic performances in transparent conductive electrodes. To the best of our knowledge, in spite of these great potentials, there has not been a study that has explored the possibility of using electrospinning for fabrication of Cu/CNT submicron diameter nanofibers.

Herein, the fabrication of continuous Cu/CNT composite nanofibers through an electrospinning process with potential applications in portable and transparent electronics is reported. Electrospinning has proven to be a simple, scalable, and fast method for production of polymer-based fibers [12]. It has also been used for fabrication of submicron diameter metallic and ceramic fibers [11, 13-16], but not for producing metal/CNT composite fibers thus far. This is possibly due to the following difficulties: (i) inorganic fibers produced with electrospinning usually exhibit rough surface and porous structure [10, 11, 16], (ii) small amounts of CNT can easily clog the electrospinning needle and stop the process, and (iii) CNT has poor affinity towards metal source and segregates in the polymeric carrier. In this study, these challenges were overcome by tuning the surface chemistry of CNTs and introducing CuNW to the precursor solution. Electrospun Cu/CNT single fiber has conductivity of 3.4×10^6 S/m, while the conductivity of a single Cu fiber containing CuNW is 7.6×10^6 S/m which is the highest shown in the literature to the best of our knowledge. When these fibers are deposited on a transparent substrate, the Cu and CNT/Cu mats show sheet resistance of 25 Ω/□ at 85% and 39 Ω/□ at 79% transmittance, respectively. Considering the facile scalable fabrication method coupled with remarkable electrical performance presented here, these novel composite fibers have potential applications in portable electronics, touch screens, foldable displays, and interactive electronics.

4.2. Experimental procedure

4.2.1. Materials

Copper acetate, polyvinyl alcohol (PVA) (Mw= 125,000 g/mol), and polyvinylpyrrolidone (PVP) (Mw = 1,300,000 g/mol) were purchased from Sigma-Aldrich and used as received. Pristine few wall CNT (P-CNT) with average diameter of 15 nm and average length of 5 μm, with theorical density of 2 g/ml were purchased from Arkema. The surface of MWCNTs were functionalized using carboxyl (O-CNT) or thiol (SH-CNT) groups according to [4]. CuNWs were synthesized using KBr as a co-capping agent according to the procedure described in [17].

4.2.2. Fiber production

In a typical process, 5 to 15 mg P-CNT or functionalized CNTs (f-CNT) were mixed with 20 mg CuNWs in 3 ml ethanol under sonication for 15 min. Simultaneously, 0.4 g of PVA was dissolved in 7 ml of DI-water at 80 °C. Subsequently, 0.5 g copper acetate was added to this solution and was stirred as it cooled down to the room temperature. After the copper acetate was dissolved, the CNT-CuNW solution was added and the mixture was stirred for 15 min followed by sonication for 15 min. The electrospinning process was carried out at a steady flow rate of 0.1 ml/min and external voltage of 10 kV. The shear stress caused by the needle aligns the CNTs and CuNWs in the direction of the fiber and increases the density. The fibers were heated at 350 °C in air for 4 h to remove the PVA and then in nitrogen- 5vol% hydrogen (reforming gas) at 300 °C for 2 h to reduce the CuO to Cu.

4.2.3. Characterization

The morphology and composition of the fibers were studied using scanning electron microscopy (SEM) (FEI ESEM Quanta 600 FEG) equipped with Energy-dispersive X-ray

spectroscopy (EDS) (Oxford Instruments). Transmission electron microscopy (TEM) (JEOL JEM 2010) was used to analyze the CNT-CuNW interactions. Fibers were attached to standard microchips using focused ion beam (FIB) to measure the electrical conductivity (FEI FIB200 system at 30 keV and 13 pA). X-ray photoelectron spectroscopy (XPS) (Omicron DAR 40 dual Mg/Al x-ray source) was used to determine the surface chemistry of functionalized CNTs. XPS plots were deconvoluted based on Gaussian–Lorentzian peaks and Shirley background subtraction [4]. UV–Vis absorbance spectra were acquired with a UV–Vis–NIR spectrophotometer (Shimadzu, UV-3600) on glass transparent electrodes containing electrospun fibers.

Electrical resistance of individual electrospun fibers is measured by applying a DC current using Keithley 4200-SCS semiconductor characterization system. The electrical conductivity was calculated according to following equation, $\sigma = I/V \times L/A$ where V is the applied voltage (V), I is the measured current (A), L is the length of fiber (m), A is the cross-section area of the fiber (m^2). The ampacity of the fibers was similarly measured by applying a DC current. To increase the current an amplifier was used. The sheet resistance of the fibers was obtained using a four-point-probe (Signatone, SP4-40045TBY) on a 1 cm^2 surface area.

Thermogravimetric analysis (TGA) (Q500 TA Instruments) was carried out on composite fibers after the polymer removal but before the reduction to avoid the effect of Cu reduction on the results. Measurements were performed in oxygen purging at 40 mL/min at a heating rate of 10 °C from room temperature to 800 °C with a 15 min isotherm at 250 °C to determine the concentration of CNTs in fibers. The difference in weight after decomposition at ~450 °C and 600 °C was defined as the wt.% of CNTs present in the CNT/CuO fibers. By replacing the CuO

molar mass to Cu molar mass, the CNT weight ratio in CNT/Cu fiber was estimated. Finally, vol.% of composite fibers were obtained by considering the density of 2 and 8.96 g/ml for CNTs and Cu, respectively. To obtain the CNT content in the CNT-Cu fibers, TGA was performed on CuO-CNT fibers. This was done prior to reduction of CuO to Cu for simplicity since the oxidation of copper may interfere with CNT decomposition.

4.3. Results and discussion

Figure 4-1 schematically represents the fabrication process of high-aspect-ratio composite CNT-Cu fibers using electrospinning. The process starts with mixing the copper nitrate and CuNW-CNT dispersions with polymer aqueous solution as described in the experimental section. Electrospinning was carried out at room temperature and the humidity was controlled to less than 40% to facilitate the solvent evaporation. After electrospinning, the fibers were calcinated at 400 ºC in air to remove the polymer and decompose the copper source to CuO, followed by annealing at 300 ºC in reforming gas to reduce the CuO into copper-based fibers. The complex precursor used here showed poor spinnability and the fabricated fibers after heat treatments were short and non-uniform. It was observed that introduction of a small amount of CuNW to the precursor proved to be an effective approach for overcoming this issue. CuNW acts as a foundation for decomposing copper nitrate, and can improve the CNT dispersion in the precursor solution which leads to smooth, uniform, and long ultrasmall-diameter copper-based fibers. As a result, a fixed amount of CuNW was included in the precursor for process optimization, alongside water, Cu acetate and the polymer. The effects of CuNW on fiber quality and electrical properties will be further discussed in detail.

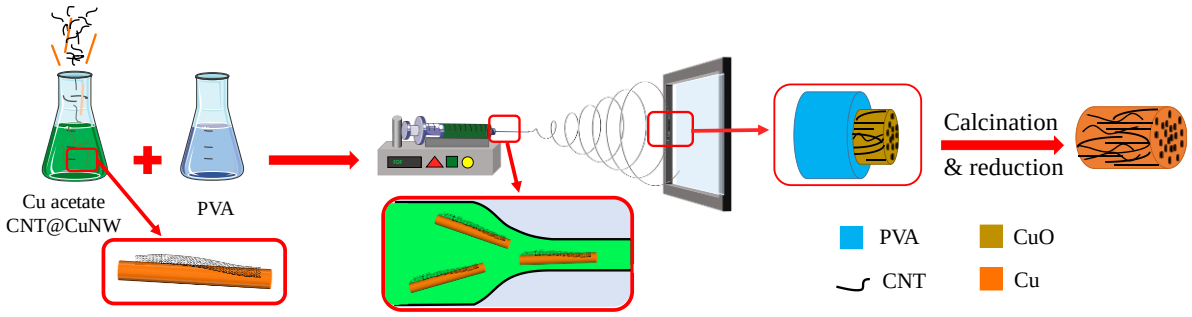

Figure 4-1. The schematic of fabricating CNT/Cu composite fibers. Through proper surface modification of CNTs, they form a stable colloidal suspension with CuNW in the precursor solution. The spinning process aligns the CNT-CuNW hybrids in the direction of fiber.

Electrospinning process and the quality of the fibers can be affected by many parameters including voltage, type of polymer, salt, and solvent [10]. PVP and PVA are the most common polymers that are used as a carrier for fabrication of inorganic fibers via electrospinning [11, 14, 18-20]. To dissolve the PVA in water properly, it is suggested to first stir the solution overnight at room temperature and then increase the temperature to at least 85 ºC for three to four hours. To avoid polymer hydrolysis and maximizing the stability of the Cu acetate-PVA solution, a small amount of acetic acid can be added [10]. In comparison, PVP can be easily dissolved in water at room temperature in less than two hours and there is no concern about its hydrolysis in the presence of Cu acetate. Even though preparing a PVP aqueous solution is simpler, our results show that PVA and copper nitrate can produce copper-based fibers with significantly better quality. After electrospinning of the precursor and heat treatment steps, it is observed that the fibers made by using PVA are more uniform, smooth, continuous, and have high aspect ratio. The weight ratio between copper nitrate and polymer also plays a major role in quality of the fibers. When this ratio is too high, a stable electrospinning jet cannot form; as a result, no fiber is produced. If the ratio is too low, after removing the polymer, discrete particles or short fibers are obtained. The CuNW content is another parameter that was

optimized. Taylor cone at low CuNW loading is unstable which leads to short and inhomogeneous fibers, and at high CuNW content no fibers is formed.

CNT concentration and its surface chemistry are among other important parameters. The effect of these parameters on spinnability and morphology of the calcinated fibers is presented in Figure 4-2. As it can be observed, by functionalization and lowering the CNT loading, quality of the fabricated fibers improves. Surface chemistry of CNTs has a major role on the spinnability and properties of the fibers in two different ways: (a) CNT dispersion and (b) CNT-copper interactions. CNT agglomeration can clog the spinning syringe and destabilize the jet which leads to non-uniform and short fibers, if any. This is more significant for pristine CNTs (P-CNT); by adding only 5 vol% P-CNT into the precursor, the spinning process can only go on for 8-10 minutes, and higher CNT content does not lead to fiber formation (Figure 4-2a). Acid treatment of CNTs creates carboxyl groups on the surface and enhances their dispersion in polar solvents and improves their interaction with metals [21]. By introducing oxidized CNTs (O-CNT) to the precursor, the dispersion becomes more homogenous and the electrospinning process could be continuously carried out in 5 vol% to 15 vol%. As the O-CNT content increases, the smoothness and quality of the fibers deteriorate. At higher O-CNT loading, the Taylor cone becomes unstable and after a few minutes the process stops.

Another functionalization approach investigated here is thiol activation. Previous research has reported that thiol activated CNTs (SH-CNT) show enhanced affinity towards Cu [4, 22]. Consequently, through a facile wet chemistry technique described in the experimental section, CNTs were functionalized with thiol groups. By incorporating SH-CNT, the Taylor cone is stable at 20 vol% filler loading and fibers have generally better quality. It is worth noting that

SH-CNT in water and ethanol have poor dispersion, but in the presence of CuNW, the dispersion stability improves significantly. Similar results have been previously reported for SH-CNTs in water-gold colloids [23]. Therefore, for achieving the best result, a colloid dispersion of CuNW – SH-CNT with mass ratio of 1:1 to 1:4 before adding the Cu acetate was prepared. As it can observed in Figure 4-2b and Figure 4-2c, SH-CNTs have high affinity towards CuNWs and readily wrap around them, while the O-CNTs are not able to cover the CuNWs as much. Therefore, it is speculated that during the spinning process, CuNWs will act as carrier for SH-CNT and increase the CNT content in the CNT/Cu fiber. On the other hand, P-CNT has poor affinity towards metallic source, i.e., copper acetate, which leads to its segregation in the polymer, i.e., PVA. This conjecture is supported by the thermogravimetric analysis (TGA) results (Figure 4-3). TGA experiments were carried out on fibers after calcination but before the reduction step, i.e., on CNT/CuO fibers. Before TGA, samples were washed twice with ethanol and water and dried in vacuum oven over night to remove any loose CNTs. Results for the P-CNT/Cu and 5 vol% O-CNT/Cu samples are not reported since the achieved value was below 1 wt% and close to margin of error. As it can be observed, by thiol activation, comparatively more CNTs are transferred and encapsulated in the Cu fibers. Also, it was noticed that by increasing the SH-CNT loading, a lower fraction of loaded filler is found inside the composite fiber. This is attributed to the insufficient amount of CuNW to stabilize CNT in the precursor solution. At low SH-CNT concentration, all the CNTs are able to bind with the CuNW but as the loading increases there is less CuNW surface available for SH-CNT adsorption.

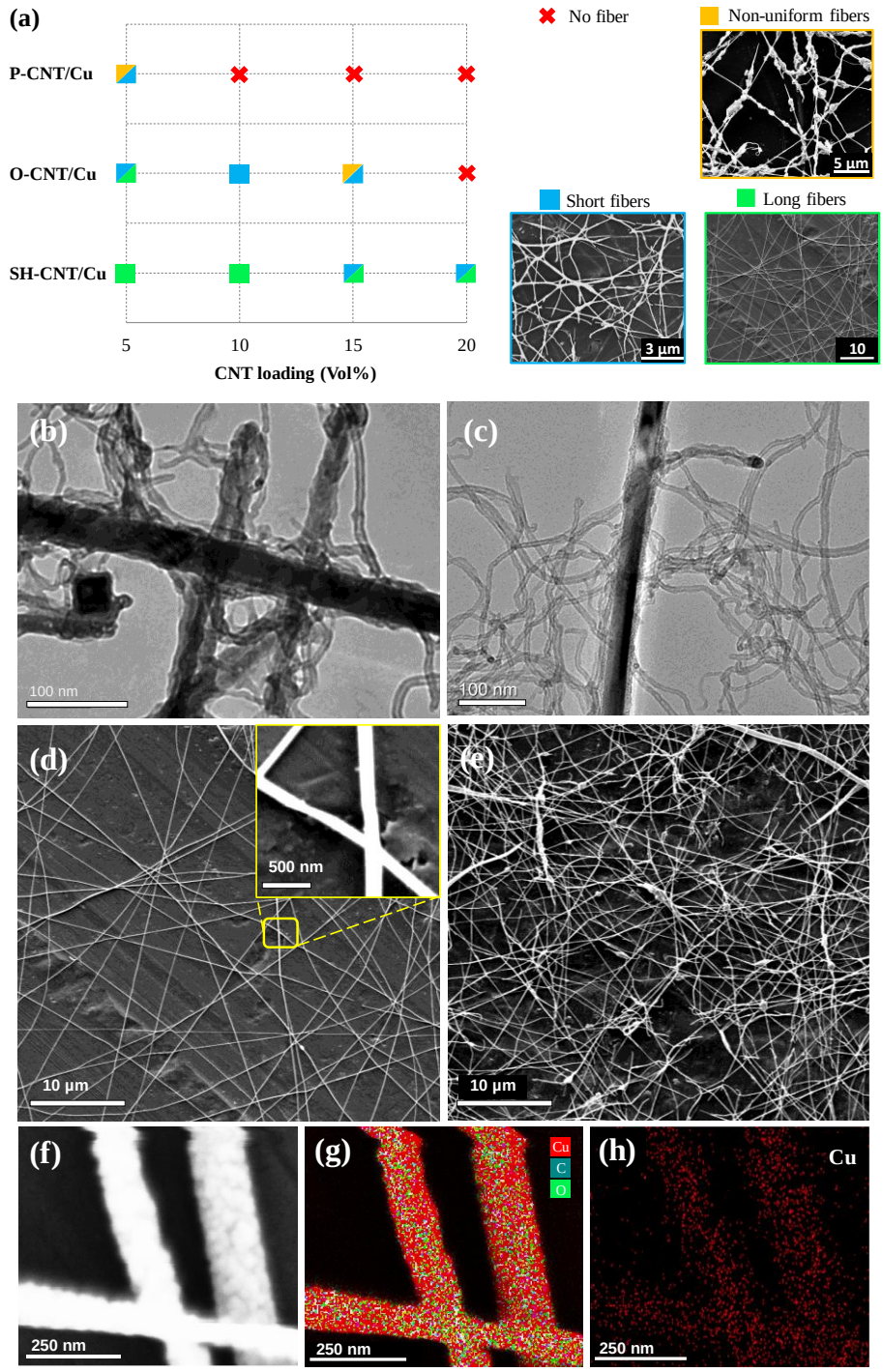

Figure 4-2. (a) Typical composite fiber morphologies with respect to CNT functionalization and loading. Representative TEM images of SH-CNT (b) and O-CNT (c) interactions with CuNWs. SEM images show that ultralong and smooth Cu fibers can be produced with the help of CuNW (d). Incorporation of CNTs causes non-uniformity in the fibers (e). Corresponding EDS mapping of Cu fibers show the composition of the electrospun fibers (f-h).

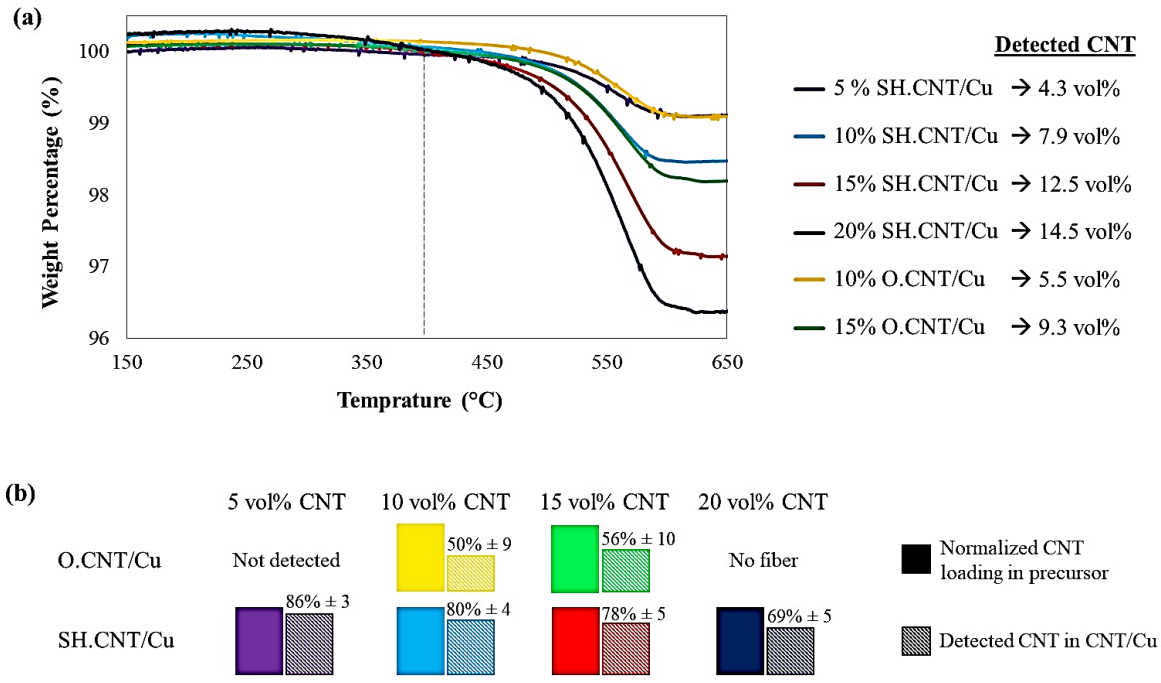

Figure 4-3. TGA results confirms the presence of CNTs inside the composite electrospun fibers (a). Moreover, based on these results, it is deduced that the surface functionalization of CNTs have a significant impact on the composition of produced fibers. The detected CNT content in the composite fibers based on the normalized CNT loading is presented in (b).

The electrical conductivity of single Cu, and composite fibers were measured by two-point probe method and the results are presented in Figure 4-4a. The conductivity of a single electrospun Cu fiber is 7.6×10^{6} S/m which is seven times lower than bulk copper. This issue has been previously observed for metal fibers produced by spinning techniques and it is mainly attributed to the impurities, rough surface, and microstructural defects of spun fibers [10, 11, 16, 24, 25]. However, when the Cu nanofiber is produced with CuNW in the precursor solution, the conductivity becomes almost one order of magnitude higher than the values reported in the previous works [16, 25]. When electrons migrate through the surface of conductive nanofiber, the surface roughness may deteriorate the electrical conductivity of the fibers. It is observed that employing a small amount of CuNW results in significantly smoother, more uniform, and

higher aspect ratio fibers which facilitate the electron transfer through the wire. High resolution SEM image indicates that the copper crystalline grains firmly combined with each other forming a solid continuous. High resolution SEM image indicates that the copper crystalline grains firmly combined with each other forming a solid continuous fiber (Figure 4-2b).

The effect of CNT inclusion and its surface chemistry on the electrical properties of composite fibers are also studied by using 15 vol% O-CNT/Cu and 20 vol% SH-CNT/Cu samples. For composite fibers lower electrical conductivities were recorded; the former showed conductivity of 3.6×10^{6} and the latter 3.4×10^{6} S/m. As observed in Figure 4-2a, CNTs generally increase the surface roughness and inhomogeneity in composite samples. Moreover, presence of fillers in the matrix can promote the electron scattering due to contact resistance and interfacial defects [26]. Despite the fact that 20 vol% SH-CNT/Cu sample has 50% higher CNT content compared with 15 vol% O-CNT/Cu (TGA results: Figure 4-3a), they have almost similar room temperature conductivities. It has been previously reported that due to strong interaction, Cu can readily wet the SH-CNT surface and form dense hybrid structure [4]. It was also observed that upon mixing, SH-CNTs wrap around the CuNW and form a uniform and stable dispersion (Figure 4-2d). This, not only improves the CNT-Cu interactions, but also regulates the CNT transfer from the syringe to the Taylor cone creating relatively smoother and more uniform fibers (Figure 4-2 c). Therefore, the superior performance of SH-CNT/Cu sample despite having more filler is attributed to its better morphology and filler-matrix interaction.

The ampacity of the fibers was measured by mounting two sides of the fiber on a silicon wafer using silver paste and applying DC current. Voltage was gradually increased while the current was recorded. At lower current densities, voltage is linearly proportional to the current

(ohmic behavior). By increasing the voltage, more current passes through the wire creating heat in the wire, i.e. Joule heating. Due to this heat electron scattering and as a result electrical resistance increases. By further increasing the voltage, current reaches its maximum and starts to decrease. By dividing the maximum current by the wire cross section, the ampacity was obtained. It is worth noting that the electrical conductivity of the fibers was obtained from the linear portion of the I–V curve. As represented in Figure 4-4b, the ampacity of the SH-CNT/Cu reaches 8.2×10^5 A/cm^2, which is comparable to bulk copper. These remarkable results show that by proper surface modification it is possible to fabricate highly conductive CNT/Cu nanostructures using spinning techniques for versatile applications in stretchable electronics to transparent conductive electrodes (TCE), and others.

Indium tin oxide (ITO) is the most common used material in TCEs in numerous applications, from touch screens to solar cells. In addition to high cost, their poor mechanical flexibility encouraged researchers to develop new alternatives. Due to their high ductility and electrical conductivity, metal-based electrodes are intriguing candidates for this purpose. These TCEs are mainly fabricated by using nanowires (NW) or spun fibers of Ag and Cu. For instance, Ag nanowire-based TCEs can have low sheet resistance ($10 < Rs < 50$ Ω/□) at high transmittance ($T > 80\%$) [27-31]. High cost of silver has derived scientists towards using CuNW (1% the cost of silver and 1000 times more abundant than silver and indium [32]). Their conductivity-transmission performance is similar to their Ag-based counterparts, but they are susceptible to oxidation [33-37]. Despite the promising performance, nanowire systems suffer from high contact resistance, oxidation, and low processability. Consequently, spinning techniques are being studied for fast production of metallic meshes for TCEs [11, 24].

Generally, there is an excellent controllability over the size of the fabricated fibers and submicron ultralong fibers can be made. When the diameter and length of the final fiber form are increased to submicron and centimeter scales, the issues regarding oxidation and contact resistance are alleviated since there are fewer contact points in a network of longer fibers. However, the scope of metal-based TCE applications is limited by their inherent high light reflection and temperature-dependent performance [28, 38]. In this study, the application of these novel electrospun CNT/Cu fibers for transparent electrodes are investigated.

To study the photoelectric properties of Cu and CNT/Cu electrospun fibers, sheet resistance of samples with different transmittance and composition at wavelength of 550 nm was measured. The sheet resistance is a function of electrospinning duration; as electrospinning takes longer more fibers are deposited on the substrate. As a result, the sheet resistance and transparency both decrease. This is attributed to the fact that at the first stages of electrospinning, a connected mat of spun fibers cannot be formed. Moreover, the time required for making a conductive pathway is longer for CNT/Cu fibers. It is known that in such conductive networks, the resistance is dominated by the inter-fiber resistance and the contribution from the individual fiber resistance is negligible [39]. As observed in Figure 4-2e, composite fibers are generally shorter compared with Cu fibers, meaning they require more fibers to form a conductive network. For the same reason, the ultralong Cu sample fabricated here outperforms the similar TCEs in the literature such as [13]. As discussed before, CuNW incorporation produces smooth and highly conductive fibers with length that can reach to a few millimeters. This significantly reduces the number of junctions per unit area of the film, which provides a path for electron transportation within the network with less electron scattering due

to surface defects and contact resistance. Figure 4-4g shows that the Cu electrospun mesh can be successfully transferred onto flexible substrates such as gloves and still preserve its conductivity. It is speculated that this remarkable performance is a result of CuNW introduction which regulates the spinning process and produces ultralong fibers. The sheet resistance of the CNT/Cu fibers are slightly lower and they require longer spinning duration to form a conductive network. This was not surprising since these fibers are comparatively shorter. Nevertheless, their performance is still excellent compared to solution-processed metallic NWs [13, 37, 38, 40-42], polymers coatings [43, 44], graphene-based electrodes [45], and CNT thin films [39, 46].

4.4. Conclusion

In conclusion, conductive Cu-CNT composite fibers with high aspect-ratio and excellent ampacity are fabricated using electrospinning. There are two key points in the successful process demonstrated here: (a) addition of CuNW and (b) proper surface modification of CNTs. By addition of CuNW, smooth and long fibers with aspect ratio of more than 5000 times and conductivity of 7.6×10^{6} S/m were produced. The composite fiber shows an impressive ampacity of 8.2×10^{5} A/cm^2 which is around 40% higher than Cu fibers. Moreover, it is shown that this method can be used to fabricate highly conductive transparent electrodes; for the Cu mat the sheet resistance was 25 Ω/□ at transparency of 85%, outperforming the previous works based on electrospun metallic fibers. These fibers have high ductility and can be transferred to flexible substrates such as gloves. The CNT/Cu composite fibers also show low sheet resistance at transparency below 85%, comparable to the commercial ITO based TCEs. These findings are not limited to electrospinning and can be readily modified and used in other spinning methods

which may result in even better properties. The continuous electrospinning used to prepare extra-long metal submicron fibers has great potential for numerous applications, ranging from light-weight portable electronics to solar cells.

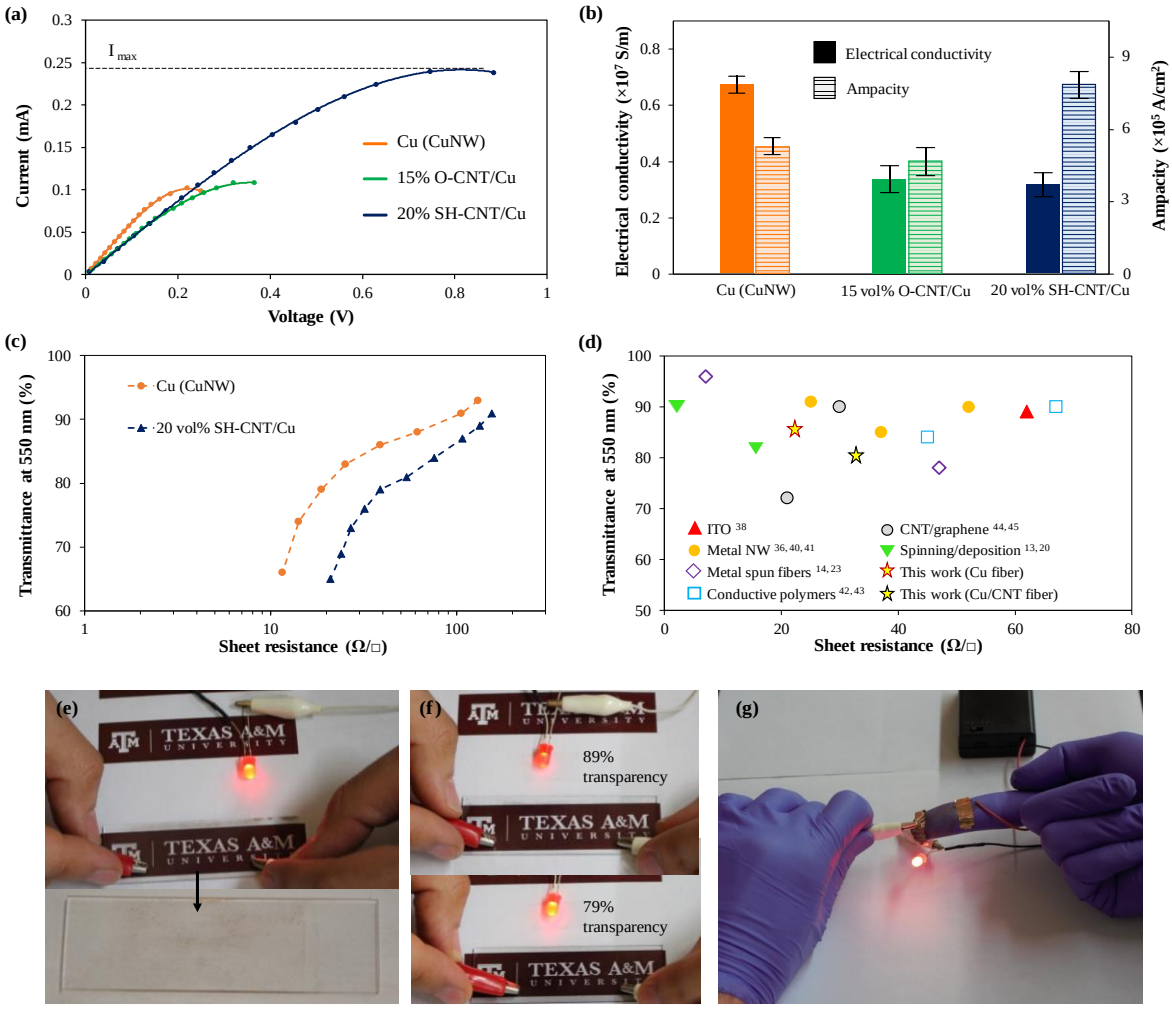

Figure 4-4. The electrical performance of Cu-based electrospun fibers. (a) I–V curves and the corresponding resistance of individual electrospun fibers. I_{max} is the maximum current that passes through the fiber, after which the current Joule heating dominates the electrical performance. The conductivity of each fiber is calculated based on the slope of the I-V curve at the linear section of the plot and the result are presented in (b). The transmittance versus sheet resistance of these submicron fibers are presented in (c). Compared to the previous works, the composite electrospun fibers have remarkable performance, comparable to the common commercial options (d). Demonstration of Cu (e) and CNT/Cu (f) performance in LED circuit. In (f), the top image represents the performance of a TCE with 89% transmittance and the one below is for TCE with 81% transmittance. The Cu electrospun fibers can be transferred to other substrates including gloves showing their potential application in stretchable electronics (g).

4.5. References

1. Collins, P.G., et al., *Current saturation and electrical breakdown in multiwalled carbon nanotubes.* Physical review letters, 2001. **86**(14): p. 3128.

2. Wang, X., et al., *High-Ampacity Power Cables of Tightly-Packed and Aligned Carbon Nanotubes.* Advanced Functional Materials, 2014. **24**(21): p. 3241-3249.

3. Subramaniam, C., et al., *One hundred fold increase in current carrying capacity in a carbon nanotube–copper composite.* Nature communications, 2013. **4**: p. 2202.

4. Daneshvar, F., et al., *Tuning the composition and morphology of carbon nanotube-copper interface.* Carbon, 2019.

5. Han, B., et al., *Fabricating and strengthening the carbon nanotube/copper composite fibers with high strength and high electrical conductivity.* Applied Surface Science, 2018. **441**: p. 984-992.

6. Tran, T.Q., et al., *High-Performance Carbon Fiber/Gold/Copper Composite Wires for Lightweight Electrical Cables.* Journal of Materials Science & Technology, 2019.

7. Han, B., et al., *Fabrication and densification of high performance carbon nanotube/copper composite fibers.* Carbon, 2017. **123**: p. 593-604.

8. Xu, G., et al., *Continuous electrodeposition for lightweight, highly conducting and strong carbon nanotube-copper composite fibers.* Nanoscale, 2011. **3**(10): p. 4215-4219.

9. Milowska, K.Z., et al., *Breaking the electrical barrier between copper and carbon nanotubes.* Nanoscale, 2017. **9**(24): p. 8458-8469.

10. Khalil, A., et al., *Electrospun metallic nanowires: Synthesis, characterization, and applications.* 2013. **114**(17): p. 12_1.

11. Wu, H., et al., *Electrospun metal nanofiber webs as high-performance transparent electrode.* 2010. **10**(10): p. 4242-4248.

12. Greiner, A. and J.H. Wendorff, *Electrospinning: a fascinating method for the preparation of ultrathin fibers.* Angewandte Chemie International Edition, 2007. **46**(30): p. 5670-5703.

13. Yang, X., et al., *Large-scale stretchable semiembedded copper nanowire transparent conductive films by an electrospinning template.* 2017. **9**(31): p. 26468-26475.

14. Hsu, P.-C., et al., *Passivation coating on electrospun copper nanofibers for stable transparent electrodes.* 2012. **6**(6): p. 5150-5156.

15. Einert, M., et al., *Electrospun CuO nanofibers: stable nanostructures for solar water splitting.* 2017. **1**(7): p. 326-340.

16. Bognitzki, M., et al., *Preparation of sub-micrometer copper fibers via electrospinning.* 2006. **18**(18): p. 2384-2386.

17. Aziz, A., et al., *1D copper nanowires for flexible printable electronics and high ampacity wires.* Nanoscale, 2017. **9**(35): p. 13104-13111.

18. Lee, H., et al., *Fabrication and electrical properties of platinum nanofibres by electrostatic spinning.* 2009. **42**(12): p. 125409.

19. Xiang, H., et al., *A novel and facile method to prepare porous hollow CuO and Cu nanofibers based on electrospinning.* 2011. **13**(15): p. 4856-4860.

20. Wu, H., et al., *A transparent electrode based on a metal nanotrough network.* 2013. **8**(6): p. 421.

21. Banhart, F.J.N., *Interactions between metals and carbon nanotubes: at the interface between old and new materials.* 2009. **1**(2): p. 201-213.

22. Rigo, A., et al., *Interaction of copper with cysteine: stability of cuprous complexes and catalytic role of cupric ions in anaerobic thiol oxidation.* 2004. **98**(9): p. 1495-1501.

23. García-González, R., et al., *Dispersion studies of carboxyl, amine and thiol-functionalized carbon nanotubes for improving the electrochemical behavior of screen printed electrodes.* Sensors and Actuators B: Chemical, 2013. **181**: p. 353-360.

24. Bai, X., et al., *Continuous draw spinning of extra-long silver submicron fibers with micrometer patterning capability.* 2017. **17**(3): p. 1883-1891.

25. Hansen, N.S., D. Cho, and Y.L.J.S. Joo, *Metal Nanofibers with Highly Tunable Electrical and Magnetic Properties via Highly Loaded Water-Based Electrospinning.* 2012. **8**(10): p. 1510-1514.

26. Milowska, K.Z., et al., *Carbon nanotube functionalization as a route to enhancing the electrical and mechanical properties of Cu–CNT composites.* 2019. **11**(1): p. 145-157.

27. Ahn, Y., et al., *Improved thermal oxidation stability of solution-processable silver nanowire transparent electrode by reduced graphene oxide.* 2012. **4**(12): p. 6410-6414.

28. Khaligh, H.H. and I.A.J.N.r.l. Goldthorpe, *Failure of silver nanowire transparent electrodes under current flow.* 2013. **8**(1): p. 235.

29. Krantz, J., et al., *Solution-processed metallic nanowire electrodes as indium tin oxide replacement for thin-film solar cells.* 2011. **21**(24): p. 4784-4787.

30. Tokuno, T., et al., *Fabrication of silver nanowire transparent electrodes at room temperature.* 2011. **4**(12): p. 1215-1222.

31. Yu, Z., et al., *Highly flexible silver nanowire electrodes for shape-memory polymer light-emitting diodes.* 2011. **23**(5): p. 664-668.

32. Yao, S. and Y.J.A.m. Zhu, *Nanomaterial-enabled stretchable conductors: strategies, materials and devices.* 2015. **27**(9): p. 1480-1511.

33. Zhang, T., et al., *Solution-Processable Oxidation-Resistant Copper Nanowires Decorated with Alkyl Ligands.* 2019.

34. Zhang, T., et al., *Synthesis of oxidation-resistant electrochemical-active copper nanowires using phenylenediamine isomers.* 2019. **162**: p. 154-161.

35. Hwang, C., et al., *Controlled aqueous synthesis of ultra-long copper nanowires for stretchable transparent conducting electrode.* 2016. **4**(7): p. 1441-1447.

36. Dou, L., et al., *Solution-processed copper/reduced-graphene-oxide core/shell nanowire transparent conductors.* 2016. **10**(2): p. 2600-2606.

37. Chu, H.-C., et al., *Spray-deposited large-area copper nanowire transparent conductive electrodes and their uses for touch screen applications.* 2016. **8**(20): p. 13009-13017.

38. Ji, S., et al., *Haze-free transparent electrodes using metal nanofibers with carbon shells for high-temperature stability.* 2019. **483**: p. 1101-1109.

39. Hecht, D.S., L. Hu, and G.J.A.m. Irvin, *Emerging transparent electrodes based on thin films of carbon nanotubes, graphene, and metallic nanostructures.* 2011. **23**(13): p. 1482-1513.

40. Guo, F., et al., *High-performance semitransparent perovskite solar cells with solution-processed silver nanowires as top electrodes.* 2015. **7**(5): p. 1642-1649.

41. Zhang, D., et al., *Synthesis of ultralong copper nanowires for high-performance transparent electrodes.* 2012. **134**(35): p. 14283-14286.

42. Jiu, J., et al., *Facile synthesis of very-long silver nanowires for transparent electrodes.* 2014. **2**(18): p. 6326-6330.

43. Vosgueritchian, M., D.J. Lipomi, and Z.J.A.f.m. Bao, *Highly conductive and transparent PEDOT: PSS films with a fluorosurfactant for stretchable and flexible transparent electrodes.* 2012. **22**(2): p. 421-428.

44. Kee, S., et al., *Highly Deformable and See-Through Polymer Light-Emitting Diodes with All-Conducting-Polymer Electrodes.* 2018. **30**(3): p. 1703437.

45. Bae, S., et al., *Roll-to-roll production of 30-inch graphene films for transparent electrodes.* 2010. **5**(8): p. 574.

46. Liu, K., et al., *Cross-Stacked Superaligned Carbon Nanotube Films for Transparent and Stretchable Conductors.* 2011. **21**(14): p. 2721-2728.

5. TIN OXIDE AS AN INTERMEDIATE LAYER FOR COPPER OXIDE- CARBON NANOTUBE SUPERCAPACITORS [*]

5.1. Introduction

Stringent environmental regulations, ever-increasing interest in electric vehicles (EV), and their fast market growth have enticed automotive companies to push for EVs sooner than anticipated. Extensive work on rechargeable batteries made this transition feasible. However, there are still significant obstacles to overcome. One of the deficiencies of rechargeable batteries occurs during acceleration of EVs when the battery is required to provide a huge amount of energy in a short period of time. This rapid energy depletion can damage the electrode materials, and reduce the battery's lifetime [1]. Therefore, there has been an effort to develop novel electrode materials with higher power density and better stability [2, 3]. An alternative solution has been implemented: a complementary system alongside the battery, which has high cyclability and can provide the demanded energy during acceleration [4, 5]. Supercapacitors or electrochemical capacitors (ECs) are an attractive option due to their high-power density, long life span, high cyclic efficiency, safety and rapid charge-discharge rates [5-7].

Based on energy storage mechanisms, supercapacitors are categorized into two groups: electrical double layer capacitors and pseudocapacitor. The former purely works based on electron storage at double layer while in the latter, faradic redox reactions occur which results

[*] Reprinted with permission from "Porous SnO_2–Cu_xO nanocomposite thin film on carbon nanotubes as electrodes for high performance supercapacitors" by Daneshvar, Farhad, et al., *Nanotechnology* 30.1 (2018): 93-109. Copyright 2018 by IOP Publishing, Ltd.

in significantly higher specific capacitance and energy density [8, 9]. Pseudocapacitors typically are made of either polymers or transition metal oxides (TMOs). While polymers have good specific capacity and electrical conductivity, they suffer from poor cyclability due to substantial volume changes [10]. TMOs, on the other hand, generally possess higher specific capacitance, but their electrical conductivity is poor [11, 12]. Because pseudocapacitance relies on faradic reactions at the surface, a higher specific surface area provides more sites for metal oxide redox reactions, which improves the specific capacitance of the TMOs. In addition to specific surface area, electrical conductivity and microstructure also play major roles on capacitive behavior of TMOs.

Copper oxide is one of the promising TMOs for supercapacitor applications. It is an inexpensive and abundant material that possesses high theoretical capacity [13-15]. Therefore, recently these oxides, either in CuO or Cu_2O form, have attracted considerable interest as EC electrode material [14-20]. However, the electrochemical performance of these oxides suffers due to low conductivity and limited specific surface area [20, 21]. To tackle the obstacle of low electrical conductivity, hybridization with conductive carbon-based materials such as carbon black, graphene, or carbon nanotubes (CNTs) has been suggested [17, 22-26]. Among these, CNTs have attracted particular attention due to their high electrical conductivity, specific surface area, mechanical strength, electrochemical stability, and low electrical percolation threshold. As Liu et al. [18] has shown, by introducing CNTs to electrode materials a conductive network is created which facilitates charge transfer through the electrode and enhances the specific capacitance of CuO nano-sheets significantly.

However, progress in integrating CNTs in supercapacitors has been limited. For instance, Zhang et al. [23] observed that substituting CNT for carbon black as an additive in CuO electrode material not significantly increased the specific capacitance (from 137 F/g to 150 F/g). Nevertheless, previous research has shown that using CNTs during the synthesis of active material can yield advantages far beyond just forming a conductive network. In this case, CNTs can yield strong bonds with metal oxides by acting as supports or templates for nucleation and growth of active material. This not only enhances the charge transfer, but also results in size refinement, hinders agglomeration, and creates a coarse and mesoporous structure that results in higher capacitance through easier charge transfer and higher specific surface area [25, 27-29].

In addition to hybridization with carbon nanostructures, hybridization with transition metal oxides has shown to be a promising method for improving the electrochemical performance of electrodes in supercapacitors [29-32]. For instance, Sugimoto et al. [31] reported that by introducing VO_2 to RuO_2 the specific surface area was tripled and specific capacitance reached to 1210 F/g, which exceeds that of Ru_2O electrode by 60%. In addition to increasing the surface area, doping a secondary oxide can improve the electrochemical performance by enhancing the conductivity, uniformly dispersing the active material or refining the particle size. Stannic oxide is one of the oxides that has been studied as an additive in composite electrodes. SnO_2 not only has the conventional redox properties, but also is inexpensive, has high wettability, and relative to other TMOs, has higher electronic conductivity [5]. It has been observed that adding SnO_2 has a synergistic effect on electrode performance especially through increasing electrical conductivity and facilitating electron and proton conduction [32]. Therefore, regardless of the

material type, by choosing a suitable additive the electrochemical performance of the electrode can be enhanced.

In this work multi-walled CNTs (MWCNTs) were used as a template for growth of tin and copper oxides (CuO_x-SnO_2) nanoparticles using electroless deposition (ED). ED is a simple and scalable technique which provides morphology control by easily changing the parameters, such as pH and bath composition, and can produce rough and porous structures [33, 34]. Moreover, by using MWCNTs we were able to engineer the morphology of SnO_2-Cu_xO thin film in nanoscale and create a one-dimensional (1D) porous structure which offers high surface area and short transport/diffusion pathways for electrons/ions which leads to fast kinetics and high capacity. Strong bonding between the thin film and MWCNTs and 1D porous SnO_2-Cu_xO structure provides an excellent cycle stability through accommodating the volume changes caused by faradic reactions. Electrochemical tests have shown that deposition of tin and copper oxides on CNTs can result in a hybrid material which outperforms any reported copper-based and tin-based supercapacitors in the literature with respect to specific capacitance and cyclability.

5.2. Experimental procedure

5.2.1. Materials and methods

Multiwall carbon nanotubes (MWCNT) with a purity of 95 wt.%, diameter of 20-40 nm and length of 10-30 μm were supplied by Arkema Inc. All other chemicals were obtained from Sigma-Aldrich and were used as received. For obtaining a good dispersion they were exfoliated according to previous report [35]. Briefly, 250 mg as-received MWCNTs were added to a

mixture of H_2SO_4 (45 mL) and HNO_3 (15 mL) at a 3:1 volume ratio. This mixture was sonicated in a sonication bath for two hours at 25 °C [36] [40] and then washed with DI water.

Synthesis of SnO_2-Cu_xO/CNT hybrid structure by ED consists of several steps which are schematically represented in Figure 5-1. First 50 mg of oxidized MWCNTs were added to a 50 ml aqueous solution of $SnCl_2$ (0.98 g) and 0.1 ml HCl (37 wt.%). The mixture was sonicated for 15 minutes, and then washed with DI water. CNTs usually have weak interactions with metallic particles. In supercapacitor applications this can result in lower conductivity and detachment of metal oxides from the CNTs. Tin has a high wetting capability and therefore readily attaches to the surface of MWCNTs. Tin layer will act as an intermediate layer for adsorption of other metallic-based particles during following processing steps. In the next step, sensitized MWCNTs are added to 50 ml DI water solution containing 0.007 g $PdCl_2$ and 0.1 ml HCl (37 wt.%) and sonicated for 15 minutes. During this stage (i.e. activation), palladium ions replace a portion of the tin particles on the surface of MWCNTs and act as catalysts for nucleation and growth of copper. Finally, after washing with DI water, activated MWCNTs are dispersed in 50 ml copper electroless deposition (ED) bath with the chemical composition presented in Table 5-1. After 15 minutes of stirring at 60 °C, 0.2 ml formaldehyde solution was added gradually to reduce the copper ions. After 30 minutes of stirring at 60 °C copper coated MWCNTs were washed and separated by centrifuge.

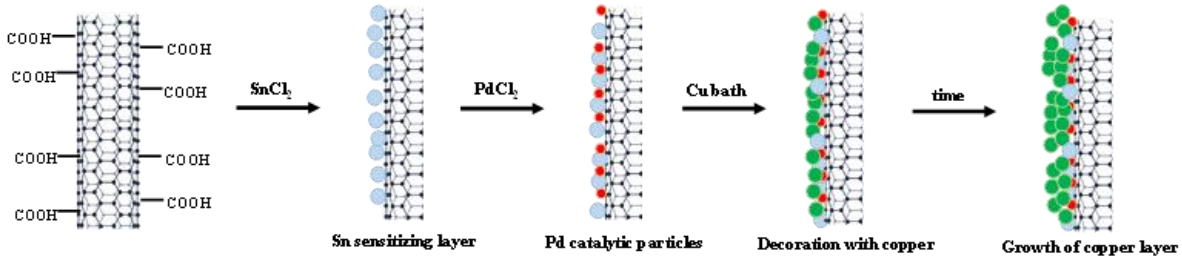

Figure 5-1. A schematic of an electroless deposition process on CNTs. Blue, red and green spheres represent Sn, Pd and Cu particles respectively.

5.2.2. Characterization

For assessing the coating morphology transmission electron microscope (TEM, FEI Teccai G2 S-Twin, Philips) was used. The crystallographic phases of all of the samples were investigated using an X-ray diffractometer (XRD, Bruker D8 Advance ECO) with CuK_{α} incident radiation (λ=0.1506 nm). X-ray photoelectron spectroscopy (XPS) was obtained from an Omicron's DAR 40 dual Mg/Al X-ray source for XPS measurements and the HIS 13 He UV source for UPS measurements. STEM and EDX images were obtained using a FEI Tecnai Osiris S/TEM working at 200 keV. The EDX detectors are FEIs Super-X system employing 4 Bruker silicon drift detectors (SDD) for high collection efficiency (>0.9 sr solid angle) and high-count rates (>250 kcps).

5.2.3. Materials and methods

The electrochemical performance of the supercapacitors was tested in a conventional three-electrodes (versus Ag/AgCl)) and two electrodes coin cells. All the electrochemical measurements including cyclic voltammetry and galvanostatic charge/discharge were conducted using Iviumstat Electrochemical Interface. Cyclic voltammetry tests have been carried out with the two-electrode cells. Electrodes were prepared by mixing the hybrid material with poly-vinylidene fluoride (PVDF) and carbon black (CB) (80:10:10 in mass ratio)

using a pestle and mortar. Cyclic voltammetry (CV) measurements were recorded in a 6 M KOH aqueous electrolyte in the range of -0.4 to 0.4 V at different scan rates.

Table 5-1. Chemical composition of copper electroless bath.

Chemical composition	Quantity
$CuSO_4.5H_2O$	6.2 g/l
2Na-EDTA	40 g/l
Na_2SO_4	35 g/l
HCOONa	60 g/l
CHOH (37 vol% in water)	20 ml/l
Temperature	60 °C
pH (NaOH)	13

5.3. Results and discussion

The chemical composition of the hybrid system was investigated by XPS, XRD and EDX. Figure 5-2a represents the XPS spectrum where the peaks at binding energies of 284.4, 486.5 and 933.9 eV correspond to C 1s, Sn 3d and Cu 2p, respectively. The C 1s peak is associated with the sp^2 C-C bond of MWCNTs and can be deconvoluted into C=C at 284.3 eV, C-O at 285.8 eV and C=O at 288.2 eV [37-39]. The presence of these peaks underneath the C 1s is an indication of functional groups on the surface of MWCNTs created during acid treatment. These groups not only enhance the bonding between the metal oxides and MWCNTs, but also increase the wettability and hydrophilicity of the hybrid system which helps increase electrolyte ion transport within the structure. Moreover, Pan, et al. [40] observed redox peaks in CV curves of functionalized CNTs indicating that these oxygenated groups on the surface may induce faradic redox reactions which can enhance the specific capacitance. Finally, it should be noted that proper acid treatment can increase the specific surface area of MWCNTs either by creating

defects at the surface or dissolving the catalysts and opening the tube ends. As a result, due to capillary forces during ED process, metallic ions can diffuse and deposit inside the tube.

The peaks related to Sn are situated at 495 eV and 486.6 eV belonging to Sn 3d3/2 and Sn 3d5/2, respectively. These results are identical to the reference data for Sn 3d in SnO_2 [42]. As represented in Figure 5-2d, the high-resolution XPS spectra for Cu consist of 4 peaks. The peaks observed at 933.9 eV and 953.3 eV are attributed to Cu 2p3/2 and Cu 2p1/2, respectively [42]. Moreover, two strong satellite peaks are seen at higher binding energies compared to the main peaks: a sharp peak at 962.35 eV and a broad peak between 941 to 945 eV. The overall spectrum is similar to CuO. However, by analyzing the main Cu 2p1/2 peak more carefully, it can be noted that at lower binding energies another peak exists; therefore, the Cu 2p3/2 peak can also be deconvoluted into two peaks by Gaussian method. The new peak at lower binding energy (932.3 eV) has a low intensity and is characteristic of Cu_2O [43, 44], confirming that CuO and Cu_2O oxides coexist in the deposited coating which is in accordance with XRD results (Figure 5-2e).

The morphology and microstructure of the hybrid system is represented in Figure 5-2f. It can be observed that the coating has a rough surface in nanoscale and contains pores less than 1 nm in size which makes this structure suitable for aqueous electrolytes [6]. Also, thickness of the coating is generally 10-15 nm. Such a fine and porous structure provides a large accessible surface area and facilitates electrolyte penetration [2]. As a result most of the nanocomposite can take part in faradic reactions which has a positive effect on capacitance.

From STEM images and nanoscale elemental maps (Figure 5-3) of the electroless deposited MWCNT, it is observed that the tube is present at the core and is uniformly covered with tin

and copper oxides. Images with lower magnification show that some of the MWCNTs are completely and some partially covered with metal oxide layer (the effect of coating density will be discussed). No observable x-ray signal was seen from palladium, which could be due the fact that it was completely covered by the Cu layer and the quantity was too small to be detectable.

As can be observed in Figure 5-2f and Figure 5-3, MWCNTs act as a template for deposition of fine copper nanoparticles and created a core-shell structure [45]. The C-OH and C=O bonds created during the acid treatment provide sites for adsorption of Sn/palladium ions. Since these defects eventually act as nucleation sites for copper, it is expected that application of functionalized MWCNTs also plays a major role in size refinement and morphology control [28]. The adsorbed Pd/Sn nuclei subsequently act as catalyst for reduction and nucleation of copper according to the following reaction [46]:

$$2HCHO + Cu^{2+} + 4OH^{-} \rightarrow 2HCOO^{-} + H_2 + 2H_2O + Cu \qquad 5\text{-}1$$

It should be noted that the produced copper in particles are in nanoscale therefore dissolved oxygen in water readily oxidizes the Cu and Sn particles. This can lead to finer particle size since copper growth favorably occurs on the fresh copper nuclei and oxidation hinders copper particle growth.

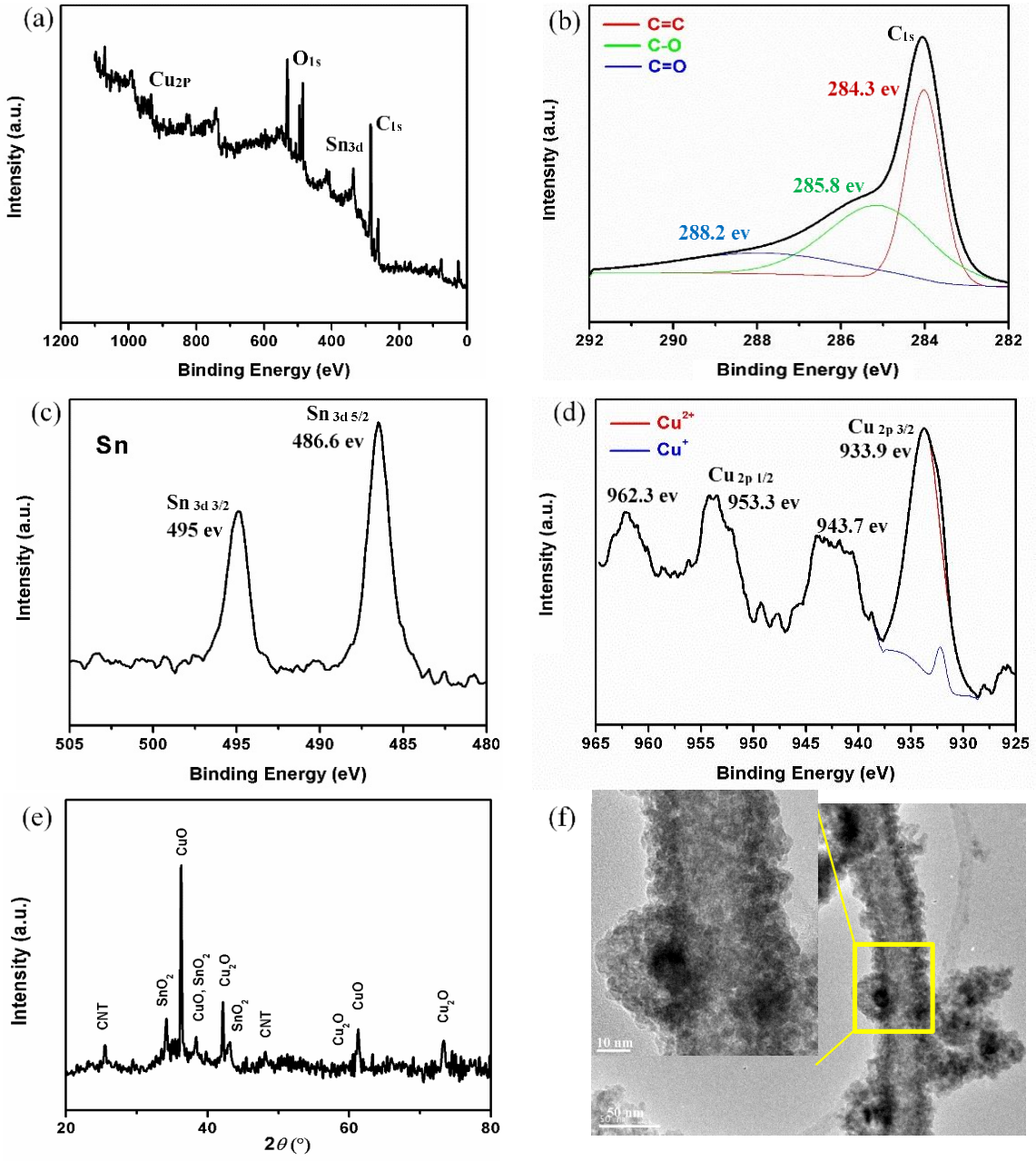

Figure 5-2. XPS spectra of (a) hybrid system, (b) C 1s of CNT, (c) Sn 3d of SnO_2, (d) Cu 2p spectrum of CuO/Cu_2O, (e) XRD of the hybrid sample and (f) TEM images of coated CNTs. The scale bar in the intersected picture is 10 nm.

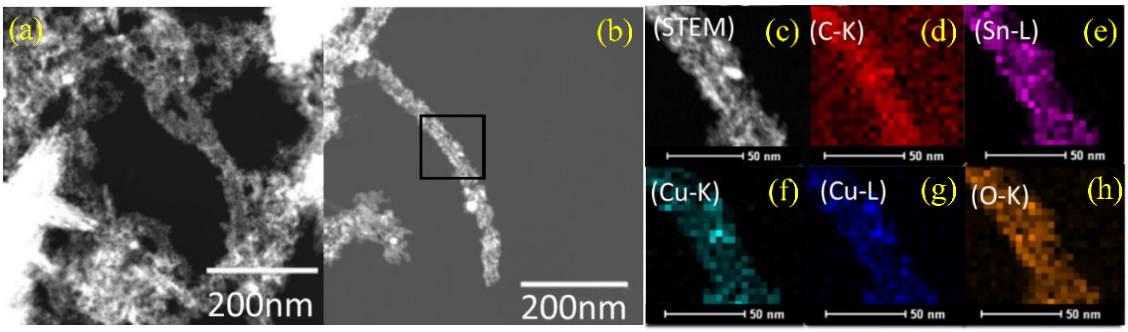

Figure 5-3. STEM (a-c) and EDX (d-h) of an electroless coated representative CNT. Black box shows the location where the elemental map is obtained.

Using a MWCNT backbone structure not only improves the electrical conductivity but also increases the surface area. As it can be seen in Figure 5-2f, deposited metal oxides adopt the 1-D structure of MWCNT and the maximum thickness reaches to 15 nm. By considering the porous structure of the thin film, we can assume that most of metal oxides are accessible by the electrolyte. Moreover, assembling these 1-D hybrid structures of SnO_2-Cu_xO/CNT creates a three-dimensional (3-D) porous conductive network which further enhances the electrolyte accessibility and promotes both electron and ion transport within the electrode material. Furthermore, we observed that the morphology, density and size of deposited particles are affected by the MWCNT surface modification method. If the oxidation of CNTs is not sufficient, the coating will be scarce. It should be noted that if the MWCNTs are fully coated with a thick layer of metal oxide, the conductivity of the hybrid system and as a result the capacitance of the electrode reduces [47]. It should be added that before performing TEM analysis, the sample was diluted in water and went through a sonication step. The fact that the coating is still attached after the sonication process shows that there is a strong interaction between the MWCNT and copper coating which can help to preserve the integrity of the

electrode through charge-discharge cycles and enhance the capacitance performance of the hybrid material [47-49].

The electrochemical performance of the supercapacitor electrode was assessed by cyclic voltammetry (CV) and galvanostatic charge/discharge tests in a two-electrode coin cell configuration. Figure 5-4a shows the CV curves of the MWCNT and the SnO_2-Cu_xO/CNT electrodes at scan rates 5 mV/s using a potential window from -0.4V to 0.4 in 6 M KOH solution. The CV curves of pure MWCNT show a nearly rectangular shape without any obvious redox peaks, indicating that the capacitance is primarily originated from double-layer capacitance. By utilizing SnO_2-Cu_xO/CNT as the electrode, two distinct reduction peaks and one oxidation peak were observed. While the observation of the redox peaks is a sign of pseudocapacitance contribution. The background current is significantly higher for SnO_2-Cu_xO/CNT than for MWCNT, which couples with the rectangular shape of the CV curve, suggests a double layer capacitance contribution from the copper oxide coating on MWCNTs. The pseudocapacitance behavior in the CV scans is associated with the following reactions [14, 50, 51]:

$$CuO + H_2O + 2e^- \rightarrow Cu_2O + 2OH^- \quad (5\text{-}2)$$

$$Cu_2O + H_2O + 2OH^- \rightarrow 2Cu(OH)_2 + 2e^- \quad (5\text{-}3)$$

$$CuOH + OH^- \rightarrow Cu(OH)_2 + e^- \quad (5\text{-}4)$$

$$CuOH + OH^- \rightarrow CuO + H_2O + e^- \quad (5\text{-}5)$$

$$SnO_2 + H_2O + e^- \rightarrow SnOOH + OH^- \quad (5\text{-}6)$$

$$SnOOH + e^- \rightarrow SnO + OH^- \quad (5\text{-}7)$$

One anodic peak and two cathodic peaks are observed in the operated potential range. The anodic peak can be ascribed to the oxidation of either Cu_2O or CuOH to CuO and/or $Cu(OH)_2$. It is possible that these two peaks have overlapped with each other. The cathodic peaks are attributed to the reduction of CuO and/or $Cu(OH)_2$ to Cu_2O and/or CuOH [14, 50]. It should be noted that based on the previous works in this potential range SnO_2 does not show clear redox peaks [51-55] therefore it can be concluded that the overall shape of the CV curve is dominated by copper oxides performance. Also it has been reported before that the pseudocapacitance contribution of CuO is mainly governed by the reduction of Cu^{2+} to Cu^{+} in KOH solutions [3, 56, 57]. Detecting two reduction peaks in the current study suggests that copper ions are existing in two oxidation states which is in agreement with XPS results. It is possible that the presence of carbon stabilizes the Cu^{+} oxidation states. At early stages of ED process it was observed that if the tube ends are open due to capillary forces tin and copper deposit inside the MWCNTs. These well-defined and narrow channels inside CNTs possess unique electronic properties that make the confined metal oxide particles stay in a more reduced state. This phenomenon has been previously reported for some metal oxides such as manganese [58], tin [59], and Iron [60]. This confinement can enhance the capacitance of the nanocomposite electrode; due to curvature, π-electron is denser at the outer surface of CNT which leads to electron deficiency inside interior hollow cavity of CNTs. As a result the charge transfers from electron donor metal oxide to compensate for the electron deficiency inside the nanotube. This is helpful in adsorption-desorption process of positive ions in the electrolyte such as K^{+} and H^{+} [58, 59] and enhance the capacity. Also density functional theory calculations of Ng et al. [61] and experimental works on confined Sn particles within CNTs [59] have shown

that CNTs with encapsulated Sn has higher electrical conductivity compared with standalone CNTs which also can enhance the capacitance.

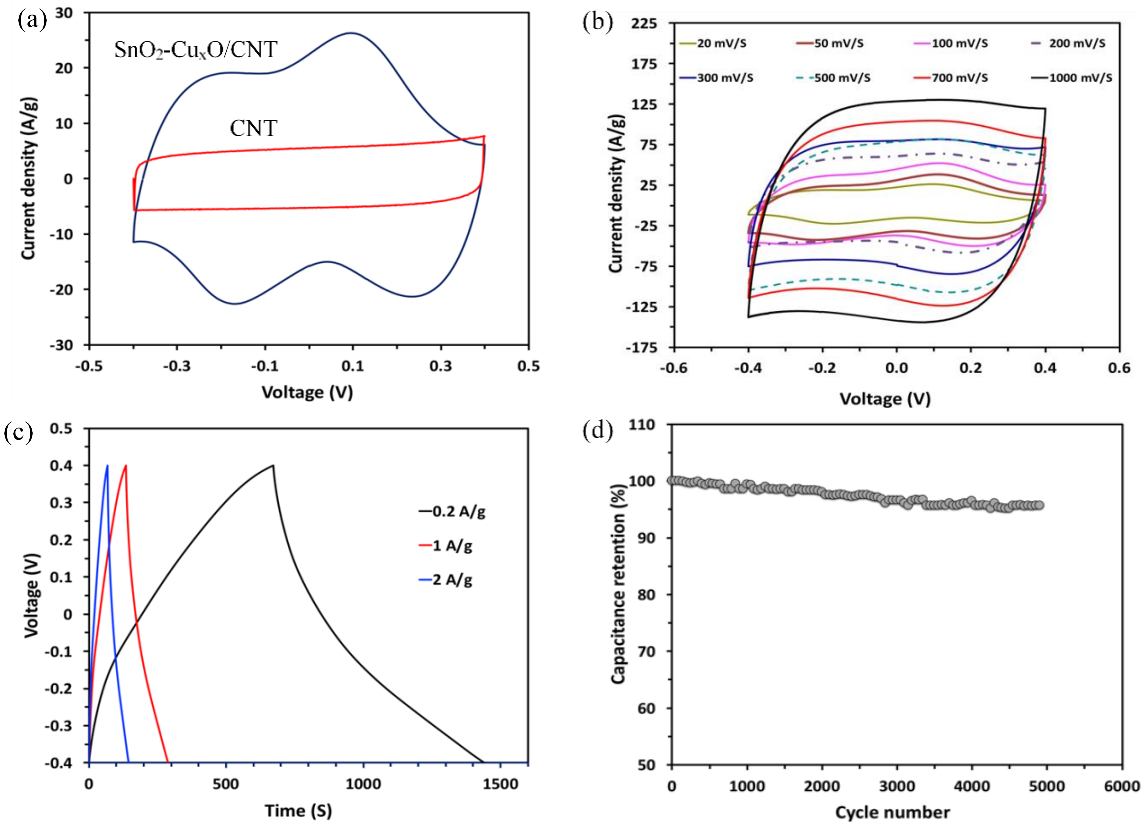

Figure 5-4. The electrochemical performance of the SnO2-CuxO/CNT electrode. (a) CV of CNT and electroplated CNT electrode at 5 mV/S, (b) CV of the electroplated electrode at different scan rate (c) charge discharge curve at different current density, and (d) cycling performance at current density of 1 A g^{-1}.

The capacitance performance of the core-shell structure was evaluated with cyclic voltammograms in a scan rate range of 20 to 1000 mV/s. As it can be observed in Figure 5-4b, with increasing scan rate, the redox peaks almost vanished, and the CV curves of the hybrid system become featureless, suggesting the faradic reactions are diffusion limited. The CV curve, however, maintains a nearly rectangular and good mirror images of the zero-current line even at high scan rates indicating an ideal capacitive behavior [19].

We have also used galvanostatic charge/discharge analysis for practical evaluation of the SnO_2-Cu_xO/CNT electrode capacitance in an alkali electrolyte (Figure 5-4c). The curve for the MWCNT is nearly triangular and shows linear charge and discharge profiles, indicating purely capacitive behavior [62]. The SnO_2-Cu_xO/CNT shows a pair of bending points at potentials close to those in the CV curve. In both cases, the charge/discharge curves were symmetrical, indicating good electrochemical capacitive characteristics and excellent reversible redox reaction. Interestingly, the SnO_2-Cu_xO/CNT electrode displays almost no drop in internal resistance (IR) at the beginning of the discharge curve, indicating low overall IR of the nanocomposite electrode. The corresponding specific capacitance was calculated from the slopes of the discharge branch of the curve using the following equation:

$$C_s = \frac{4\,i}{-\frac{\Delta V}{\Delta t}m} = \frac{4\,i}{-slope \times m} \qquad 5\text{-}8$$

in which i is the current applied, $\Delta V/\Delta t$ is the slope of the discharge curve, and m is the mass of the nanocomposite electrode. The SnO_2-Cu_xO/CNT electrode can reach a specific capacitance as high as 662 F/g at 0.2 A/g. To our knowledge, this value is the highest reported in the literature for CuO based capacitor (about 569 F/g and 545 F/g for binder free CuO nano-sheets on Ni foam at similar scan rates) [15, 63] . The supercapacitor electrode was cycled for 5000 cycles and retained about 94% of its initial capacitance (Figure 5-4d) which is much superior compared to previous results [15, 63] . The excellent cyclability performance is attributed to the 1D porous structure and strong bonding between the constituents of the nanocomposite. 1D porous structure provides space for accommodating the volume changes during charge-discharge cycles. Strong bonding between the metal oxides and MWCNTs helps

to preserve the integrity of the electrode material. In this regard tin's role is very crucial. It has relatively high electrical conductivity and excellent wettability. It readily adheres to the MWCNTs surface and makes it suitable for nucleation and growth of copper particles. Because copper is directly nucleated on tin, a strong interaction between these two components exists. Therefore tin oxide acts as an intermediate layer between copper oxide and the MWCNTs. In addition, using tin oxide can have other synergistic advantages, i.e. particle size refinement and enhancement of electronic and redox properties of the electrode material [32, 64].

To summarize, the improved performance of the SnO_2-Cu_xO/CNT electrode can be attributed to the following aspects. (i) abundant void space between the porous nanostructures not only provide short distance for the diffusion of the electrolyte but also offer a large number of electroactive sites for faradaic redox reactions to take place, hence improving the pseudo-capacitive performance, (ii) the 3D carbon network works as the backbone that provides mechanical integrity and facilitates electronic transportation within the electrodes (iii) SnO_2 has a synergistic effect on Cu_xO performance through wetting the surface of MWCNTs, modifying the particle size and enhancing the conductivity of the nanocomposite, (iv) by acid treatment the ends of MWCNTs open which results in infiltration and capsulation of metal oxide particles inside the MWCNT. These confined particles possess higher conductivity, smaller particle size and can facilitate diffusion of ions in the electrolyte which leads to higher capacitance, and (v) anchoring the CuO_x nanoparticles, which minimizes aggregation and maximizes high specific surface area.

5.4. Conclusion

Three-dimensional network of SnO_2-Cu_xO/CNT wire structure with MWCNTs as the substrate and copper oxide as the coating were synthesized through an electroless deposition technique. This facile and controllable processing method produces a unique core-shell structure with high porosity which enables fast ion and electron transports. The copper oxide nanoparticles enhance the capacitance through additional faradic redox reactions. The new hybrid shows excellent electrochemical performance as a supercapacitor electrode with a specific capacity of 662 F/g. The electrode is robust and capable of retaining more than 94% of its original capacity after 5000 cycles, indicating excellent electrochemical stability. Such an outstanding performance suggests that by engineering the CNTs surfaces and utilizing ED method, high capacity energy storage materials can be produced. Moreover, this method can be easily applied to other metal oxides to produce high performance supercapacitor electrodes.

5.5. References

1. Peterson, S. B.; Apt, J.; Whitacre, J., *Lithium-ion battery cell degradation resulting from realistic vehicle and vehicle-to-grid utilization*. Journal of Power Sources 2010, 195 (8), 2385-2392.

2. Simon, P.; Gogotsi, Y., *Materials for electrochemical capacitors*. Nature materials 2008, 7 (11), 845.

3. Ameri, B.; Davarani, S. S. H.; Roshani, R.; Moazami, H. R.; Tadjarodi, A., *A flexible mechanochemical route for the synthesis of copper oxide nanorods/nanoparticles/nanowires for supercapacitor applications: The effect of morphology on the charge storage ability*. Journal of Alloys and Compounds 2017, 695, 114-123.

4. Pay, S.; Baghzouz, Y. *In Effectiveness of battery-supercapacitor combination in electric vehicles*, Power Tech Conference Proceedings, 2003 IEEE Bologna, IEEE: 2003; p 6 pp. Vol. 3.

5. Wang, G.; Zhang, L.; Zhang, J., *A review of electrode materials for electrochemical supercapacitors*. Chemical Society Reviews 2012, 41 (2), 797-828.

6. Simon, P.; Gogotsi, Y.; Dunn, B., *Where do batteries end and supercapacitors begin?* Science 2014, 343 (6176), 1210-1211.

7. Abdelkader, A. M., *Electrochemical synthesis of highly corrugated graphene sheets for high performance supercapacitors*. Journal of Materials Chemistry A 2015, 3 (16), 8519-8525.

8. Zhang, Y.; Li, L.; Su, H.; Huang, W.; Dong, X., *Binary metal oxide: advanced energy storage materials in supercapacitors*. Journal of Materials Chemistry A 2015, 3 (1), 43-59.

9. Hao, P.; Tian, J.; Sang, Y.; Tuan, C.-C.; Cui, G.; Shi, X.; Wong, C.; Tang, B.; Liu, H., *1D Ni–Co oxide and sulfide nanoarray/carbon aerogel hybrid nanostructures for asymmetric supercapacitors with high energy density and excellent cycling stability*. Nanoscale 2016, 8 (36), 16292-16301.

10. Snook, G. A.; Kao, P.; Best, A. S., *Conducting-polymer-based supercapacitor devices and electrodes*. Journal of Power Sources 2011, 196 (1), 1-12.

11. Wu, Z.; Zhu, Y.; Ji, X., *$NiCo_2O_4$-based materials for electrochemical supercapacitors*. Journal of Materials Chemistry A 2014, 2 (36), 14759-14772.

12. Jiang, J.; Li, Y.; Liu, J.; Huang, X.; Yuan, C.; Lou, X. W., *Recent advances in metal oxide-based electrode architecture design for electrochemical energy storage*. Advanced Materials 2012, 24 (38), 5166-5180.

13. Aziz, A.; Zhang, T.; Lin, Y.-H.; Daneshvar, F.; Sue, H.-J.; Welland, M. E., *1D copper nanowires for flexible printable electronics and high ampacity wires*. Nanoscale 2017, 9 (35), 13104-13111.

14. Liu, Y.; Cao, X.; Jiang, D.; Jia, D.; Liu, J., Hierarchical CuO nanorod arrays in situ generated on three-dimensional copper foam via cyclic voltammetry oxidization for high-performance supercapacitors. Journal of Materials Chemistry A 2018.

15. Xu, P.; Liu, J.; Liu, T.; Ye, K.; Cheng, K.; Yin, J.; Cao, D.; Wang, G.; Li, Q., *Preparation of binder-free CuO/Cu 2 O/Cu composites: A novel electrode material for supercapacitor applications*. RSC Advances 2016, 6 (34), 28270-28278.

16. Chen, L.; Zhang, Y.; Zhu, P.; Zhou, F.; Zeng, W.; Lu, D. D.; Sun, R.; Wong, C., *Copper salts mediated morphological transformation of Cu 2 O from cubes to hierarchical flower-like or microspheres and their supercapacitors performances*. Scientific reports 2015, 5, 9672.

17. Kim, D.-W.; Rhee, K.-Y.; Park, S.-J., *Synthesis of activated carbon nanotube/copper oxide composites and their electrochemical performance*. Journal of Alloys and Compounds 2012, 530, 6-10.

18. Liu, Y.; Huang, H.; Peng, X., *Highly enhanced capacitance of CuO nanosheets by formation of CuO/SWCNT networks through electrostatic interaction*. Electrochimica Acta 2013, 104, 289-294.

19. Senthilkumar, V.; Kim, Y. S.; Chandrasekaran, S.; Rajagopalan, B.; Kim, E. J.; Chung, J. S., *Comparative supercapacitance performance of CuO nanostructures for energy storage device applications*. RSC Advances 2015, 5 (26), 20545-20553.

20. Moosavifard, S. E.; El-Kady, M. F.; Rahmanifar, M. S.; Kaner, R. B.; Mousavi, M. F., *Designing 3D highly ordered nanoporous CuO electrodes for high-performance asymmetric supercapacitors*. ACS applied materials & interfaces 2015, 7 (8), 4851-4860.

21. Meng, F.-L.; Zhong, H.-X.; Zhang, Q.; Liu, K.-H.; Yan, J.-M.; Jiang, Q., *Integrated Cu 3 N porous nanowire array electrode for high-performance supercapacitors*. Journal of Materials Chemistry A 2017, 5 (36), 18972-18976.

22. Li, X.; Hao, C.; Tang, B.; Wang, Y.; Liu, M.; Wang, Y.; Zhu, Y.; Lu, C.; Tang, Z., *Supercapacitor electrode materials with hierarchically structured pores from carbonization of MWCNTs and ZIF-8 composites*. Nanoscale 2017, 9 (6), 2178-2187.

23. Zhang, X.; Shi, W.; Zhu, J.; Kharistal, D. J.; Zhao, W.; Lalia, B. S.; Hng, H. H.; Yan, Q., *High-power and high-energy-density flexible pseudocapacitor electrodes made from porous CuO nanobelts and single-walled carbon nanotubes*. ACS nano 2011, 5 (3), 2013-2019.

24. Zhang, W.; Yin, Z.; Chun, A.; Yoo, J.; Diao, G.; Kim, Y. S.; Piao, Y., *Rose rock-shaped nano Cu2O anchored graphene for high-performance supercapacitors via solvothermal route*. Journal of Power Sources 2016, 318, 66-75.

25. Dong, C.; Wang, Y.; Xu, J.; Cheng, G.; Yang, W.; Kou, T.; Zhang, Z.; Ding, Y., *3D binder-free Cu 2 O@ Cu nanoneedle arrays for high-performance asymmetric supercapacitors*. Journal of Materials Chemistry A 2014, 2 (43), 18229-18235.

26. Daneshvar-Fatah, F.; Wang, C.; Shaw, L. *In Synthesis of Graphene-Supported Nano-Na3MnCO3PO4 for High Rate and High Capacity Sodium Ion Batteries*, Meeting Abstracts, The Electrochemical Society: 2015; pp 12-12.

27. Lee, C. Y.; Tsai, H. M.; Chuang, H. J.; Li, S. Y.; Lin, P.; Tseng, T. Y., *Characteristics and electrochemical performance of supercapacitors with manganese oxide-carbon nanotube nanocomposite electrodes*. Journal of the Electrochemical Society 2005, 152 (4), A716-A720.

28. Fisher, R. A.; Watt, M. R.; Ready, W. J., *Functionalized carbon nanotube supercapacitor electrodes: a review on pseudocapacitive materials*. ECS Journal of Solid State Science and Technology 2013, 2 (10), M3170-M3177.

29. Wang, K.; Zhao, C.; Min, S.; Qian, X., *Facile synthesis of Cu2O/RGO/Ni (OH) 2 nanocomposite and its double synergistic effect on supercapacitor performance*. Electrochimica Acta 2015, 165, 314-322.

30. Zhi, M.; Xiang, C.; Li, J.; Li, M.; Wu, N., *Nanostructured carbon–metal oxide composite electrodes for supercapacitors: a review*. Nanoscale 2013, 5 (1), 72-88.

31. Sugimoto, W.; Shibutani, T.; Murakami, Y.; Takasu, Y., *Charge Storage Capabilities of Rutile-Type RuO2 VO 2 Solid Solution for Electrochemical Supercapacitors*. Electrochemical and solid-state letters 2002, 5 (7), A170-A172.

32. Jayalakshmi, M.; Rao, M. M.; Venugopal, N.; Kim, K.-B., *Hydrothermal synthesis of SnO2–V2O5 mixed oxide and electrochemical screening of carbon nano-tubes (CNT), V2O5, V2O5–CNT, and SnO2–V2O5–CNT electrodes for supercapacitor applications*. Journal of Power Sources 2007, 166 (2), 578-583.

33. Shakir, I.; Ali, Z.; Bae, J.; Park, J.; Kang, D. J., *Layer by layer assembly of ultrathin V_2O_5 anchored MWCNTs and graphene on textile fabrics for fabrication of high energy density flexible supercapacitor electrodes*. Nanoscale 2014, 6 (8), 4125-4130.

34. Ramani, M.; Haran, B. S.; White, R. E.; Popov, B. N.; Arsov, L., *Studies on activated carbon capacitor materials loaded with different amounts of ruthenium oxide*. Journal of Power Sources 2001, 93 (1-2), 209-214.

35. Sun, D.; Everett, W. N.; Chu, C. C.; Sue, H. J., *Single-Walled Carbon-Nanotube Dispersion with Electrostatically Tethered Nanoplatelets*. Small 2009, 5 (23), 2692-2697.

36. Daneshvar-Fatah, F.; Nasirpouri, F., *A study on electrodeposition of Ni-noncovalnetly treated carbon nanotubes nanocomposite coatings with desirable mechanical and anti-corrosion properties*. Surface and Coatings Technology 2014, 248, 63-73.

37. Okpalugo, T. I. T.; Papakonstantinou, P.; Murphy, H.; McLaughlin, J.; Brown, N. M. D., *High resolution XPS characterization of chemical functionalised MWCNTs and SWCNTs*. Carbon 2005, 43 (1), 153-161.

38. Kundu, S.; Wang, Y.; Xia, W.; Muhler, M., *Thermal stability and reducibility of oxygen-containing functional groups on multiwalled carbon nanotube surfaces: A quantitative high-resolution xps and TPD/TPR study*. Journal of Physical Chemistry C 2008, 112 (43), 16869-16878.

39. Abdelkader, A.; Kinloch, I.; Dryfe, R., *High-yield electro-oxidative preparation of graphene oxide*. Chemical Communications 2014, 50 (61), 8402-8404.

40. Pan, H.; Poh, C. K.; Feng, Y. P.; Lin, J., *Supercapacitor electrodes from tubes-in-tube carbon nanostructures*. Chemistry of Materials 2007, 19 (25), 6120-6125.

41. An, G.; Na, N.; Zhang, X.; Miao, Z.; Miao, S.; Ding, K.; Liu, Z., *SnO2/carbon nanotube nanocomposites synthesized in supercritical fluids: highly efficient materials for use as a chemical sensor and as the anode of a lithium-ion battery*. Nanotechnology 2007, 18 (43), 435707.

42. Hussain, Z.; Salim, M. A.; Khan, M. A.; Khawaja, E. E., *X-ray photoelectron and auger spectroscopy study of copper-sodium-germanate glasses*. Journal of Non-Crystalline Solids 1989, 110 (1), 44-52.

43. Baddorf, A. P.; Wendelken, J. F., *High coverages of oxygen on Cu(110) investigated with XPS, LEED, and HREELS*. Surface Science 1991, 256 (3), 264-271.

44. Jolley, J. G.; Geesey, G. G.; Hankins, M. R.; Wright, R. B.; Wichlacz, P. L., *Auger electron and X-ray photoelectron spectroscopic study of the biocorrosion of copper by alginic acid polysaccharide*. Applied Surface Science 1989, 37 (4), 469-480.

45. Yu, Z.; Tetard, L.; Zhai, L.; Thomas, J., *Supercapacitor electrode materials: nanostructures from 0 to 3 dimensions*. Energy & Environmental Science 2015, 8 (3), 702-730.

46. Cetinkaya, T.; Uysal, M.; Guler, M. O.; Akbulut, H.; Alp, A., *Improvement cycleability of core–shell silicon/copper composite electrodes for Li-ion batteries by using electroless deposition of copper on silicon powders*. Powder Technology 2014, 253, 63-69.

47. Lang, X.; Hirata, A.; Fujita, T.; Chen, M., *Nanoporous metal/oxide hybrid electrodes for electrochemical supercapacitors*. Nature nanotechnology 2011, 6 (4), 232.

48. Zhang, L.; Tang, C.; Gong, H., *Temperature effect on the binder-free nickel copper oxide nanowires with superior supercapacitor performance*. Nanoscale 2014, 6 (21), 12981-12989.

49. Yu, L.; Jin, Y.; Li, L.; Ma, J.; Wang, G.; Geng, B.; Zhang, X., *3D porous gear-like copper oxide and their high electrochemical performance as supercapacitors*. CrystEngComm 2013, 15 (38), 7657-7662.

50. Li, Y.; Chang, S.; Liu, X.; Huang, J.; Yin, J.; Wang, G.; Cao, D., *Nanostructured CuO directly grown on copper foam and their supercapacitance performance*. Electrochimica Acta 2012, 85, 393-398.

51. Velmurugan, V.; Srinivasarao, U.; Ramachandran, R.; Saranya, M.; Grace, A. N., *Synthesis of tin oxide/graphene (SnO2/G) nanocomposite and its electrochemical properties for supercapacitor applications*. Materials Research Bulletin 2016, 84, 145-151.

52. Prasad, K. R.; Miura, N., *Electrochemical synthesis and characterization of nanostructured tin oxide for electrochemical redox supercapacitors*. Electrochemistry communications 2004, 6 (8), 849-852.

53. Li, F.; Song, J.; Yang, H.; Gan, S.; Zhang, Q.; Han, D.; Ivaska, A.; Niu, L., *One-step synthesis of graphene/SnO2 nanocomposites and its application in electrochemical supercapacitors*. Nanotechnology 2009, 20 (45), 455602.

54. Lim, S.; Huang, N.; Lim, H., *Solvothermal synthesis of SnO2/graphene nanocomposites for supercapacitor application*. Ceramics International 2013, 39 (6), 6647-6655.

55. Hwang, S.-W.; Hyun, S.-H., *Synthesis and characterization of tin oxide/carbon aerogel composite electrodes for electrochemical supercapacitors*. Journal of Power Sources 2007, 172 (1), 451-459.

56. Shinde, S. K.; Dubal, D. P.; Ghodake, G. S.; Fulari, V. J., *Hierarchical 3D-flower-like CuO nanostructure on copper foil for supercapacitors*. RSC Advances 2015, 5 (6), 4443-4447.

57. Grugeon, S.; Laruelle, S.; Herrera-Urbina, R.; Dupont, L.; Poizot, P.; Tarascon, J. M., *Particle Size Effects on the Electrochemical Performance of Copper Oxides toward Lithium*. Journal of the Electrochemical Society 2001, 148 (4), A285-A292.

58. Chen, W.; Fan, Z.; Gu, L.; Bao, X.; Wang, C., *Enhanced capacitance of manganese oxide via confinement inside carbon nanotubes*. Chemical Communications 2010, 46 (22), 3905-3907.

59. Zhang, H.; Song, H.; Chen, X.; Zhou, J., *Enhanced lithium ion storage property of Sn nanoparticles: the confinement effect of few-walled carbon nanotubes*. The Journal of Physical Chemistry C 2012, 116 (43), 22774-22779.

60. Chen, W.; Pan, X.; Willinger, M.-G.; Su, D. S.; Bao, X., *Facile autoreduction of iron oxide/carbon nanotube encapsulates*. Journal of the American Chemical Society 2006, 128 (10), 3136-3137.

61. Ng, M.-F.; Zheng, J.; Wu, P., *Evaluation of Sn nanowire encapsulated carbon nanotube for a Li-ion battery anode by DFT calculations*. The Journal of Physical Chemistry C 2010, 114 (18), 8542-8545.

62. Yu, C.; Masarapu, C.; Rong, J.; Wei, B.; Jiang, H., *Stretchable supercapacitors based on buckled single-walled carbon-nanotube macrofilms*. Advanced Materials 2009, 21 (47), 4793-4797.

63. Wang, G.; Huang, J.; Chen, S.; Gao, Y.; Cao, D., *Preparation and supercapacitance of CuO nanosheet arrays grown on nickel foam*. Journal of Power Sources 2011, 196 (13), 5756-5760.

64. Hu, C.-C.; Wang, C.-C.; Chang, K.-H., *A comparison study of the capacitive behavior for sol–gel-derived and co-annealed ruthenium–tin oxide composites*. Electrochimica acta 2007, 52 (7), 2691-2700.

6. CONCLUSIONS

Carbon nanotube (CNT)-copper nanocomposites are promising materials for light-weight high-ampacity conductors. The key issue in hybridization of CNT and metal is creating a strong bonding between them. This requires proper modification of the CNT surface. However, experimental works on determining the effect of interfacial functionalization on the properties of the metal/CNT system is scarce. In this work, the effect of CNT surface modification on the morphology, interfacial interactions, electrochemical performance, and mechanical and electrical properties Cu/CNT hybrid systems and composite fibers are investigated. For this purpose, firstly, CNTs with carboxyl, thiol, and nitrogen doped surface groups were used as substrate for growth of Cu particles via a facile electrochemical process. It is observed that not only the morphology but also the chemical state of the Cu deposits is affected by the surface functional group on CNT. Thiol group significantly enhances copper wettability towards CNT, facilitating a uniform deposition of copper, and impedes oxidation. These findings were utilized in fabrication of core-shell CNT/Cu fibers.

Metal-carbon nanotube fibers are emerging materials for light-weight conductors that can replace common metallic conductors. One of the main challenges to their development is the poor affinity of CNT towards metals, which as discussed above was improved by introducing thiol groups to the surface of CNTs. Moreover, in industrial applications and for high precision electronics, pre-seeding the substrates is a common practice to ensure obtaining a dense and highly conductive Cu deposits. Consequently, we demonstrated a new approach for fabrication of Cu/CNT core-shell fibers that outperforms the commercial Cu wires in terms of specific

conductivity, ampacity, and strength. By introducing thiol groups to the surface of carbon nanotube fibers, we eradicate the application of tin in the electroless deposition process and palladium seeds are uniformly distributed on CNT fibers. This leads to deposition of dense and high-quality Cu deposits with enhanced adhesion to the core fiber. As a result, CNT/Cu core-shell fibers with specific conductivity of 3.4×10^7 S/m and tensile strength of 642 MPa, almost three times higher than commercial Cu wires, is produced. Due to strong interaction of thiol functional groups and Cu atoms, the fiber can preserve its integrity and conductivity after > 500 bending cycles. Finally, the ampacity of the composite wire reaches to 1.03×10^5 A/cm2 which corresponds to a specific ampacity two times higher than that of commercial Cu wires. The approaches that are used here to design the interface between the carbon nanotube fibers and Cu layer are easily adaptable and can be implemented in other deposition methods including electroplating.

We realized due to strong affinity of thiol-activated CNTs towards metals, they can readily wrap around copper nanowires. This finding was used to fabricate CNT/Cu composite fibers with high electrical conductivity and high ampacity via electrospinning for the first time. This has been achieved through tailoring the surface chemistry of CNTs and introduction of copper nanowires to the precursor. After mixing, functionalized CNTs wrap around the copper nanowires, forming a stable colloidal suspension. This mixture is added to an aqueous solution of copper acetate and polyvinyl alcohol to form the electrospinning precursor. Upon subsequent heat treatment, individual spun fibers with conductivity of 3.4×10^6 S/m and ampacity of 8.2×10^5 A/cm^2, which is about three times higher than copper, were obtained. The randomly formed mats of these submicron CNT/Cu fibers exhibit sheet resistance of 39 Ω/□ at a transparency of

79%. The procedure and approaches reported here are versatile and can be readily implemented in other spinning techniques to fabricate various metal-CNT composite fibers or thin-films. Composite metal fibers produced here can be used in a wide variety of applications from portable electronics to energy conversion devices.

Hybridization with conductive nanostructured carbon-based materials such as CNTs has been proposed to improve the conductivity and increase the surface area for electrochemical energy storage. Another application of tuning the interface of CNT and metals was realized in energy storage systems. In here, we also used CNTs as template for synthesizing porous thin films of SnO_2-CuO-Cu_2O (SnO_2-Cu_xO) via electroless deposition (ED) technique. Tin with its high wettability and electrical conductivity acts as an intermediate layer between copper and CNTs and provides a strong interaction between them. We also observed that by controlling the interfacial characteristics of CNTs and varying the composition of the electroless bath, the SnO_2-Cu_xO thin film morphology can be easily manipulated. Electrochemical characterizations show that CNT/SnO_2-Cu_xO nanocomposite possesses pseudocapacitive behaviour that reaches a specific capacitance of 662 F/g and the retention is 94% after 5000 cycles which outperforms any known copper and tin-based supercapacitors in the literature. This excellent performance is mainly attributed to high specific surface area, small particle size, synergistic effect of Sn, and conductivity improvement by using CNTs. The combination of CNTs and metal oxides holds promise for supercapacitors with improved performance.